1) Heliosejsmologia

2) Streszczenie (z krótkimi uzupełnieniami) przeglądowego artykułu G. Handlera

3) Podkreślenie kilku ważnych cech oscylacji gwiazd

Kilka krótkich artykułów dla zaliczenia (egzaminu):

Dziembowski & Pamyatnykh, 1991, A&A, 248, L11-L14.
A potential asteroseismological test for convective overshooting theories.

Dziembowski & Pamyatnykh, 2008, MNRAS, 385, 2061-2068.
The two hybrid B-type pulsators: ν Eridani and 12 Lacertae.

Handler et al., 2009, ApJ, L56-L59.
Asteroseismology of hybrid pulsators made possible: simultaneous MOST space photometry and ground-based spectroscopy of γ Peg.

Lenz, Pamyatnykh, Breger & Antoci, 2008, A&A, 478, 855-863.
An asteroseismic study of the δ Scuti star 44 Tauri.

Lenz, Pamyatnykh, Zdravkov & Breger, 2010, A&A, 509, A90 (7 pages).
A δ Scuti star in the post_MS contraction phase: 44 Tauri.

Zwintz et al., 2011, A&A, 533, A133 (8 pages).
Regular frequency patterns in the classical δ Scuti star HD 144277 observed by the MOST satellite.

Heliosejsmologia

(głównie według lekcji J. Christensen-Dalsgaard)

The Sun

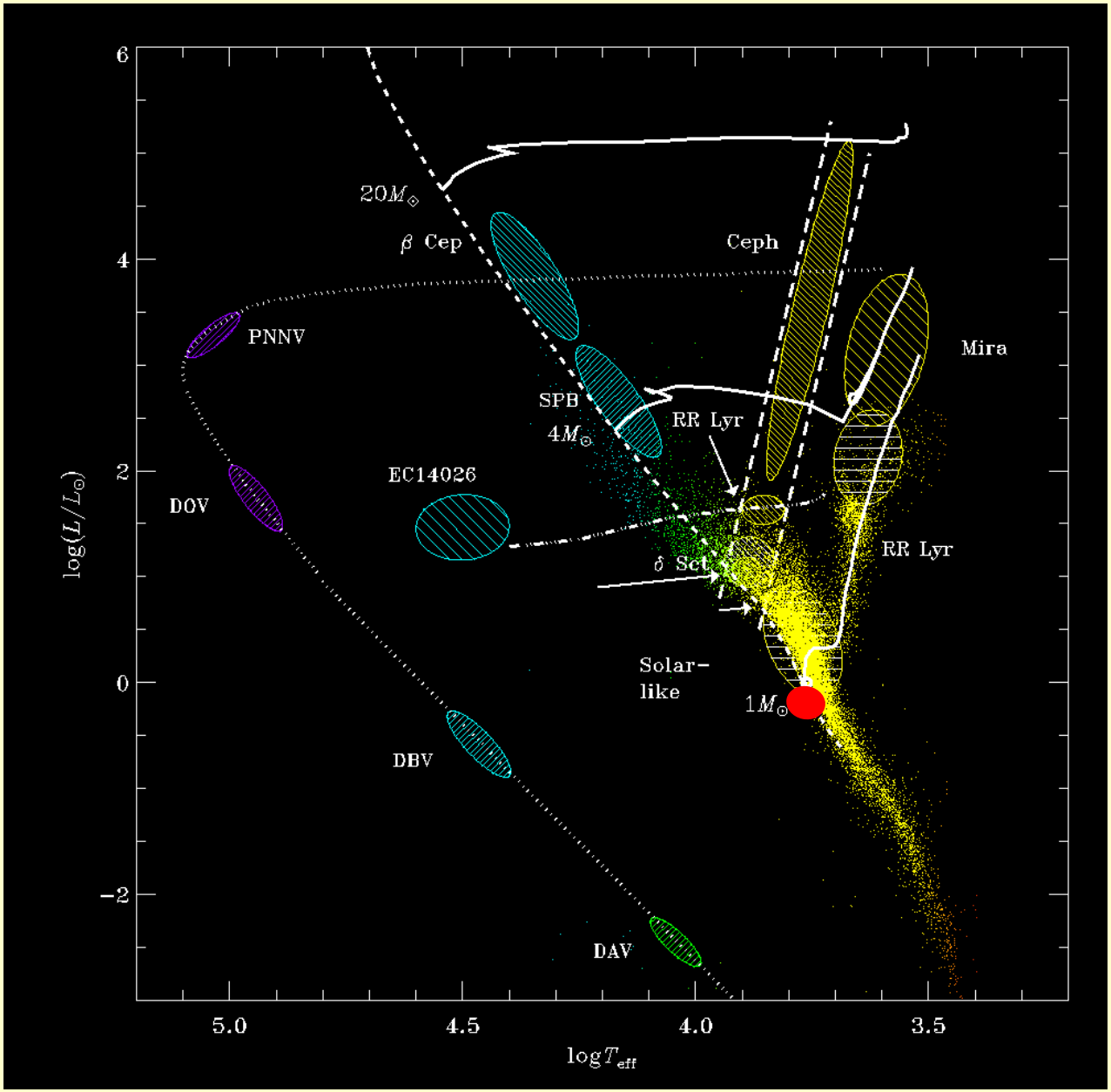
6
4
2
0
−2
log(L/L⊙)
5.0
4.5
4.0
3.5
log T_eff
20M⊙
β Cep
Ceph
PNNV
Mira
SPB
4M⊙
RR Lyr
EC14026
DOV
RR Lyr
δ Sct
Solar-
like
1M⊙
DBV
DAV

JCD

Five-min oscillations: A local phenomenon in the solar atmosphere?

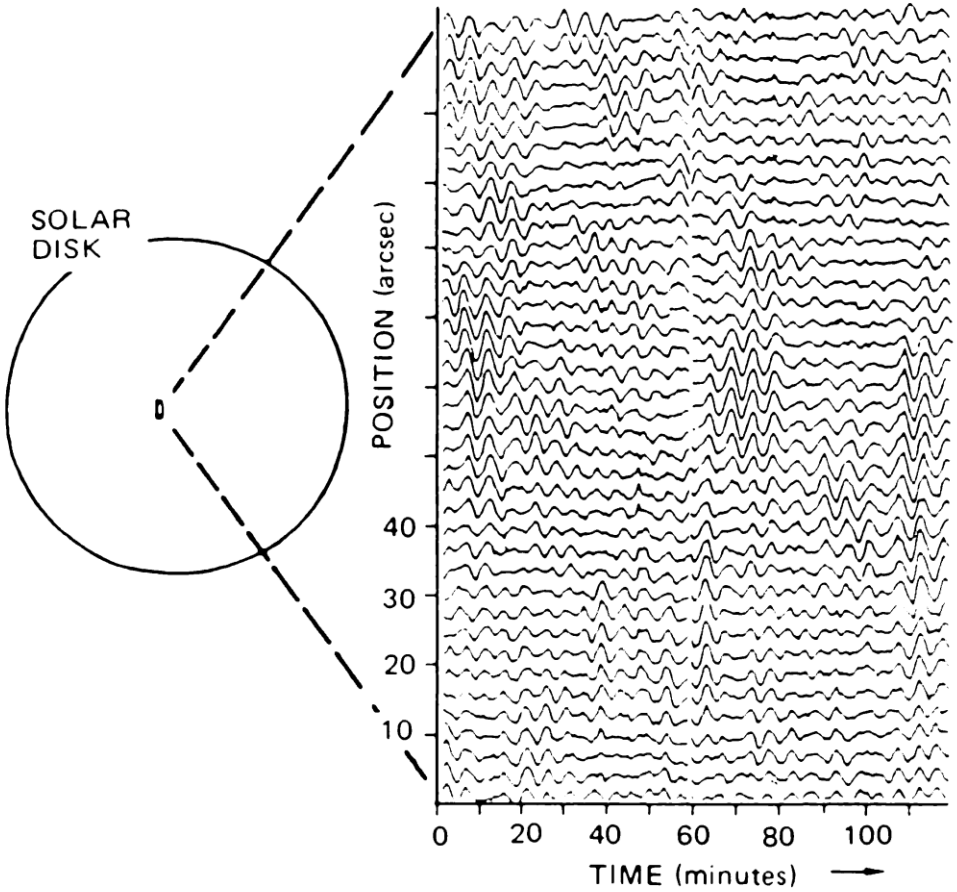

Musman & Rust

(1970; Solar Phys. 13, 261)

JCD

Oscillation modes of the Sun

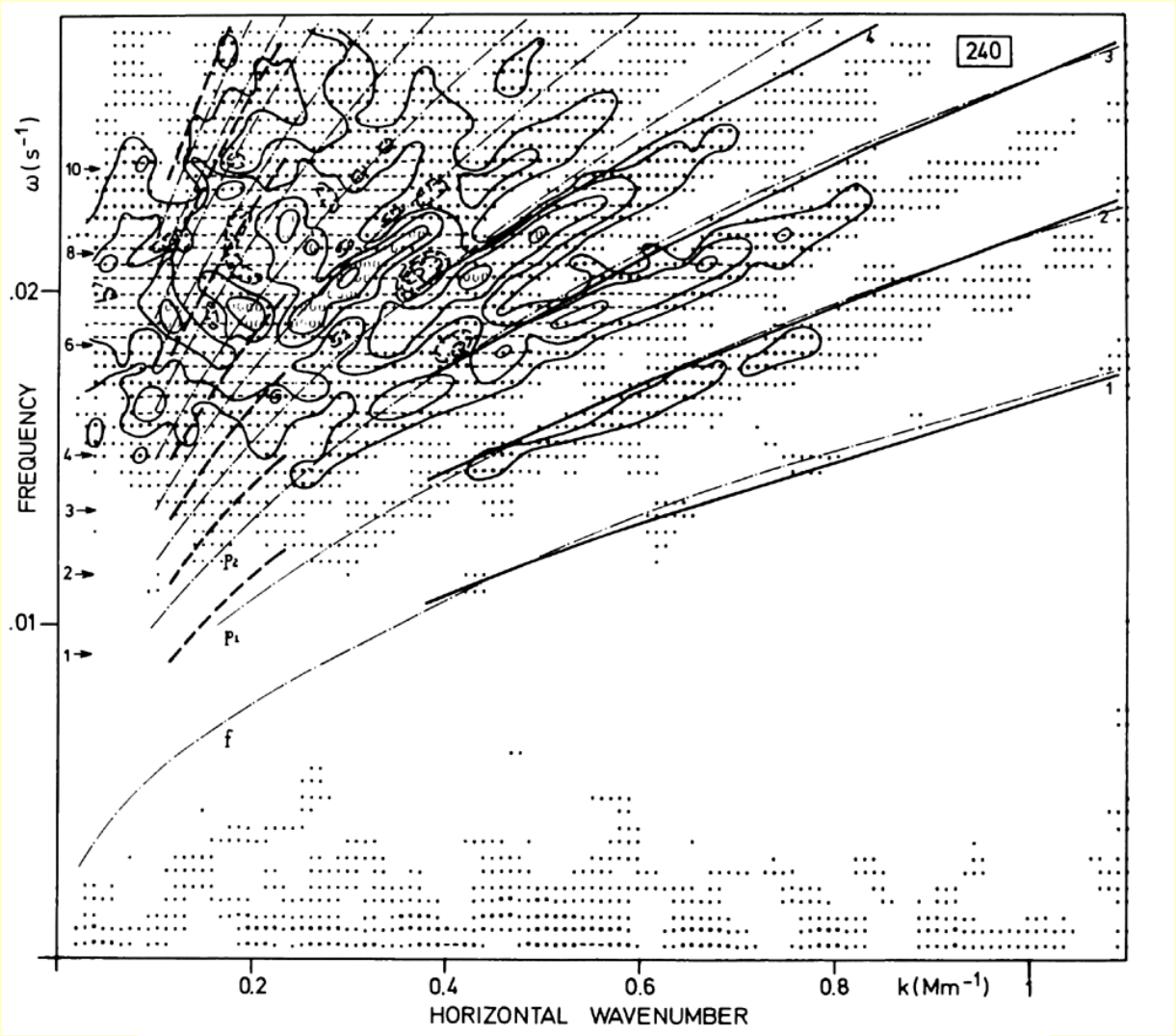

Models:

- Ulrich (1970): ——————
- Wolff (1972): — — — —
- Ando & Osaki (1975): -·-·-·-·-·-

Deubner (1975; Astron. Astrophys. 44, 371)

JCD

The start of global helioseismology

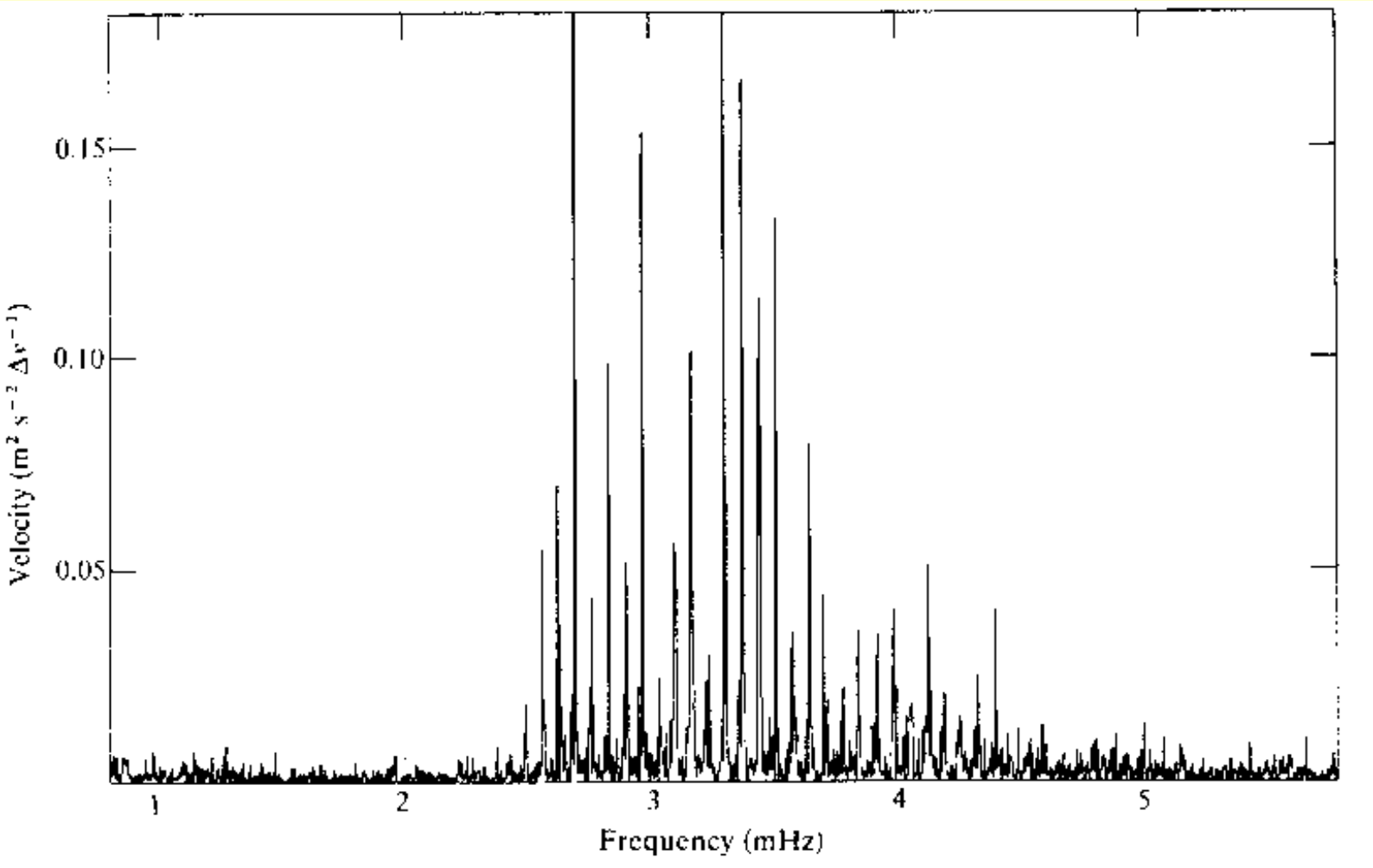

Grec et al. (1980; Nature 288, 541)

JCD

Crucial advantages

- Access to modes of degree up to 1000+
- Observations over very extended period (more than 10 years nearly continuously)
- Well-determined global parameters

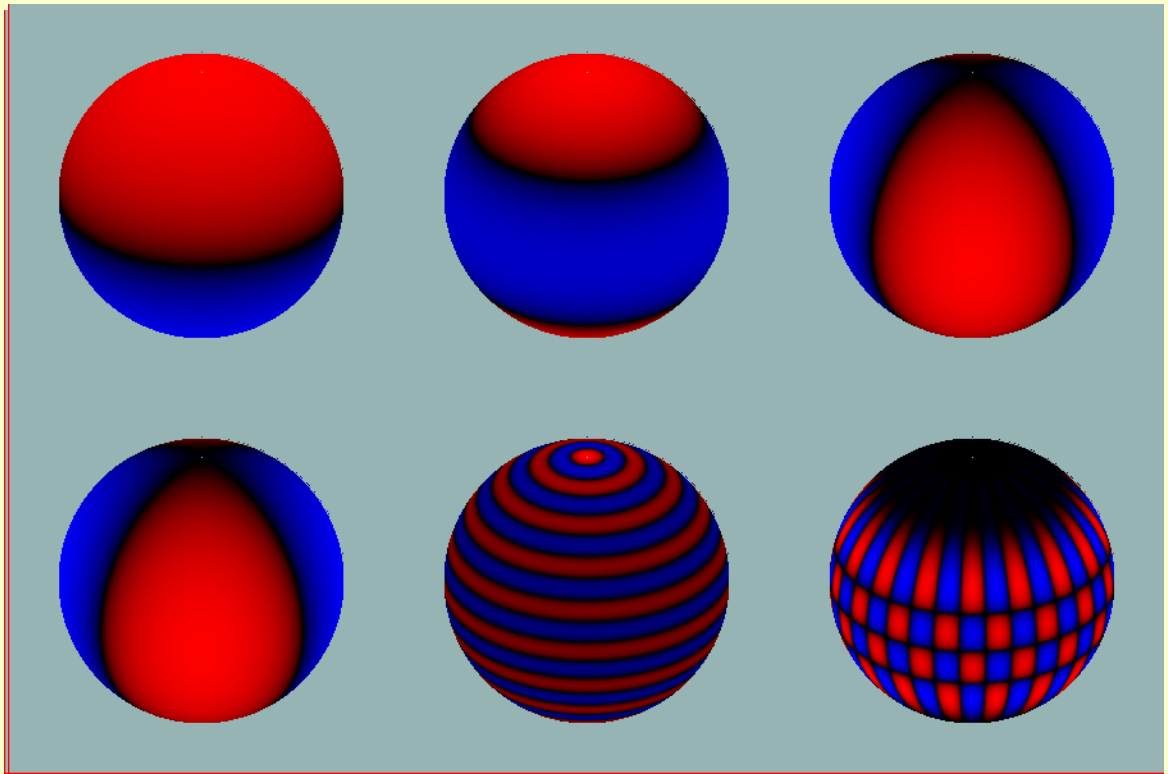

JCD

Frequencies of solar model

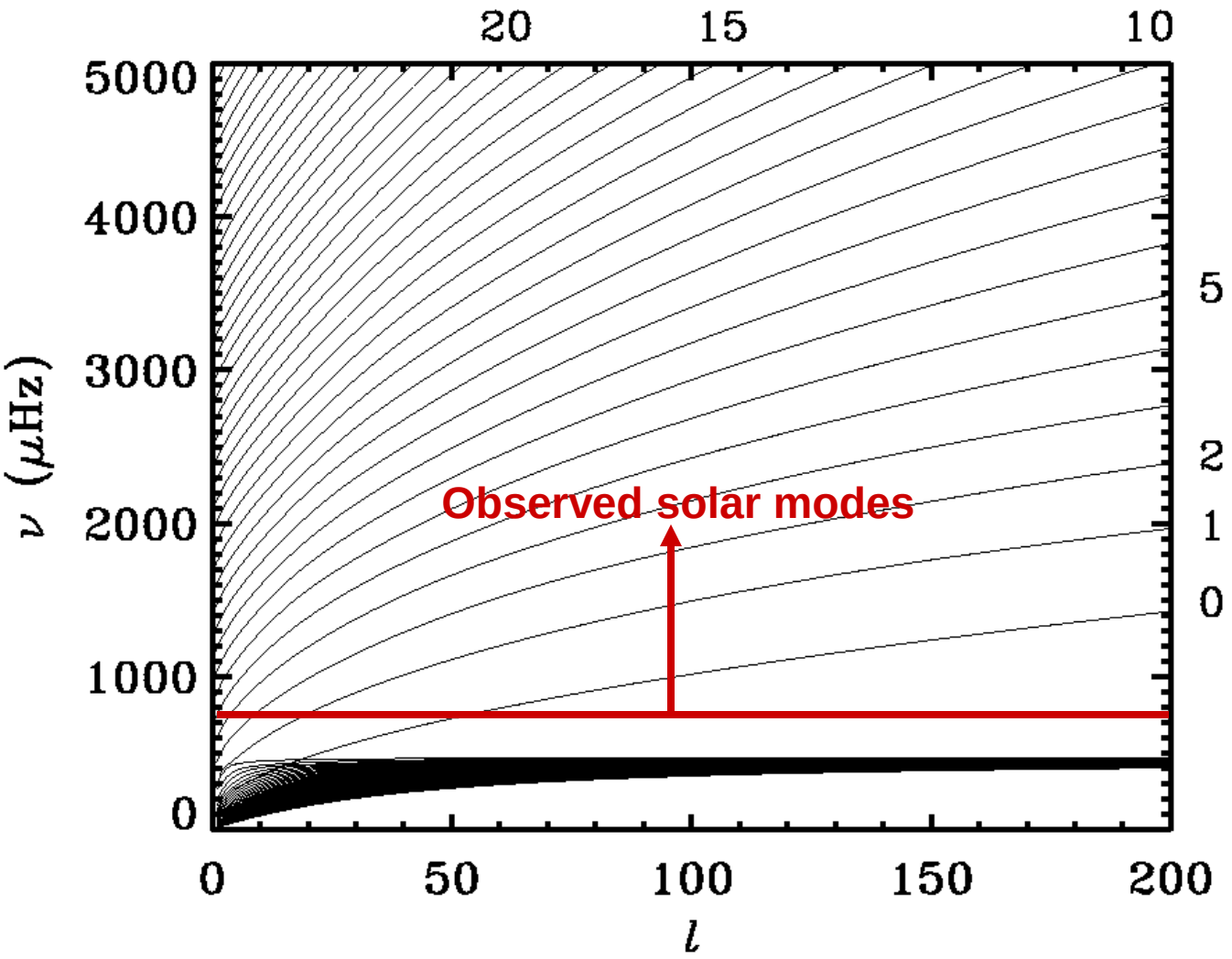

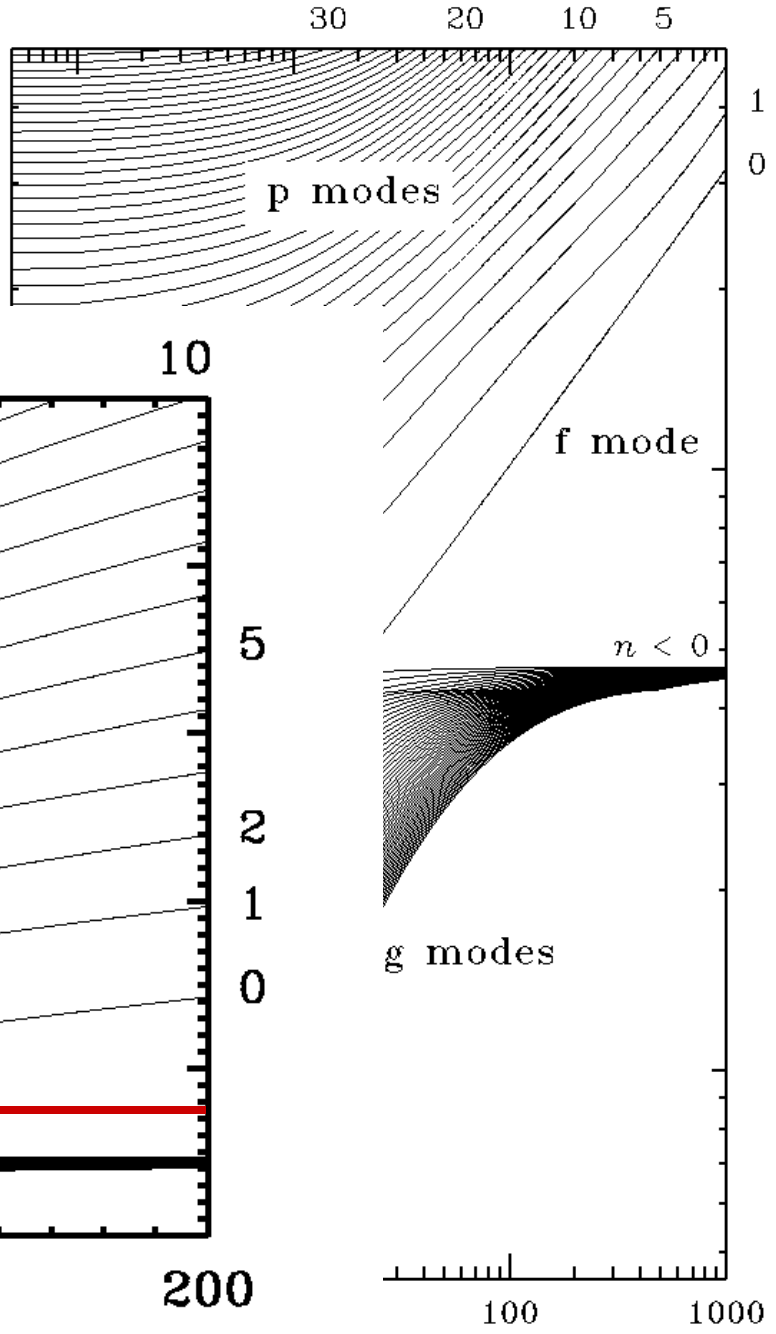

JCD


Single Dopplergram
(30-MAR-96 19:54:00)
-2500. -2000. -1500. -1000. -500. 0. 500. 1000. 1500.
Velocity (m/s)
SOI / MDI
Stanford Lockheed Institute for Spa

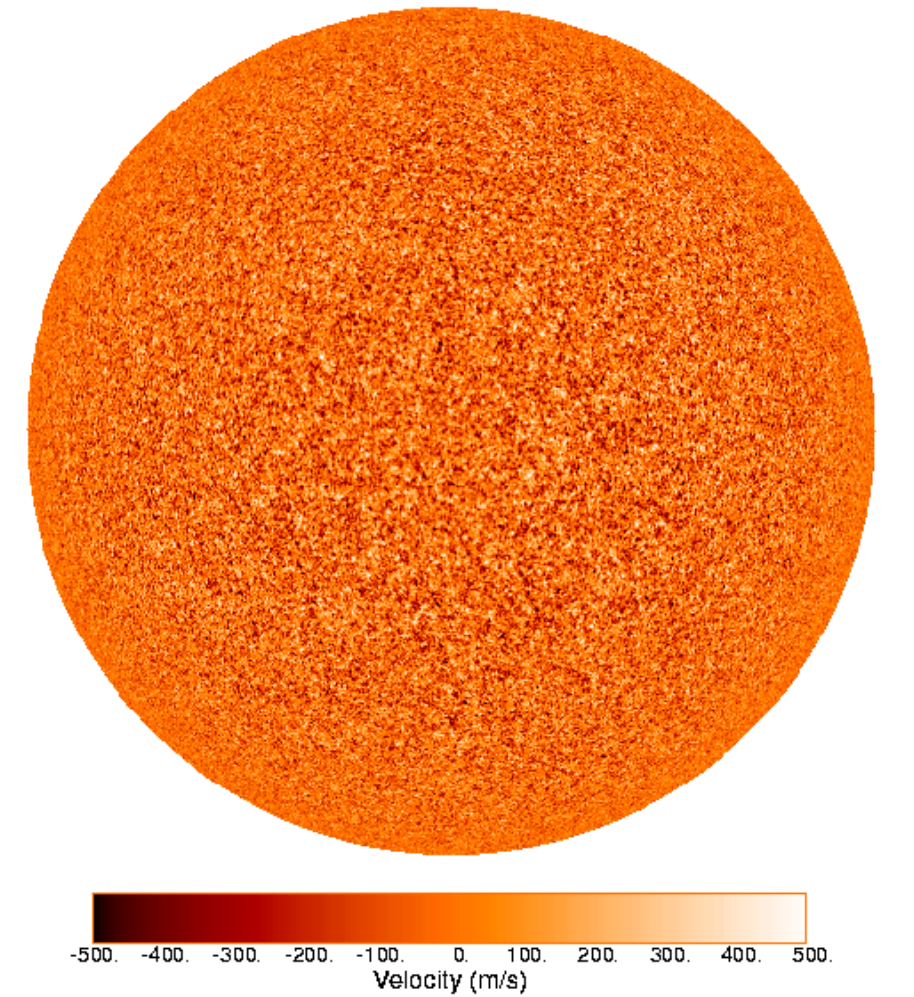
Single Dopplergram Minus 45 Images Average
(30-MAR-96 19:54:00)
-500. -400. -300. -200. -100. 0. 100. 200. 300. 400. 500.
Velocity (m/s)
SOI / MDI
Stanford Lockheed Institute for Space Research

JCD

Data on solar oscillations

Observations:

MDI on SOHO

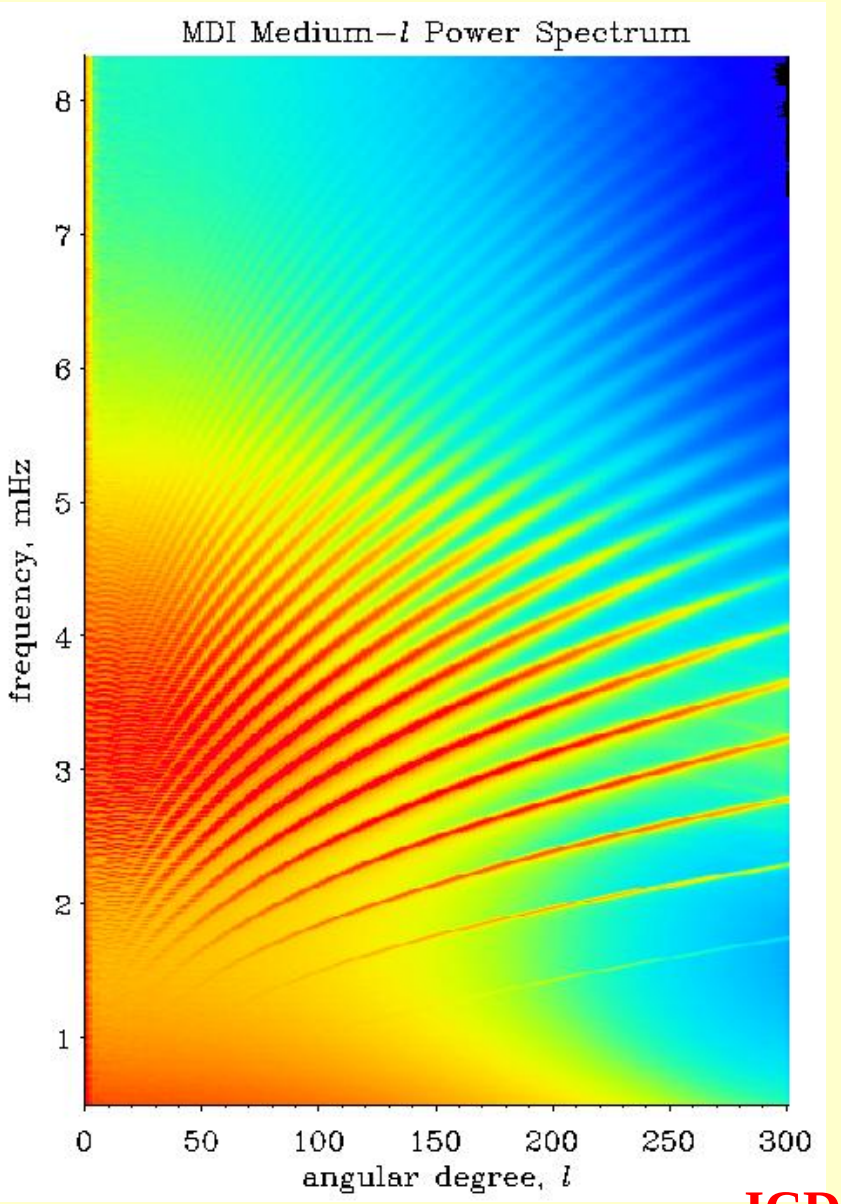

VIRGO on SOHO (whole-disk):

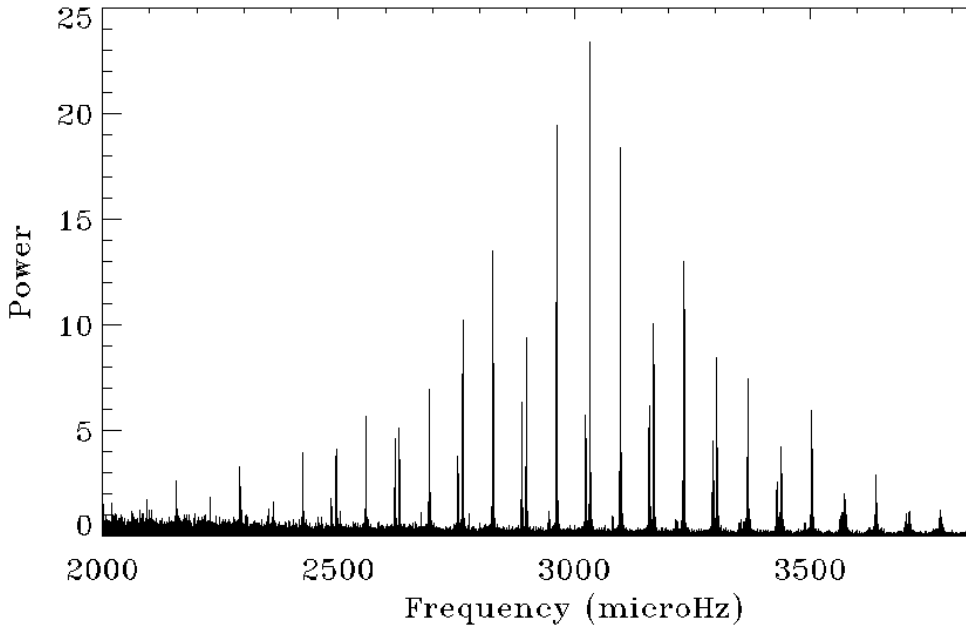

JCD

Observed frequencies

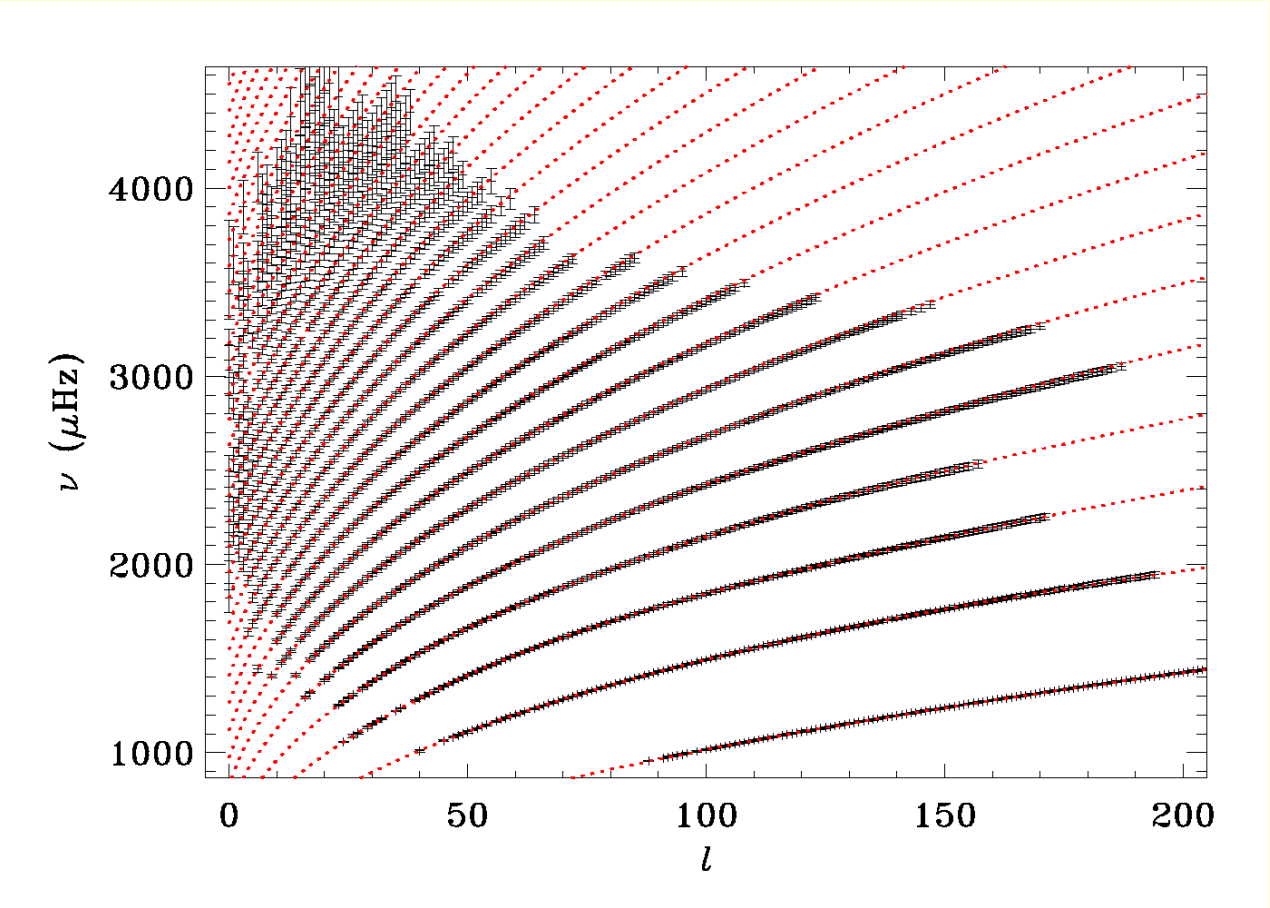

m-averaged frequencies from MDI instrument on SOHO

1000 σ error bars

JCD

The solar internal sound speed

Sun - model

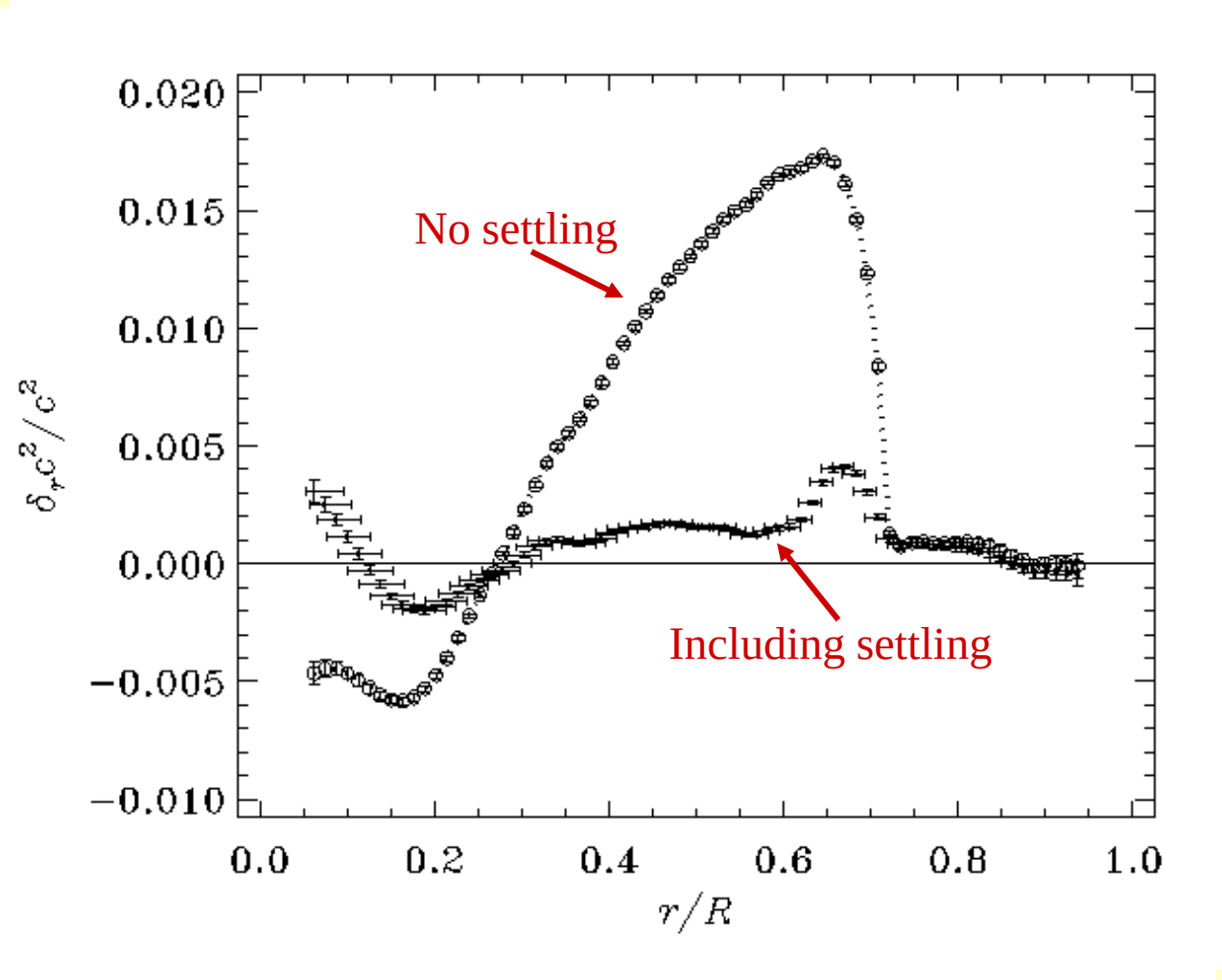

JCD

Changes in composition

The evolution of stars is controlled by the changes in their interior composition:

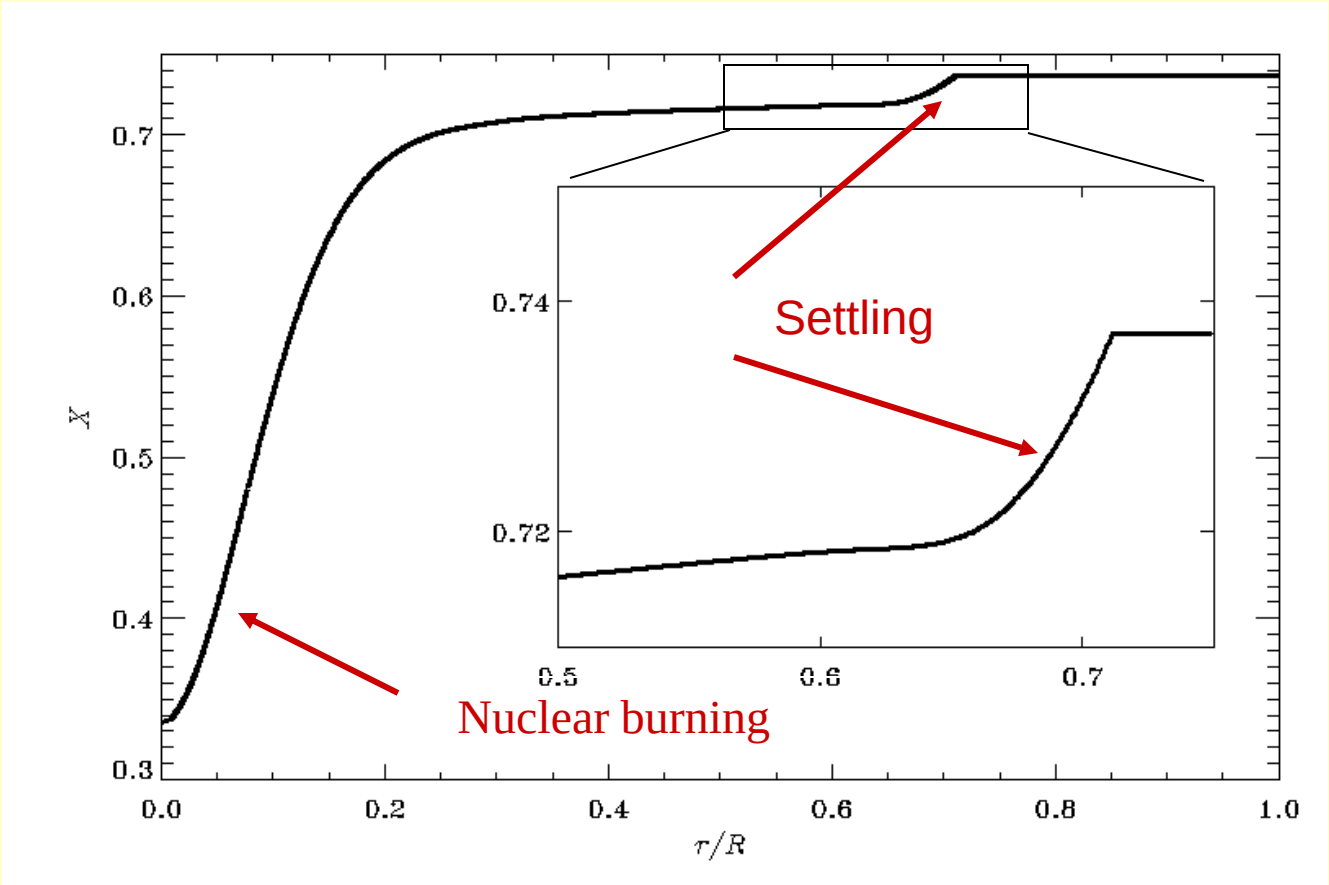

JCD

New solar composition

Asplund, Grevesse, Sauval, **"The solar chemical composition",**

2005, in "Cosmic Abundances as Records of Stellar Evolution and Nucleosynthesis",

ASP Conf. Ser., Vol. 336, p. 25 (astro-ph/0410214).

The main characteristics of the new data are :

* LARGE **DECREASE by 40 to 60 % of the abundances of C, N, O and Ne, Ar**

* SMALLER **DECREASE by 12 to 25 % of the abundances of Na, Mg, Al, P, S, K, Ca and Fe**

This means that **at fixed Z** value which is determined mainly by the C, N, O abundances,

the abundance of Fe-group elements INCREASES by approximately 20 percents.

* LARGE **DECREASE of the „metallicity", Z=0.0122, and of Z/X=0.0165**

(i.e., approximately, **X=0.74, Y=248, Z=0.012 for the Sun**).

Pamyatnykh, 2007, Goettingen

New solar chemical composition
(Asplund, Grevesse et al., 2004, 2005)

Element	GN93	A04
Hydrogen	1000	1000
Helium	98	84
Heavy elements	1.44	0.965

The new solar abundances ➔

X=0.7392, Y=02486, Z=0.0122

Z/X=0.0165 (old Z/X=0.0275)

These significant downward revisions result from:

*** the use of 3D hydrodynamical model of the solar atmosphere,**

*** non-LTE effects,**

*** the use of better atomic and molecular data.**

GN93 (old): Grevesse, Noels, 1993, in *„Origin and Evolution of the Elements”*.

A04 (new): Asplund, Grevesse, Sauval et al., 2004, A&A, 417, 751

Pamyatnykh, 2007, Goettingen

Revision of solar abundances

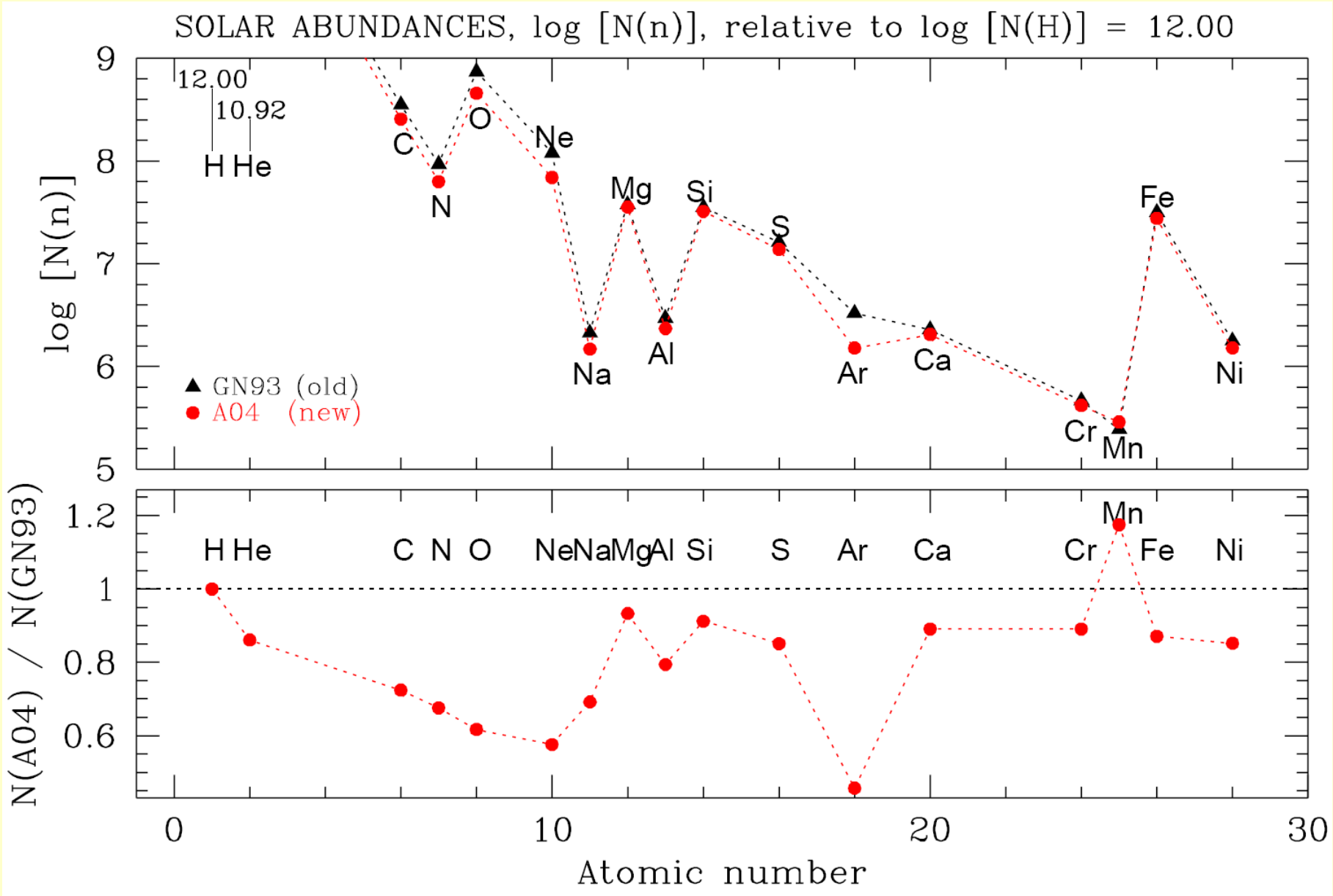

Pamyatnykh, 2007, Goettingen

Revision of solar abundances

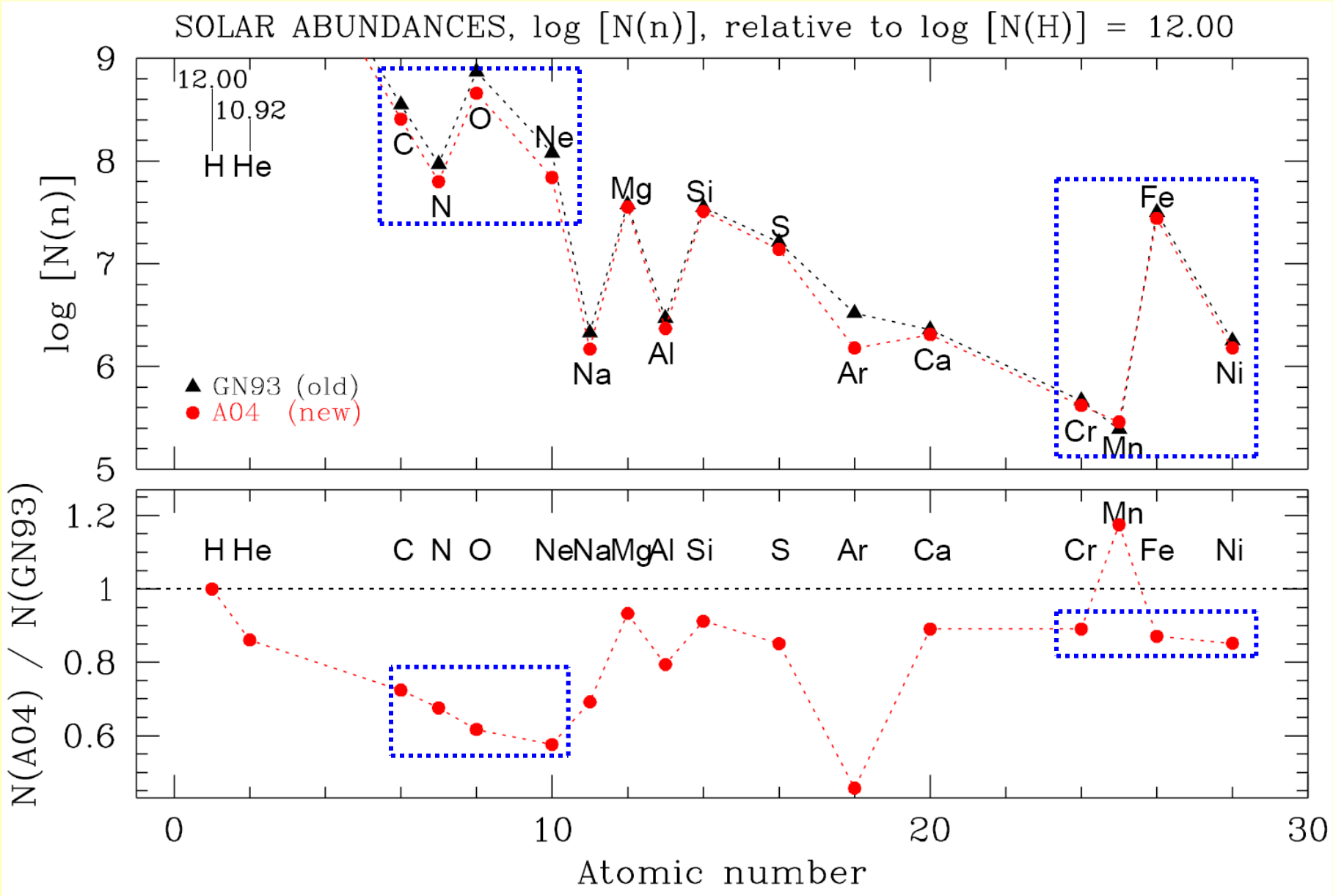

Pamyatnykh, 2007, Goettingen

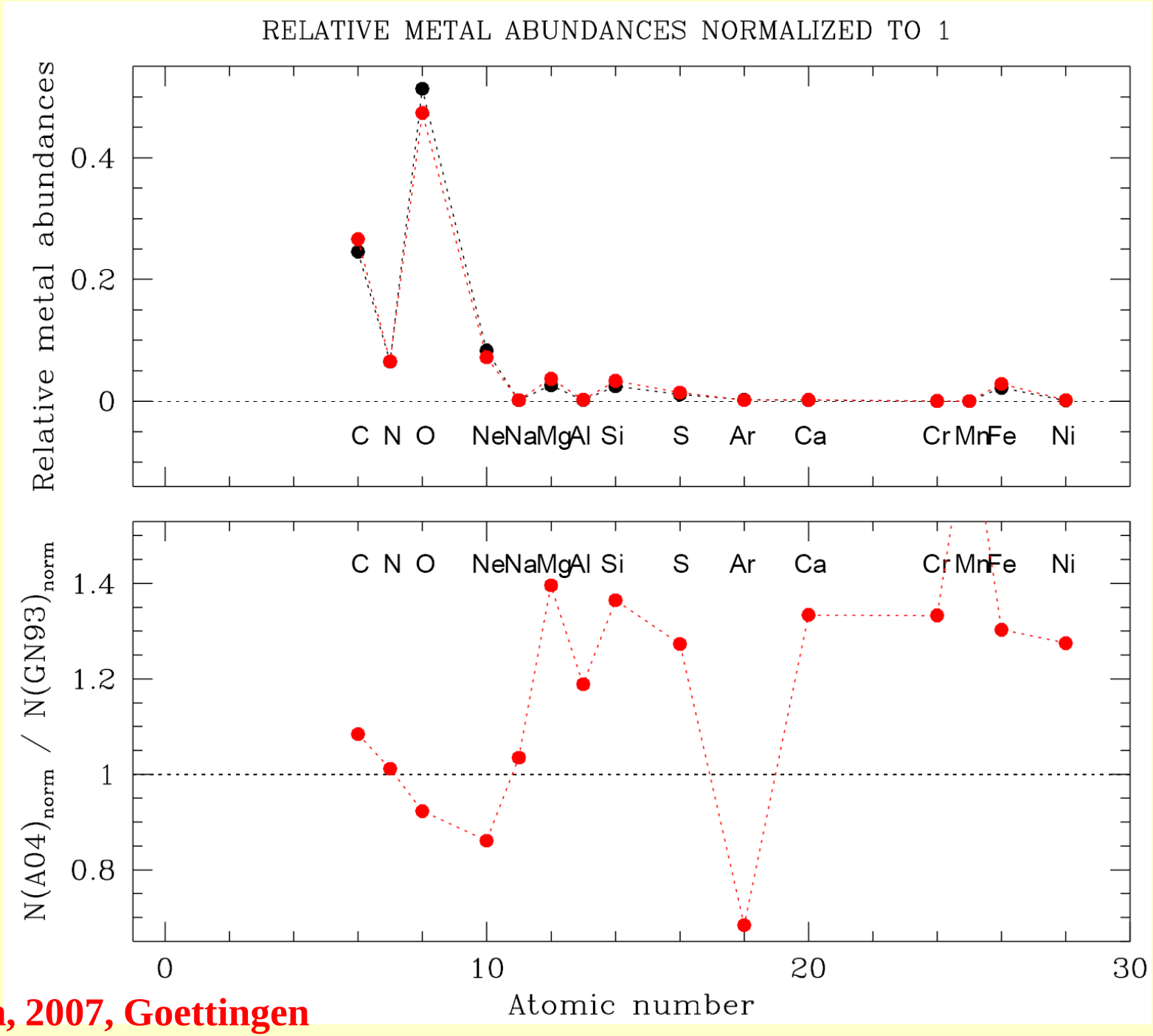

Pamyatnykh, 2007, Goettingen

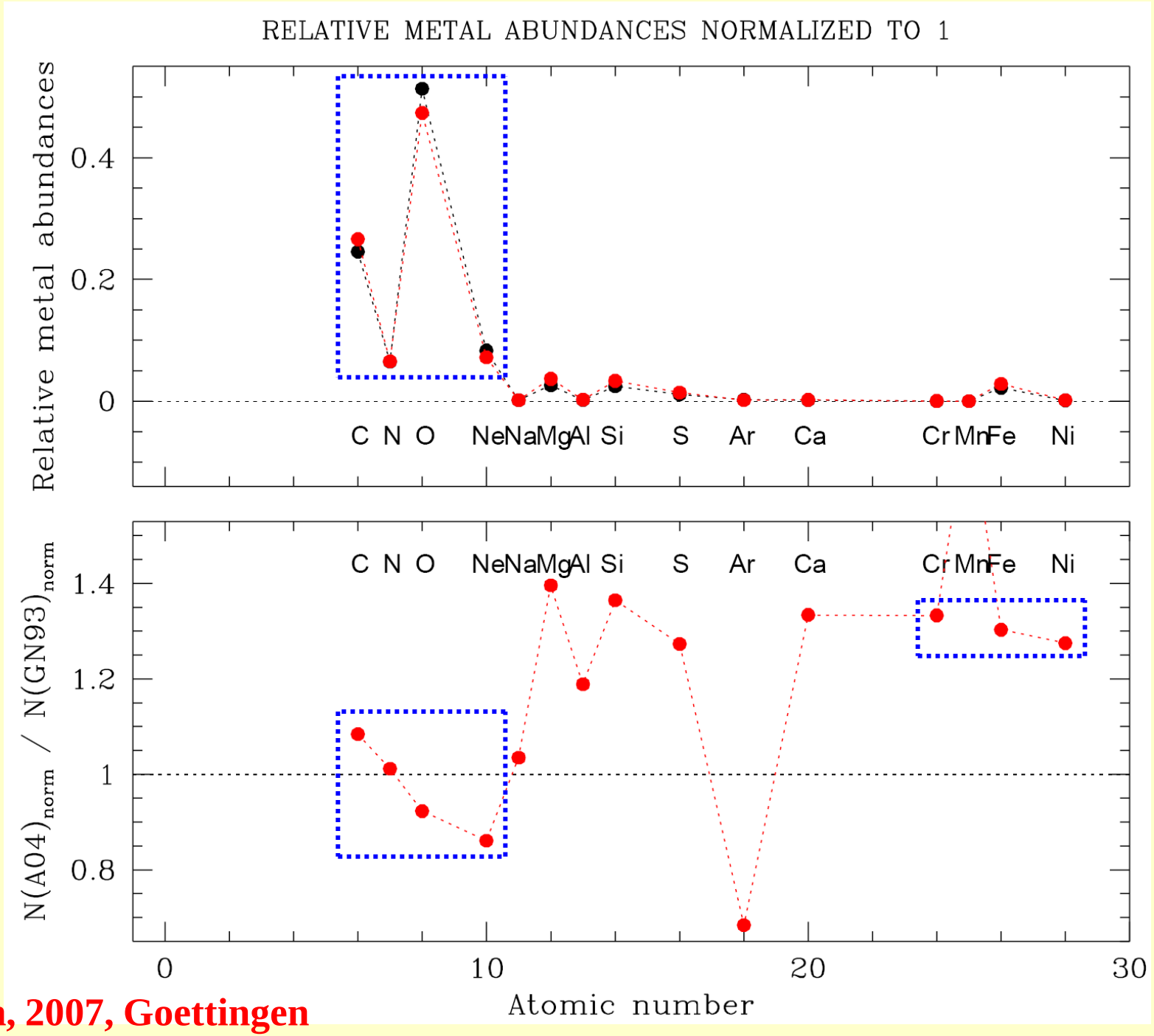

Pamyatnykh, 2007, Goettingen

Helioseismology:

R(bottom)/R = 0.713 +- 0.001
Y(surface) = 0.249 +- 0.003

κ OP, new abundances (Asplund et al. 2005):

R(bottom)/R = 0.728
(differs by 15 errors from Helioseismology)

Y(surface) = 0.229
(differs by 6.7 errors from Helioseismology)

Bahcall J. N., Serenelli A. M., Basu S., 2005, Ap J, 621, L85

Relative sound speed differences and relative density differences between solar models and helioseismological results

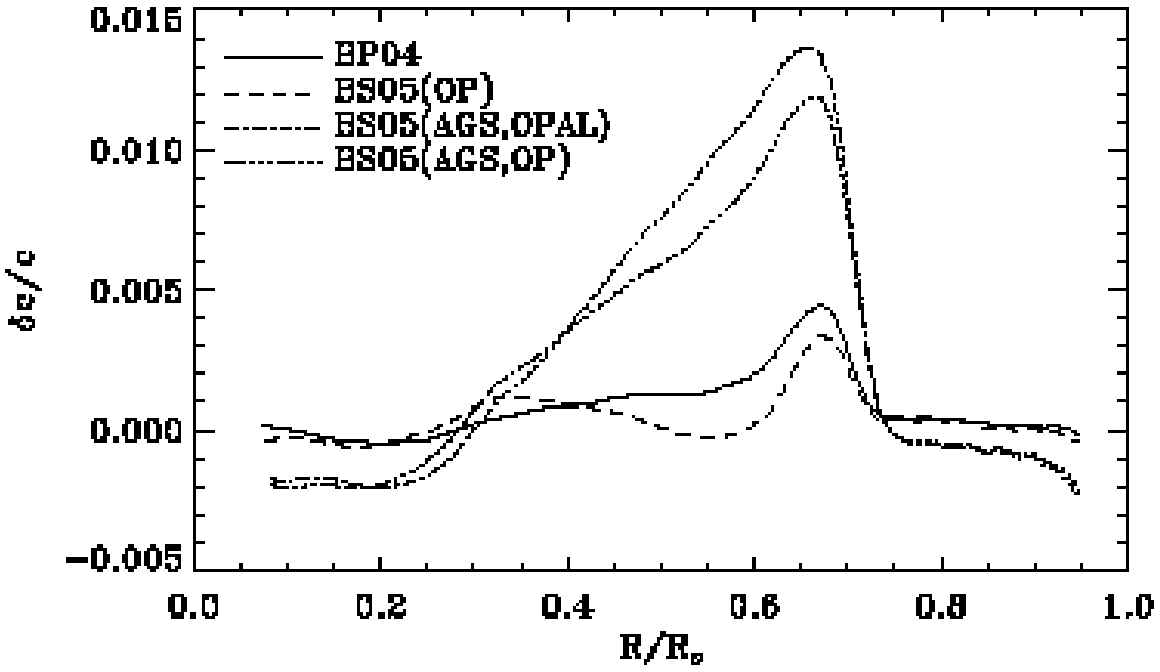

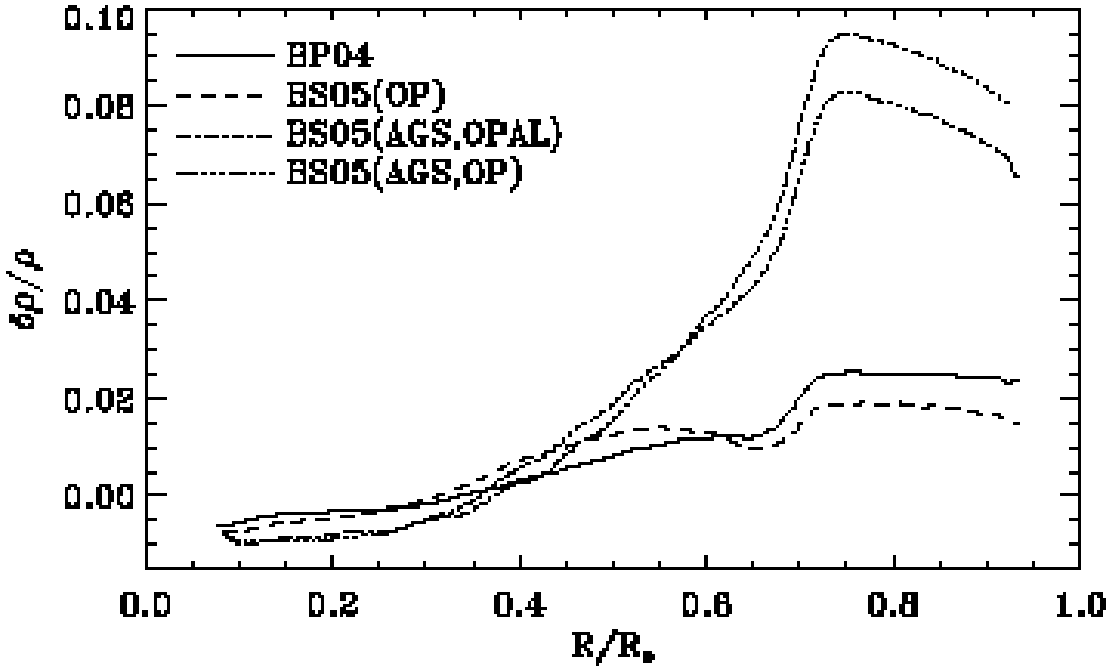

Bahcall J. N. et al. 2005

Revision of solar surface abundances

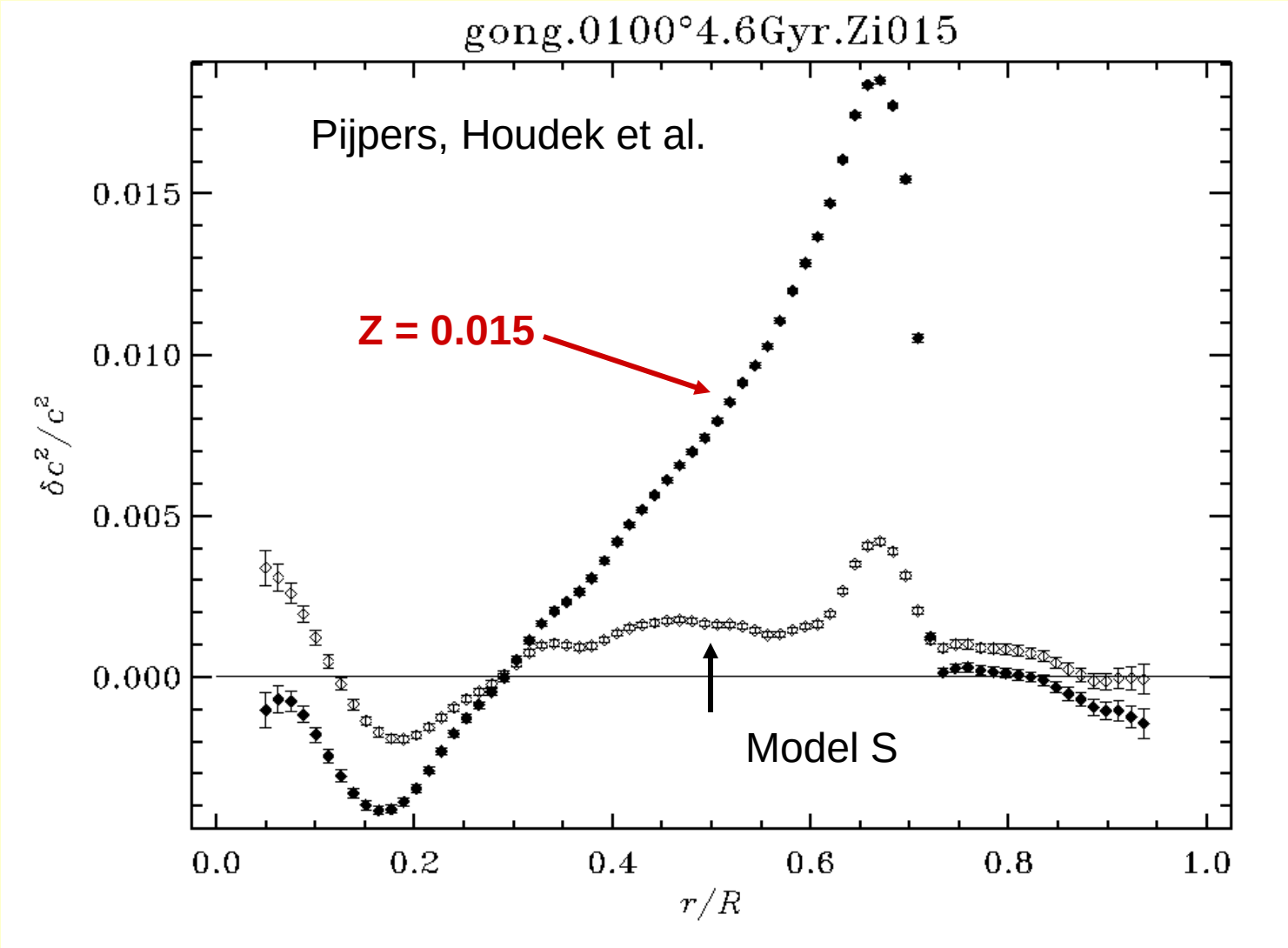

JCD

How do we correct the models?

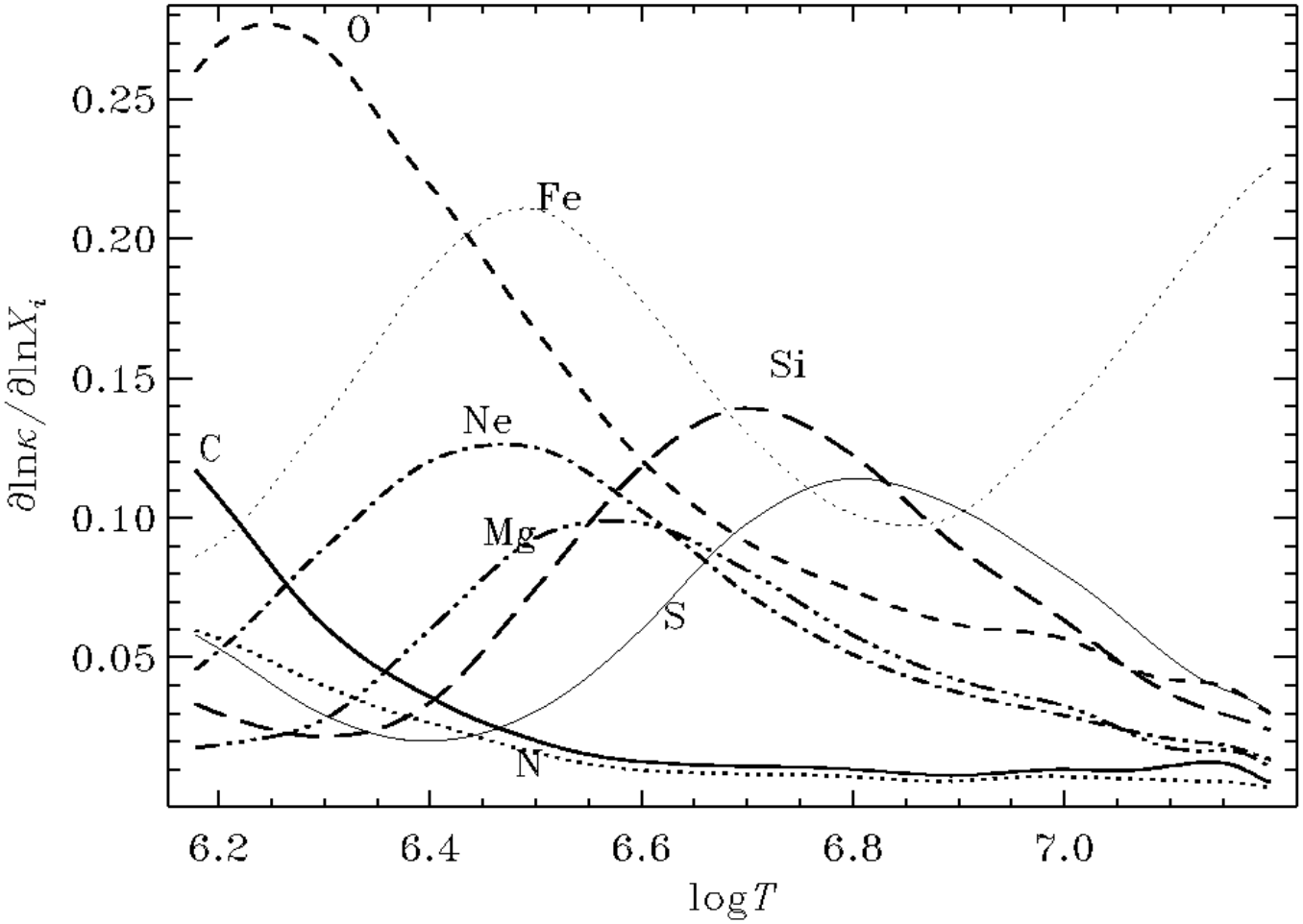

JCD

The neon story

Ne x 2.5

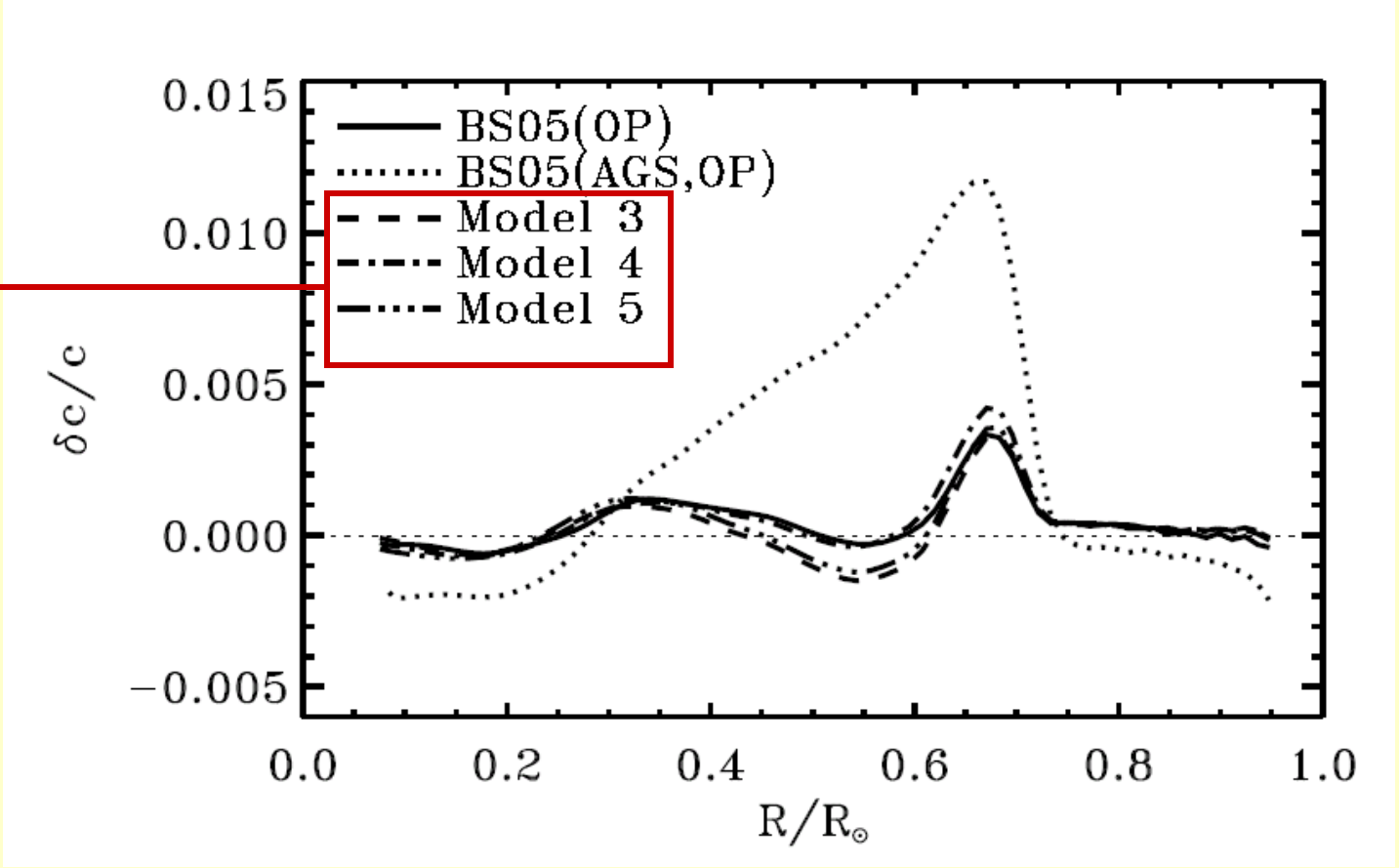

Bahcall et al. (2005; ApJ, in the press [astro-ph/0502563])

Drake & Testa (2005; Nature 436, 525): X-ray observations of nearby stars indicate such a neon increase

JCD

Internal solar rotation

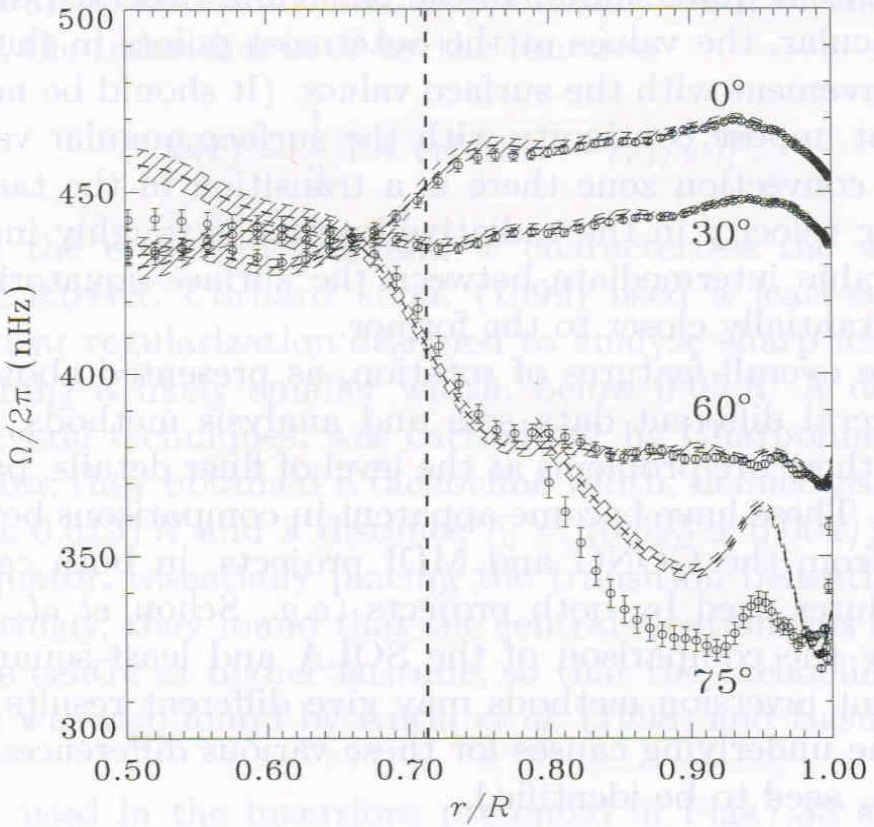

Fig. 7.35. Inferred rotation rate $\Omega/2\pi$ as a function of radius at the latitudes indicated, obtained from inversion of 144 d of MDI data. The circles with 1-σ error bars show results of a SOLA inversion, while the dashed lines with 1-σ error band were obtained with regularized least-squares inversion. The heavy vertical dashed line marks the base of the convection zone. Adapted from Schou *et al.* (1998).

Aerts, JCD, Kurtz, 2010, Asteroseismology

Streszczenie
(z krótkimi uzupełnieniami)
przeglądowego artykułu G. Handlera

Przeglądowy artykuł Geralda Handlera (38 stron)

Asteroseismology

Gerald Handler
Copernicus Astronomical Center, Bartycka 18, 00-716 Warsaw, Poland
Email: gerald@camk.edu.pl

arXiv:1205.6407v1 [astro-ph.SR] 29 May 2012

(Skany z artykułu G.Handlera, jeśli nie zaznaczono inaczej)

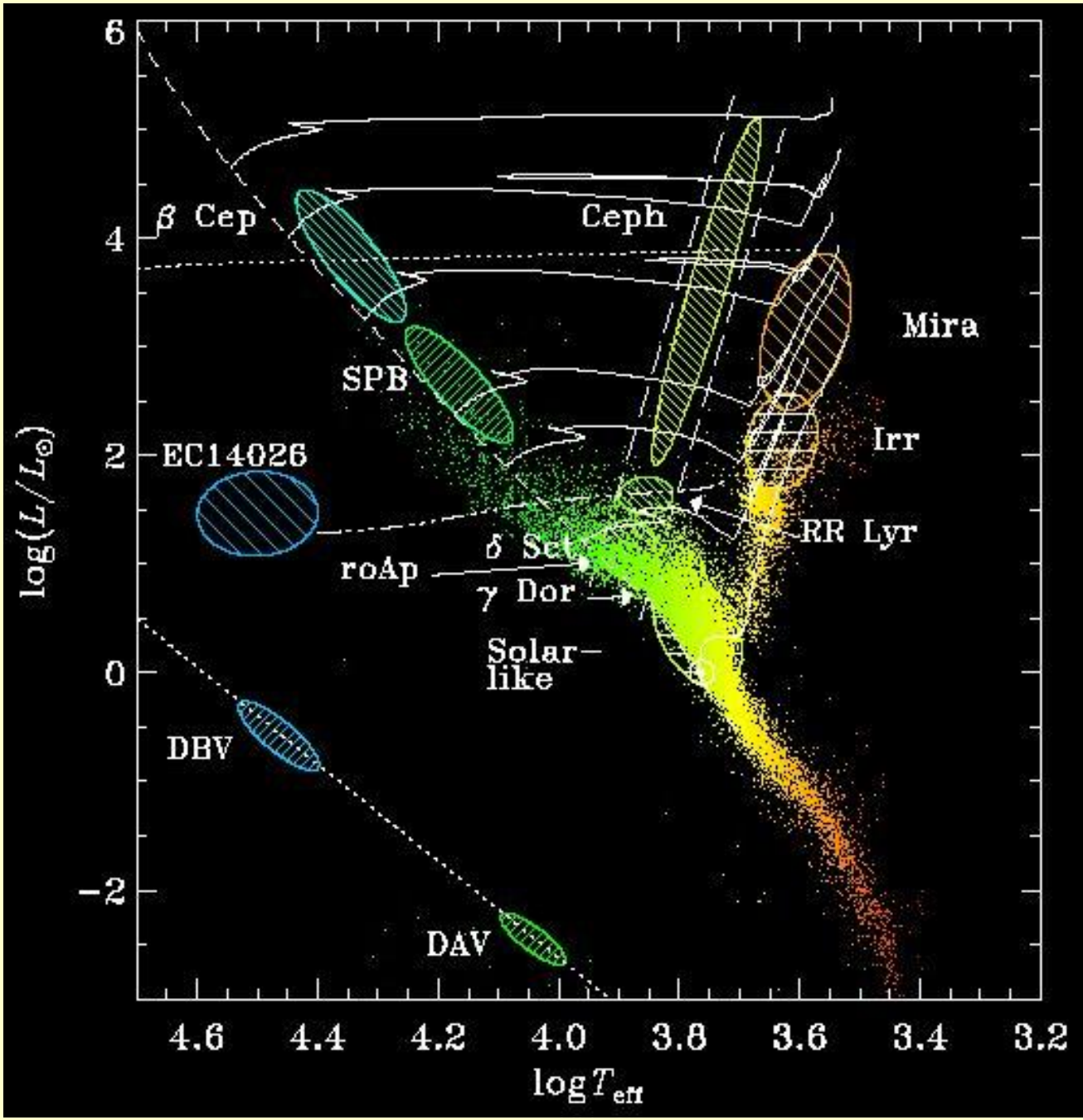

J. Christensen-Dalsgaard

Sprzed 40 lat i teraz

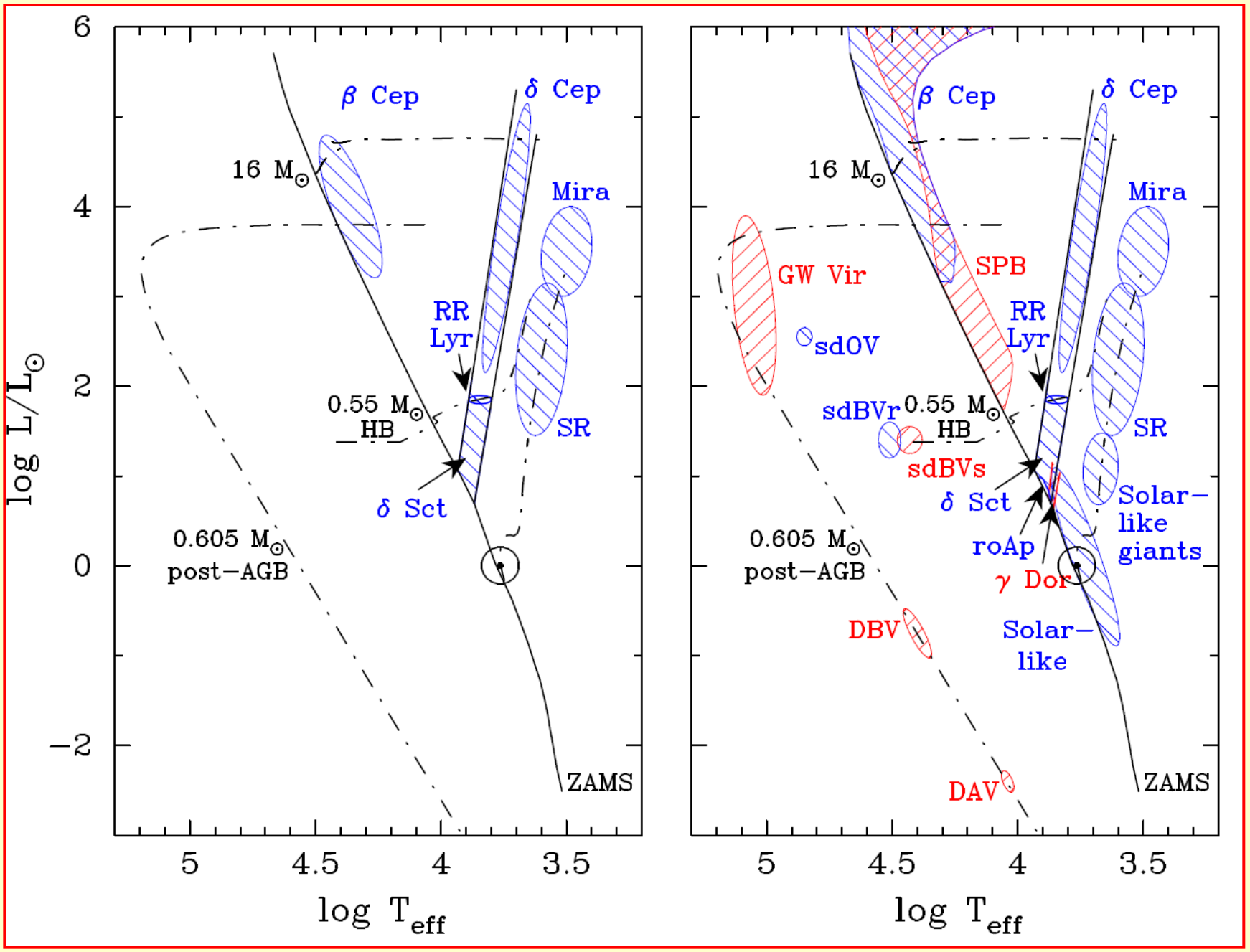

Otto Struve about 60 years ago

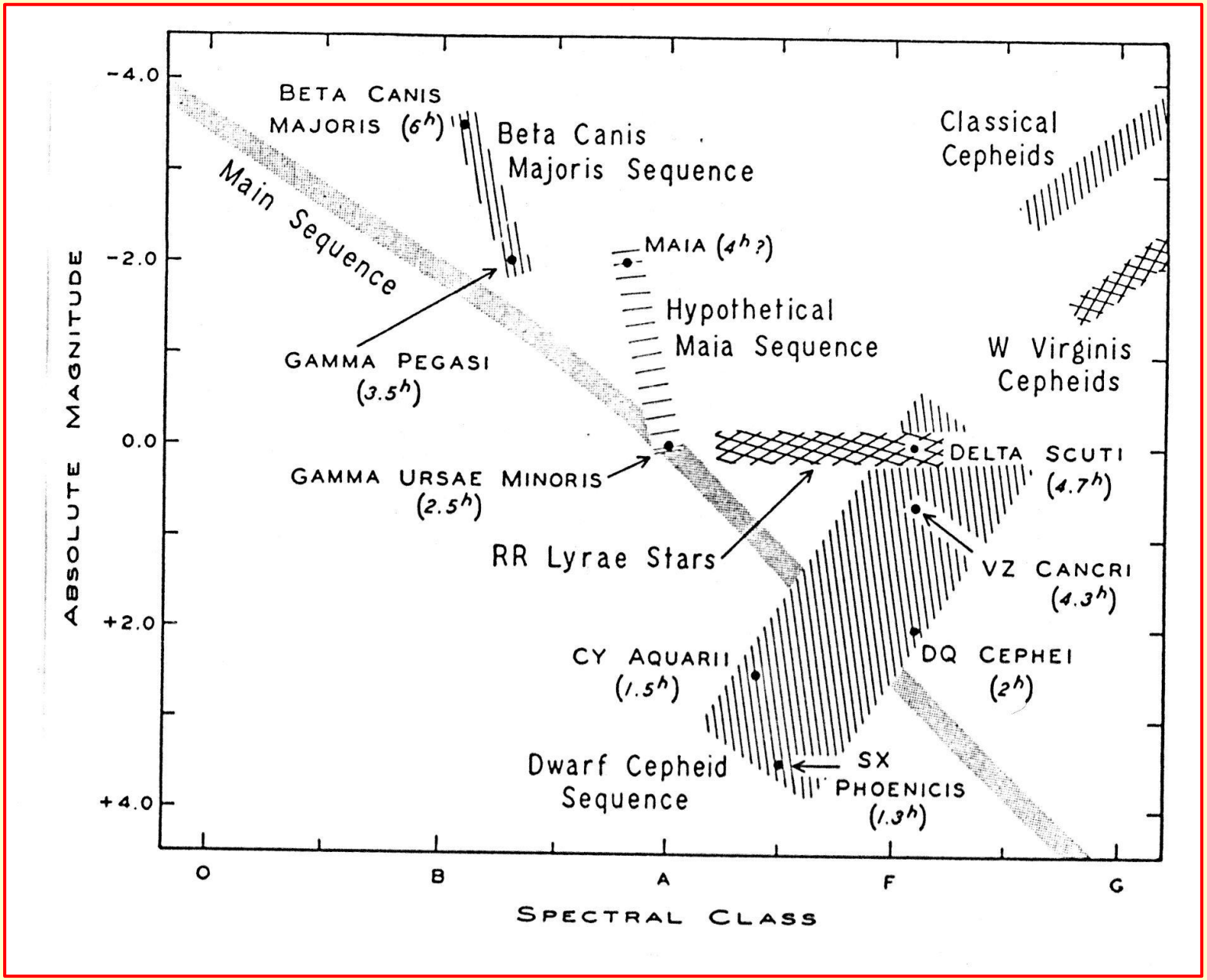

O. Struve, *Some unusual short-period variables.* Sky and Telescope, 1955, 14, 461.

Table 1: Selected classes of pulsating star

Name	Approx. Periods	Discovery/Definition
Mira variables	100 - 1000 d	Fabricius (1596)
Semiregular (SR) variables	20 - 2000 d	Herschel (1782)
δ Cephei stars	1 - 100 d	1784, Pigott, Goodricke (1786)
RR Lyrae stars	0.3 - 3 d	Fleming (1899)
δ Scuti stars	0.3 - 6 h	Campbell & Wright (1900)
β Cephei stars	2 - 7 h	Frost (1902)
ZZ Ceti stars (DAV)	2 - 20 min	1964, Landolt (1968)
GW Virginis stars (DOV)	5 - 25 min	McGraw et al. (1979)
Rapidly oscillating Ap (roAp) stars	5 - 25 min	1978, Kurtz (1982)
V777 Herculis stars (DBV)	5 - 20 min	Winget et al. (1982)
Slowly Pulsating B (SPB) stars	0.5 - 3 d	Waelkens & Rufener (1985)
Solar-like oscillators	3 - 15 min	Kjeldsen et al. (1995)
V361 Hydrae stars (sdBVr)	2 - 10 min	1994, Kilkenny et al. (1997)
γ Doradus stars	0.3 - 1.5 d	1995, Kaye et al. (1999)
Solar-like giant oscillators	1 - 18 hr	Frandsen et al. (2002)
V1093 Herculis stars (sdBVs)	1 - 2 hr	Green et al. (2003)
Pulsating subdwarf O star (sdOV)	1 - 2 min	Woudt et al. (2006)

Harmoniki sferyczne

Pulsation in *nonradial modes* causes deviations from spherical symmetry: the star changes its shape. Mathematically, this no longer results in an eigenvalue problem of the Sturm-Liouville type, and a large number of possible oscillation modes originates. The eigenfunctions are proportional to *spherical harmonics*:

$$Y_l^m(\theta,\phi) = N_l^m P_l^{|m|}(\cos\theta) e^{im\phi}, \tag{1}$$

where θ is the angle from the polar axis (colatitude), ϕ is the longitude, $P_l^{|m|}$ is the associated Legendre polynomial, N_l^m is a normalization constant and l and m are the spherical degree and azimuthal order of the oscillation. With

$$P_l^m(x) = (-1)^m (1-x^2)^{m/2} \frac{d^m}{dx^m} P_l(x) \tag{2}$$

we obtain

$$P_0^0(\cos\theta) = 1 \tag{3}$$

$$P_1^0(\cos\theta) = \cos\theta \qquad P_1^1(\cos\theta) = -\sin\theta \tag{4}$$

$$P_2^0(\cos\theta) = \frac{1}{2}(3\cos^2\theta - 1) \qquad P_2^1(\cos\theta) = -3\cos\theta\sin\theta \qquad P_2^2(\cos\theta) = 3\sin^2\theta \tag{5}$$

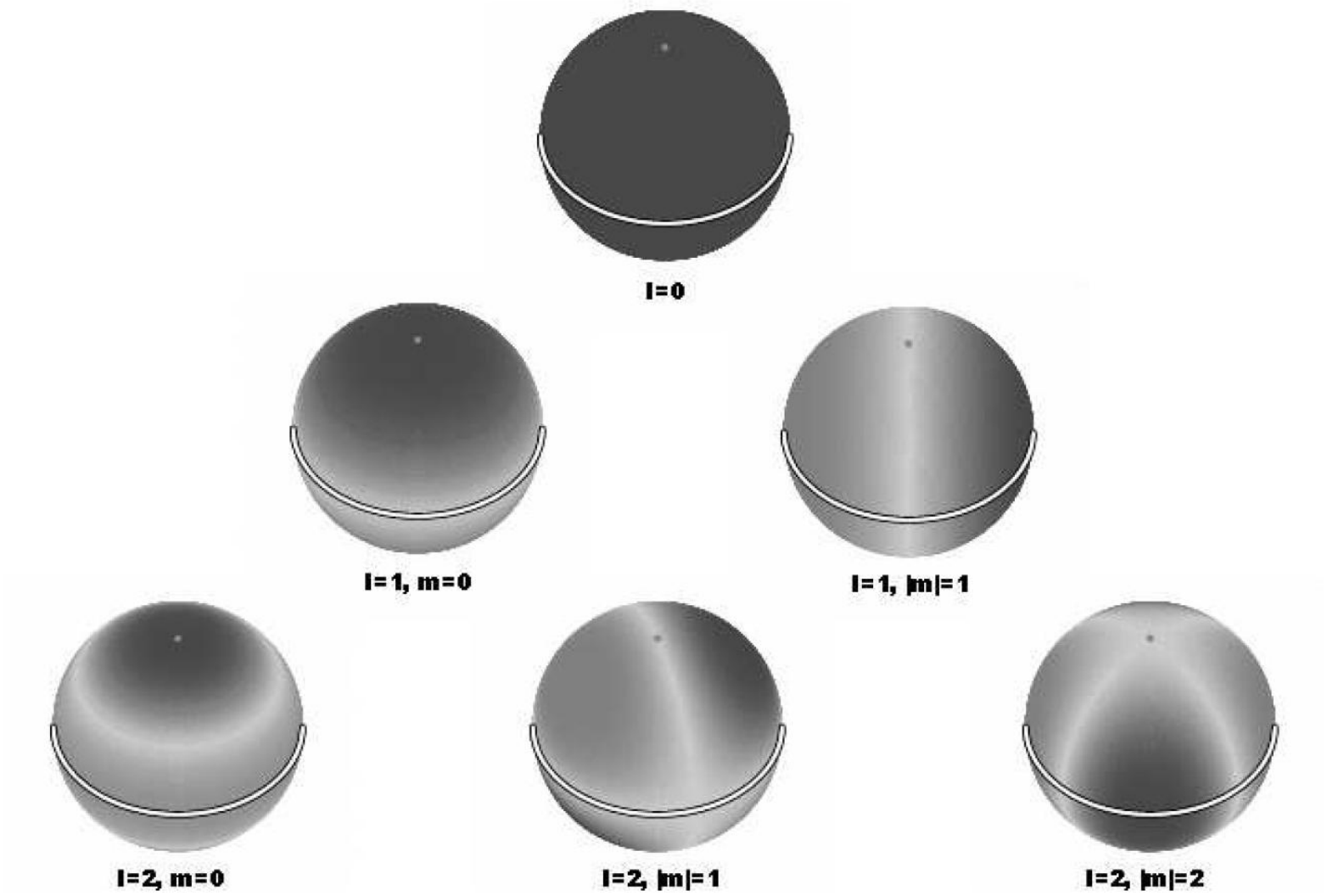

Figure 2: Schematic description of the surface distortions produced by pulsation modes with spherical degrees $0 \leq l \leq 2$, arranged in the same way as the previous expressions for the associated Legendre polynomials. Whilst the outward moving areas of the star are coloured in dark grey, the light grey areas move inward, and vice versa. The pole and equator of the star are indicated. Adapted from Telting & Schrijvers (1997).

Lokalne charakterystyczne częstotliwości wewnątrz gwiazdy

The propagation of pulsation modes in the stellar interior is governed by two frequencies. One of these is the *Lamb frequency* L_l, which is the inverse of the time needed to travel one horizontal wavelength at local sound speed. The other frequency describes at what rate a bubble of gas oscillates vertically around its equilibrium position at any given position inside a star; it is called the *Brunt-Vaisälä* frequency N. These two quantities are defined as:

$$L_l^2 = \frac{l(l+1)c^2}{r^2} \qquad N^2 = g\left(\frac{1}{p_0\gamma_1}\frac{dp_0}{dr} - \frac{1}{\rho_0}\frac{d\rho_0}{dr}\right), \tag{6}$$

where l is the spherical degree, c is the local velocity of sound, r is the radius, g is the local gravitational acceleration, p_0 and ρ_0 are local pressure and density in the unperturbed state, respectively, and $\gamma_1 = (\rho dp/pd\rho)_{\rm ad}$ is the first adiabatic exponent.

Diagram propagacji oscylacji wzdłuż promienia

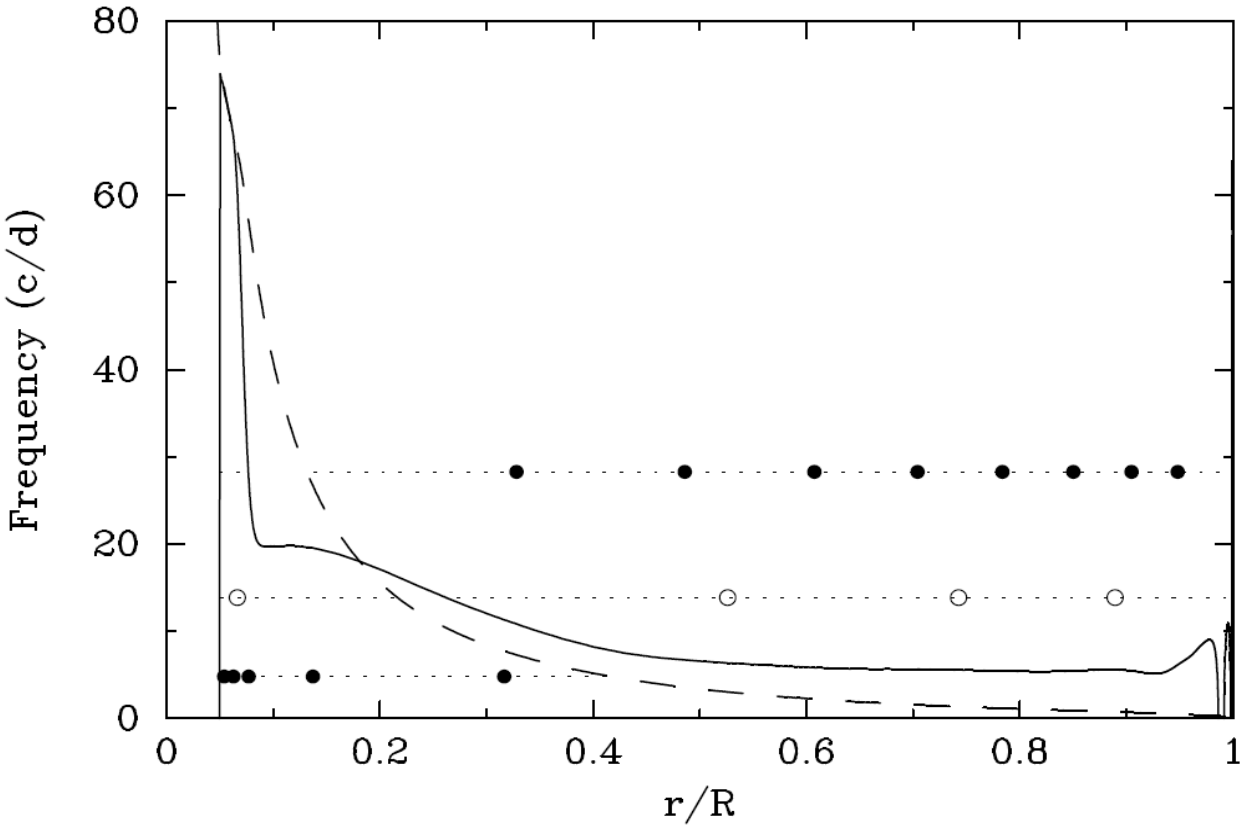

Figure 3: A propagation diagram for an evolved 2 $M_\odot$ stellar model. The run of the Lamb (dashed line) and Brunt-Vaisälä (full line) frequencies with respect to fractional stellar radius is shown. Some stellar pulsation modes are indicated with thin horizontal dashed lines, the circles are interior nodes. The lowest frequency oscillation (lowest dashed line) shown is a g_5 mode; that with the highest frequency is a p_8 mode. The oscillation with intermediate frequency is a mixed mode. Data kindly supplied by Patrick Lenz.

Ewolucja widma częstotliwości oscylacji od ZAMS ku TAMS

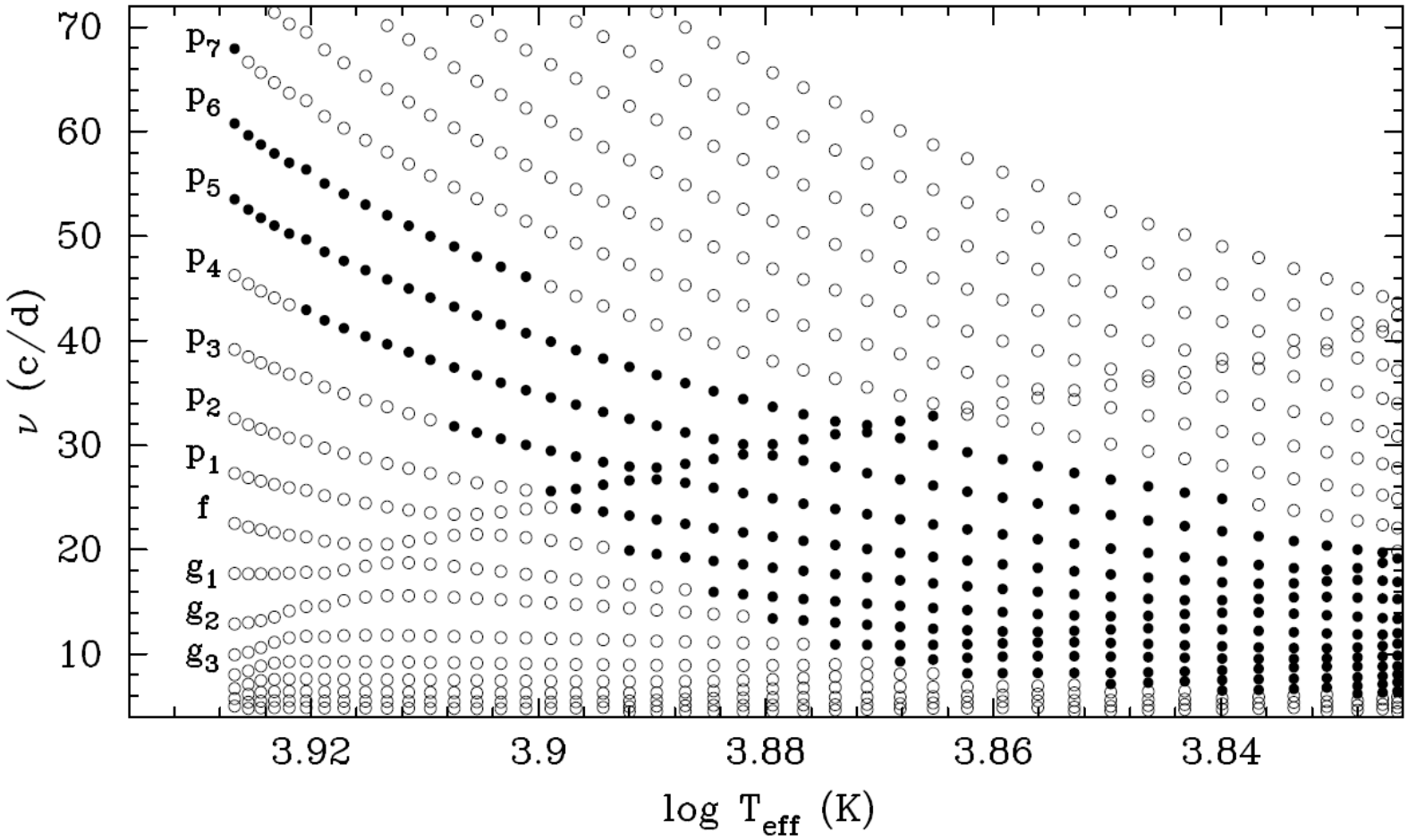

Figure 4: Theoretically predicted $l = 2$ oscillation spectra of a $1.8\,M_\odot$ main sequence model, evolving from hotter to cooler effective temperature. Pulsation modes excited in this model are shown with filled circles, stable modes with open circles. The types of mode on the Zero-Age Main Sequence (ZAMS) are given. Note the g modes intruding into the p mode domain.

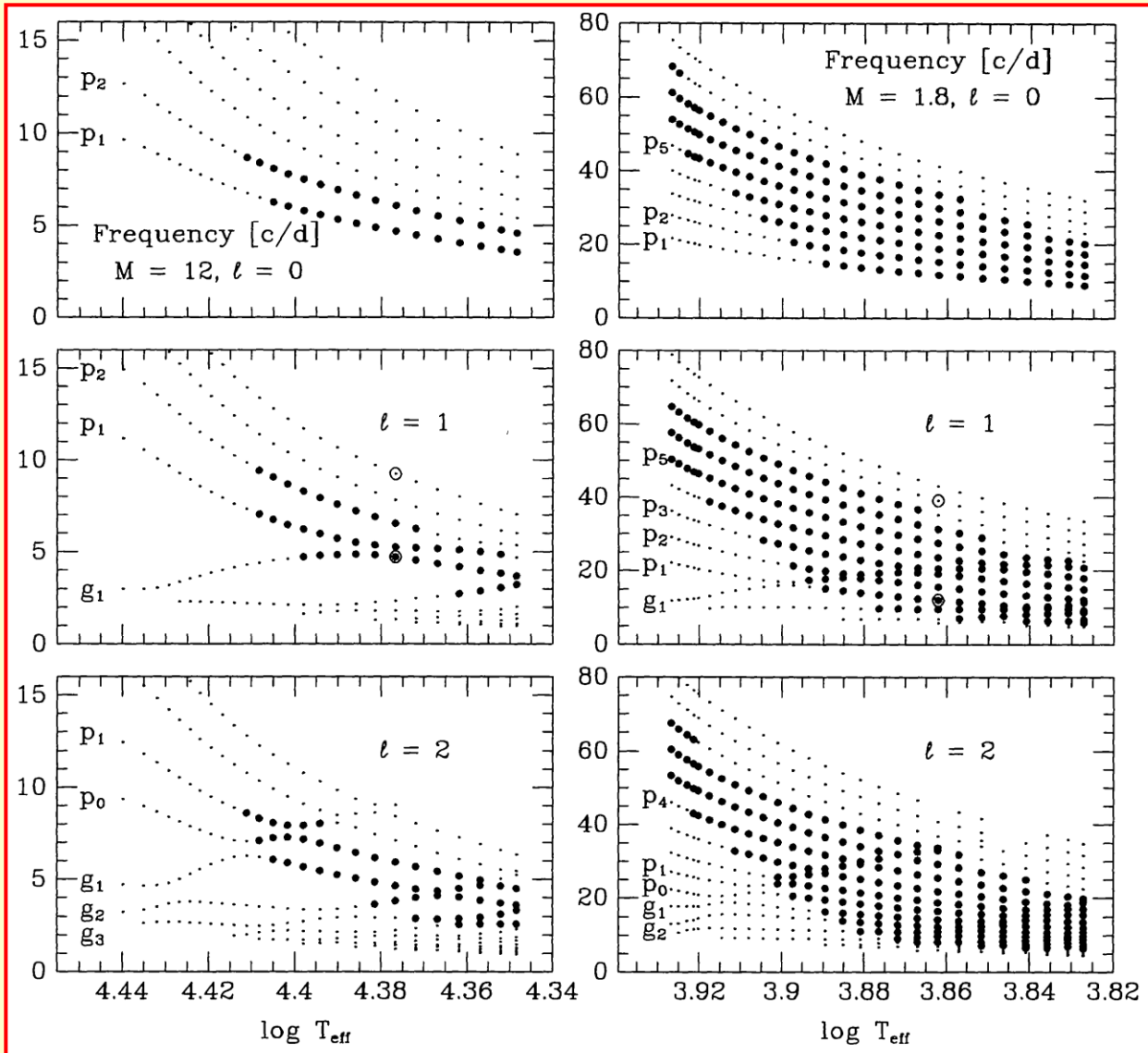

Figure 1. Frequencies of low-order p- and g-modes with low degree, ℓ, for models of 12 and 1.8 $M_\odot$ in the Main Sequence evolutionary phase. In each panel, the leftmost and rightmost points correspond to the ZAMS and TAMS models, respectively. The large dots mark unstable modes. The large open circles in the $\ell = 1$ panels mark modes which are shown in Fig. 2.

Pamyatnykh 2000

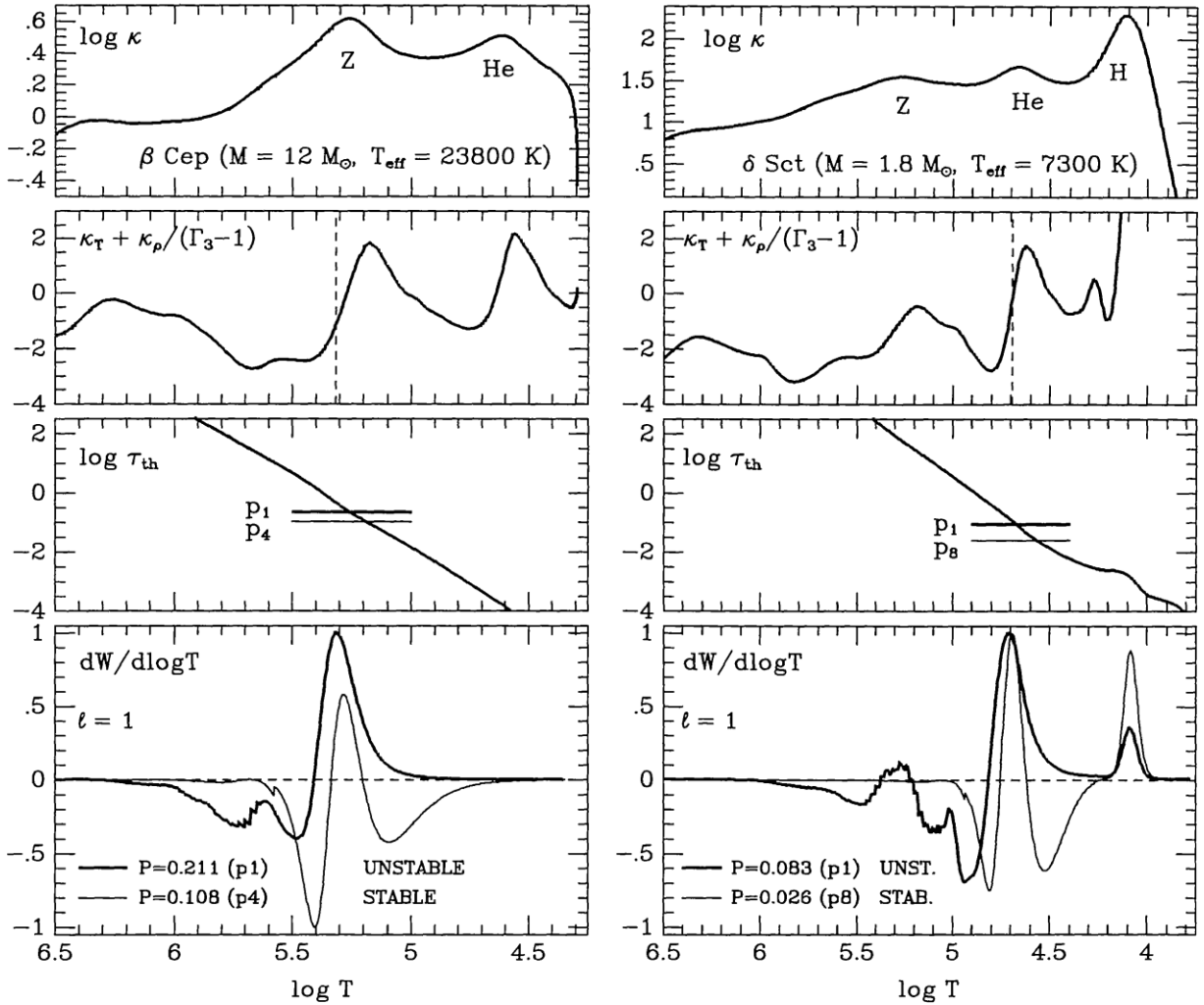

Figure 2. Opacity, κ, opacity derivative, $\kappa_T + \kappa_\rho/(\Gamma_3 - 1)$, thermal timescale, $\tau_{\rm th}$ (in days), and differential work integral, $dW/d\log T$ (arbitrary units, positive in driving zones), for selected pulsation modes (ℓ=1), plotted versus temperature for representative models of β Cephei (left) and δ Scuti (right) variables. The dashed vertical lines mark the position of the maximum driving for the unstable modes shown in the lower panels. The horizontal lines in the $\tau_{\rm th}$ diagrams correspond to the periods of selected modes.

Pamyatnykh 2000

Mode trapping in the post-MS model of 44 Tau

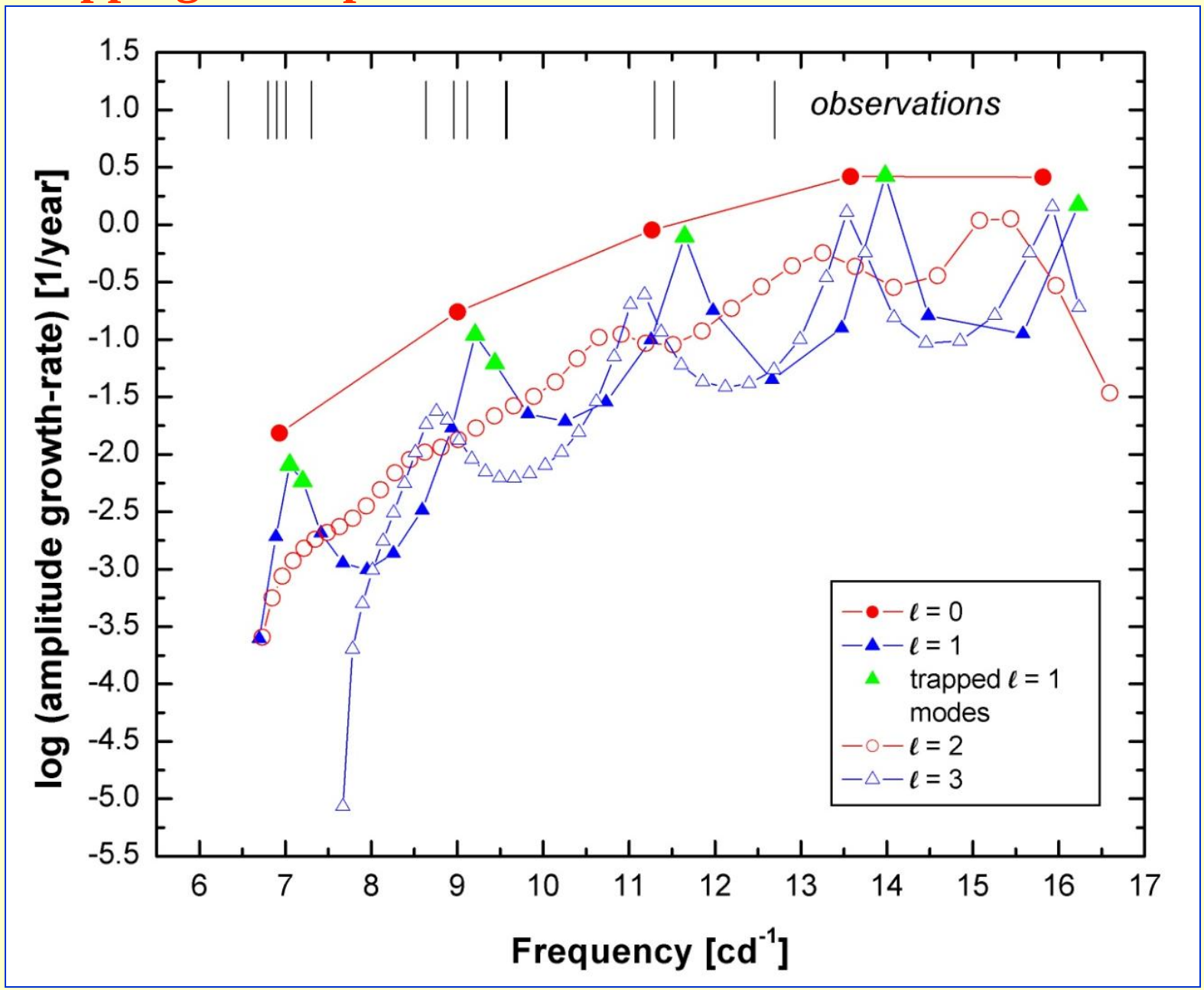

Lenz et al. 2008

Propagation diagrams for l = 1, 2, 3 modes

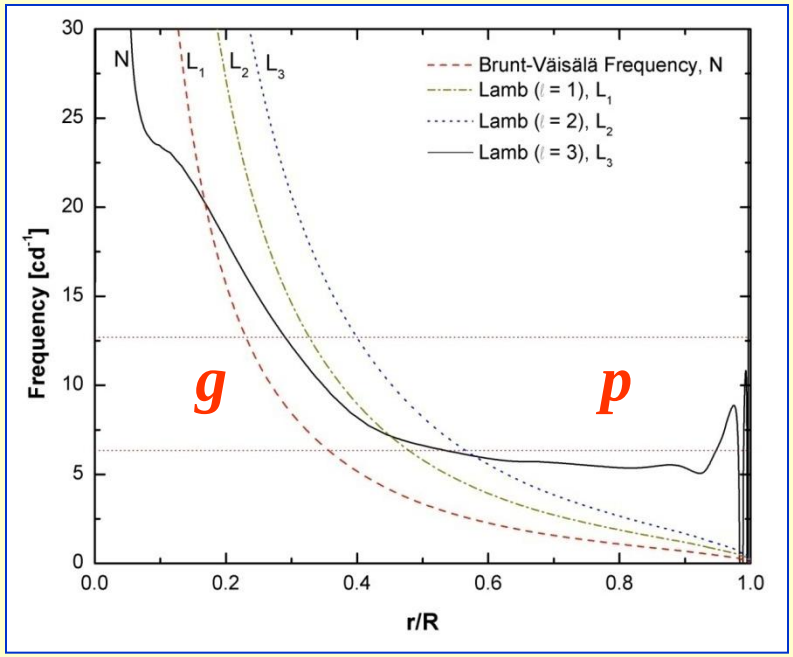

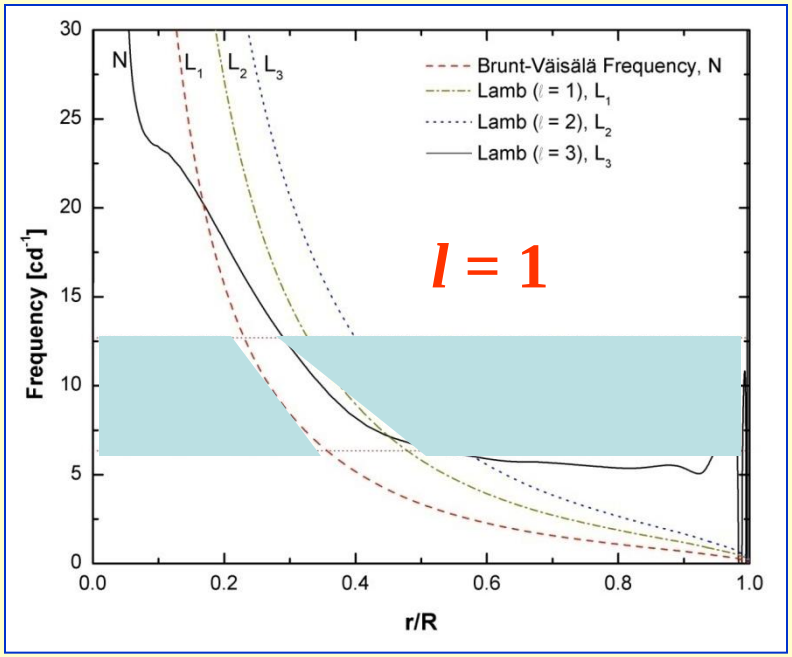

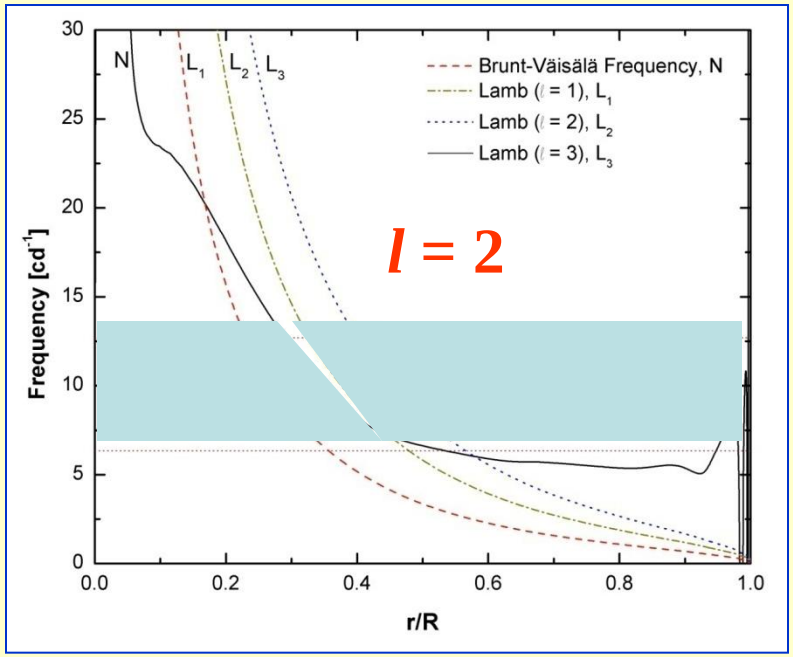

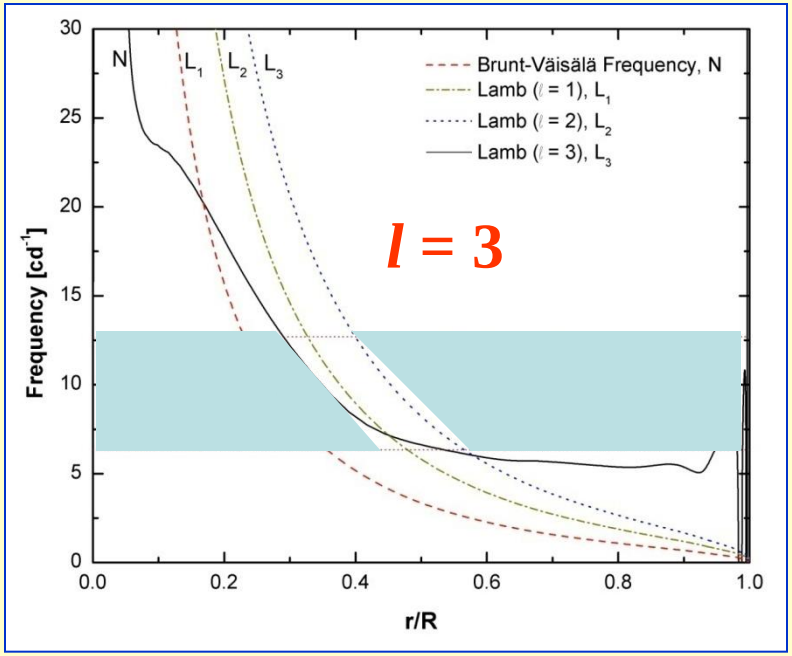

Asymptotyka wysokich owertonów p- i g-modow.

p-mody są równoodstępne w częstoliwości, g-mody – w okresach.

The frequencies of the p and g modes of pulsating stars depend strongly on their structure. However, when high radial overtones are considered, some simple relations between mode frequencies emerge. These are derived from *asymptotic theory*. The classical reference on the subject is Tassoul (1980), the instructive is Gough (1986). In the high-overtone limit one finds

$$\omega_{n,l} \simeq \Delta\omega_0 \left(n + \frac{l}{2} + \epsilon \right) - D_0 l(l+1) \tag{7}$$

for p modes, whereas for g modes

$$P_{n,l} \simeq \frac{P_0(n+\delta)}{\sqrt{l(l+1)}}, \tag{8}$$

where $\Delta\omega_0$ is the inverse sound travel time through the centre of the star, D_0 is a frequency separation dependent on the stellar evolutionary state, P_0 is the asymptotic period that is proportional to the integral of the Brunt-Vaisälä frequency throughout the star, l and n are the spherical degree and radial overtone, respectively, and ϵ and δ are stellar structure parameters, respectively.

Rotacyjne rozszczepienie częstotliwości oscylacji

In a nonrotating star, the frequencies of modes with $m \neq 0$ are the same as those of the $m = 0$ modes. However, as the $m \neq 0$ modes are travelling waves, their frequencies separate in the observer's frame when looking at a rotating star: the mode moving with rotation appears at higher frequency, the mode moving against rotation appears at lower frequency and the frequency difference to their nonrotating value is m times the rotation frequency (e.g., see Cox 1984). This effect is called *rotational frequency splitting*, and is one basic tool of asteroseismology: if such splittings are observed, the rotation frequency of the star can be determined.

Unfortunately, reality is not quite as simple as that. The Coriolis force acts on the travelling waves and modifies their frequencies. In addition, the $m \neq 0$ modes cause tidal bulges, on which centrifugal forces act. Therefore, the frequencies of these modes are often expressed as

$$\omega_{k,l,m} = \omega_{k,l,0} + m(1 - C_{k,l})\Omega + m^2 \frac{D_{k,l}\Omega^2}{\omega} \qquad (9)$$

in case of (moderately) slow stellar rotation (Dziembowski & Goode 1992). $\omega_{k,l,m}$ is the observed frequency of the mode k, l, m, Ω is the stellar rotation frequency, and $C_{k,l}$ and $D_{k,l}$ are constants that describe the effects of the Coriolis and centrifugal forces, respectively; they are also called Ledoux constants. These constants are usually determined from stellar model calculations. The rotational splitting constant $C_{k,l}$ also approaches asymptotic values for high radial overtones. For g modes, $C_{k,l}$ becomes $(l(l+1))^{-1}$, and for p modes $C_{k,l} = 0$ in the asymptotic limit.

Regularities in theoretical frequency spectra:

- high-order p-modes:

$$\nu_{nl} \approx \Delta\nu \cdot \left(n + \frac{l}{2} + \alpha\right) - \frac{l(l+1)}{4\pi^2 n} \cdot f_c$$

$$\Delta\nu = \left(2\int \frac{dr}{c}\right)^{-1}, \quad f_c = \int \frac{dc}{dr} \cdot \frac{dr}{r}$$

large separation:

$$\nu_{nl} - \nu_{n-1,l} \approx \Delta\nu$$

small separation:

$$\nu_{nl} - \nu_{n-1,l+2} = \delta\nu_{nl} \approx -\frac{4l+6}{4\pi^2 n} \cdot f_c$$

- high-order g-modes:

$$\Pi_{nl} \approx \frac{n}{\sqrt{l(l+1)}} \cdot \Delta\Pi, \quad \Delta\Pi = 2\pi^2 \left(\int \frac{N}{r}\, dr\right)^{-1}$$

$$N = g\left(\frac{1}{\Gamma_1}\frac{d\ln P}{dr} - \frac{d\ln \rho}{dr}\right)$$

- Rotational splitting: (~ Goupil et al. 2000)

$$\nu_m = \nu_0 + m\left(1 - C_{nl}\right)\frac{\Omega}{2\pi} + \frac{\Omega^2}{2\pi\nu_0}\left(D_0 + m^2 D_1\right) + m\frac{\Omega^3}{\nu_0^2}T$$

$$\Rightarrow \frac{\nu_m - \nu_{m=0}}{m} = \frac{\Omega}{2\pi}\left(1 - C_{nl} + m\mu D_1 + \mu^2 T\right)$$

$$\mu = \frac{\Omega}{\nu_0}$$

- rotation rate:

$$\frac{\nu_m - \nu_{-m}}{2m} = \Omega\left(1 - C_{nl} + \mu^2 T\right)$$

- Effective gravity:

$$g_{eff} = g - \frac{2}{3}\Omega^2 r$$

- Ledoux constant:

$$C_{nl} = \frac{\int (2yz + z^2)\rho r^4 dr}{\int (y^2 + \Lambda z^2)\rho r^4 dr} \qquad \Lambda = l(l+1)$$

y, z – radial and horizontal components of displacement

$C_{nl} \ll 1$ for high-order p-modes $(y \gg z)$

$C_{nl} \simeq \frac{1}{l(l+1)}$ for g-modes $(z \gg y)$

$C \sim \frac{1}{2}$ for gravity modes of $l = 1$

Oscylacyjne zmiany blasku i odpowiednie widmo oscylacji

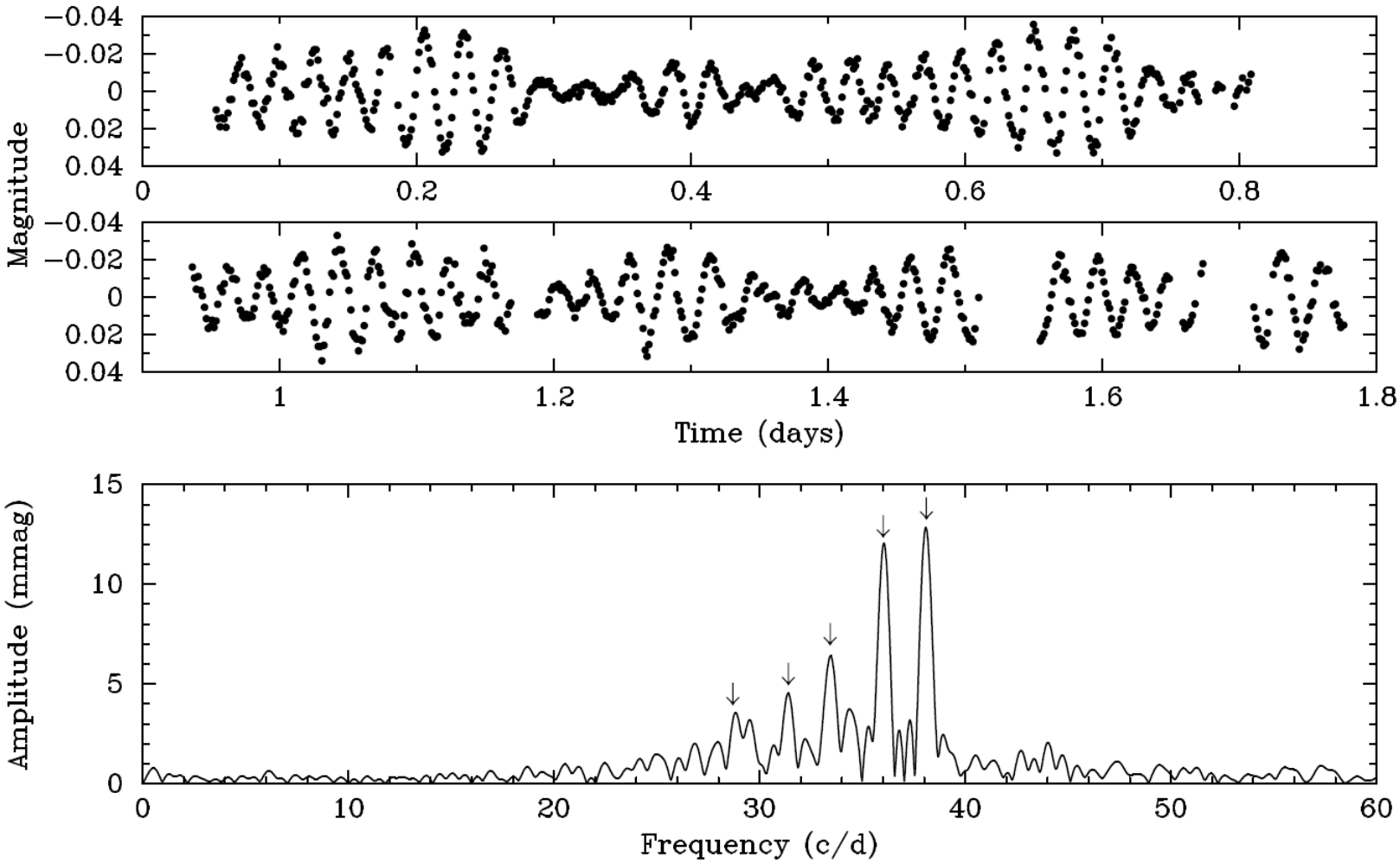

Figure 5: The light variations (upper two panels) of a pulsating star and the corresponding Fourier amplitude spectrum. The complicated beating in the light curve is reflected by the presence of several signals in the periodogram; the strongest are labelled with arrows.

Widmo słoneczno-podobnych oscylacji α Centauri

Once the oscillation frequencies of a given star have been determined, how can they be made asteroseismic use of? As an example, high-precision radial velocity measurements of the close-by star α Centauri A showed the presence of solar-like oscillations; the power spectrum (square of amplitude vs. frequency) of these data is shown in Fig. 6.

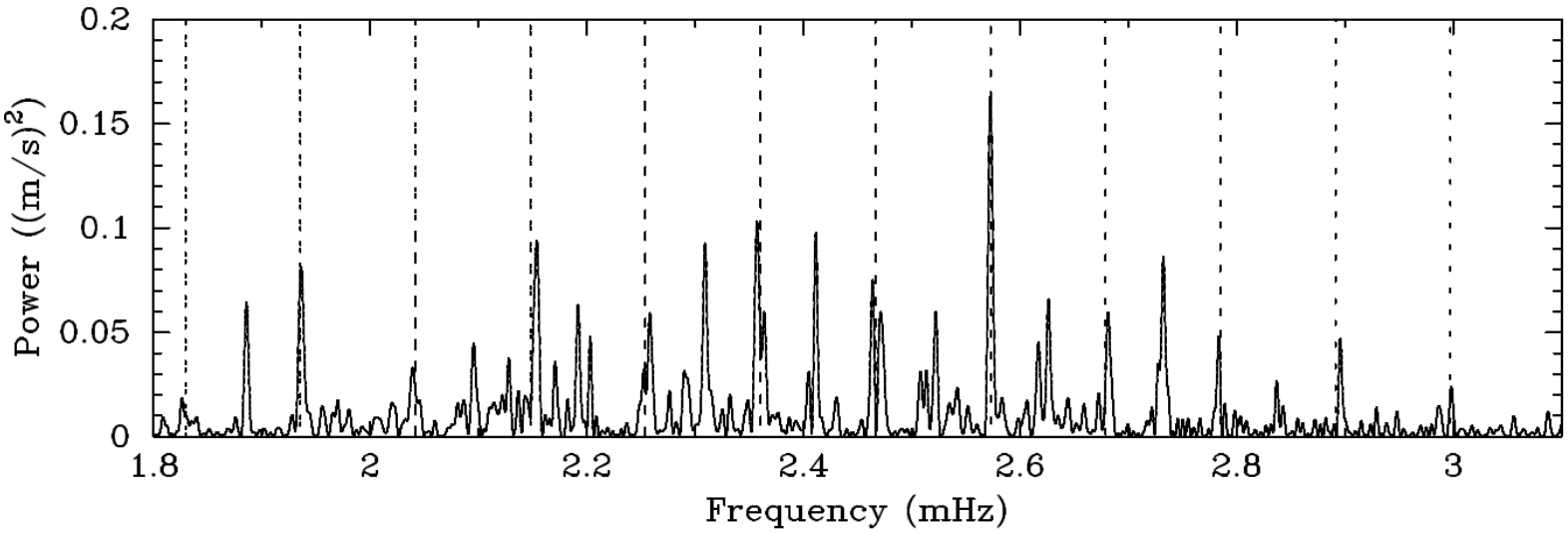

Figure 6: High-overtone p mode spectrum of the solar-like oscillator α Centauri A (Bedding et al. 2004). The vertical dotted lines are separated by 106.2 μHz.

This graph contains a series of maxima equally spaced in frequency: a high-overtone p mode spectrum, as predicted by asymptotic theory. The mean frequency spacing is 106.2 μHz. However, it is obvious that only every other of the strongest peaks conforms to this spacing; there are other signals in between. The signals halfway between the vertical lines in Fig. 6, denoting modes of spherical degree l, are a consequence of Eq. 7: these are modes with $l \pm 1$. Given the effects of geometrical cancellation, it is straightforward to assume that these are the modes of lowest l, viz. $l = 0$ and 1.

Echelle diagram dla słoneczno-podobnych oscylacji α Centauri

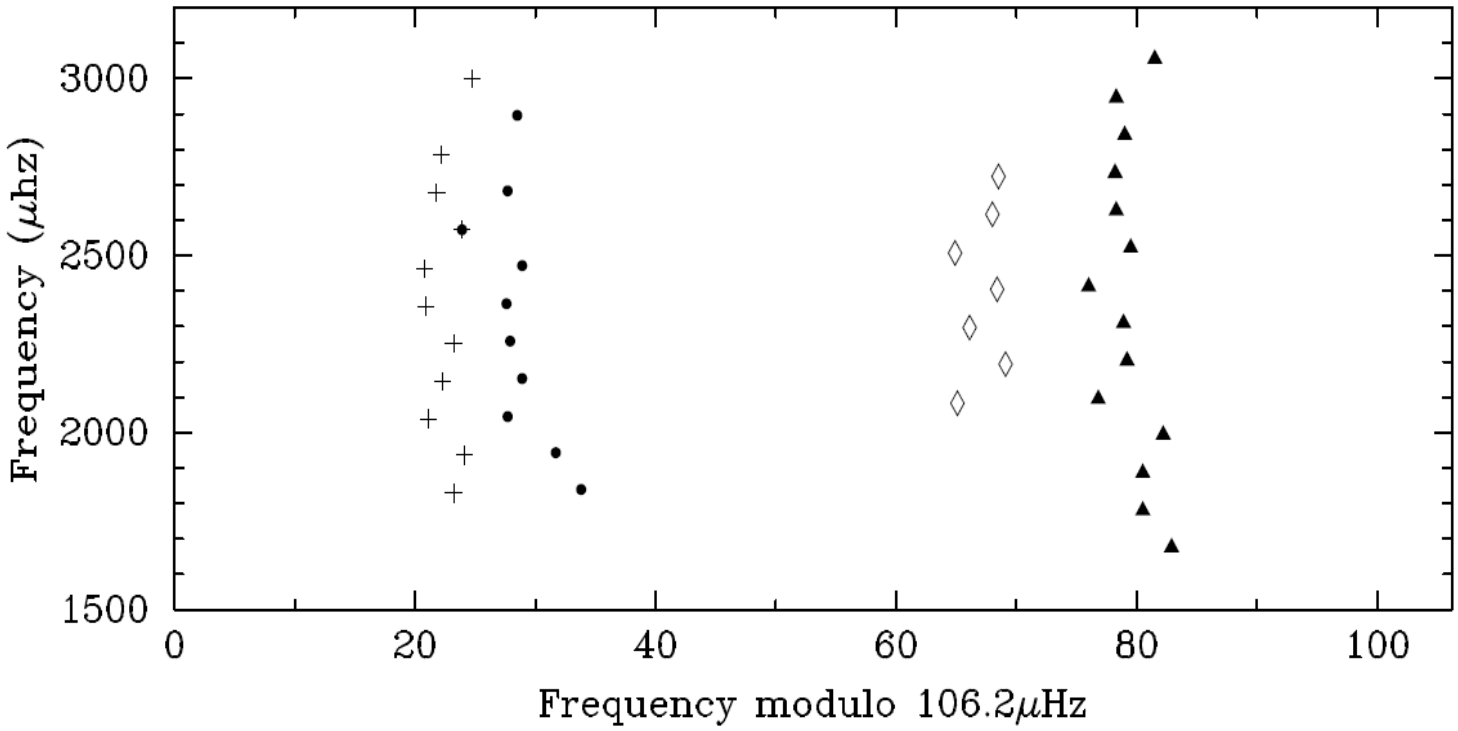

Figure 7: Echelle diagram of the frequencies determined from Fig. 6 (values from Bedding et al. 2004). Full dots represent radial modes, triangles mark dipole modes, plus signs stand for quadrupole modes and diamonds are for $l = 3$ modes.

Widmo częstotliwości
wysokich owertonów grawitacyjnych oscylacji białego karła GD 358

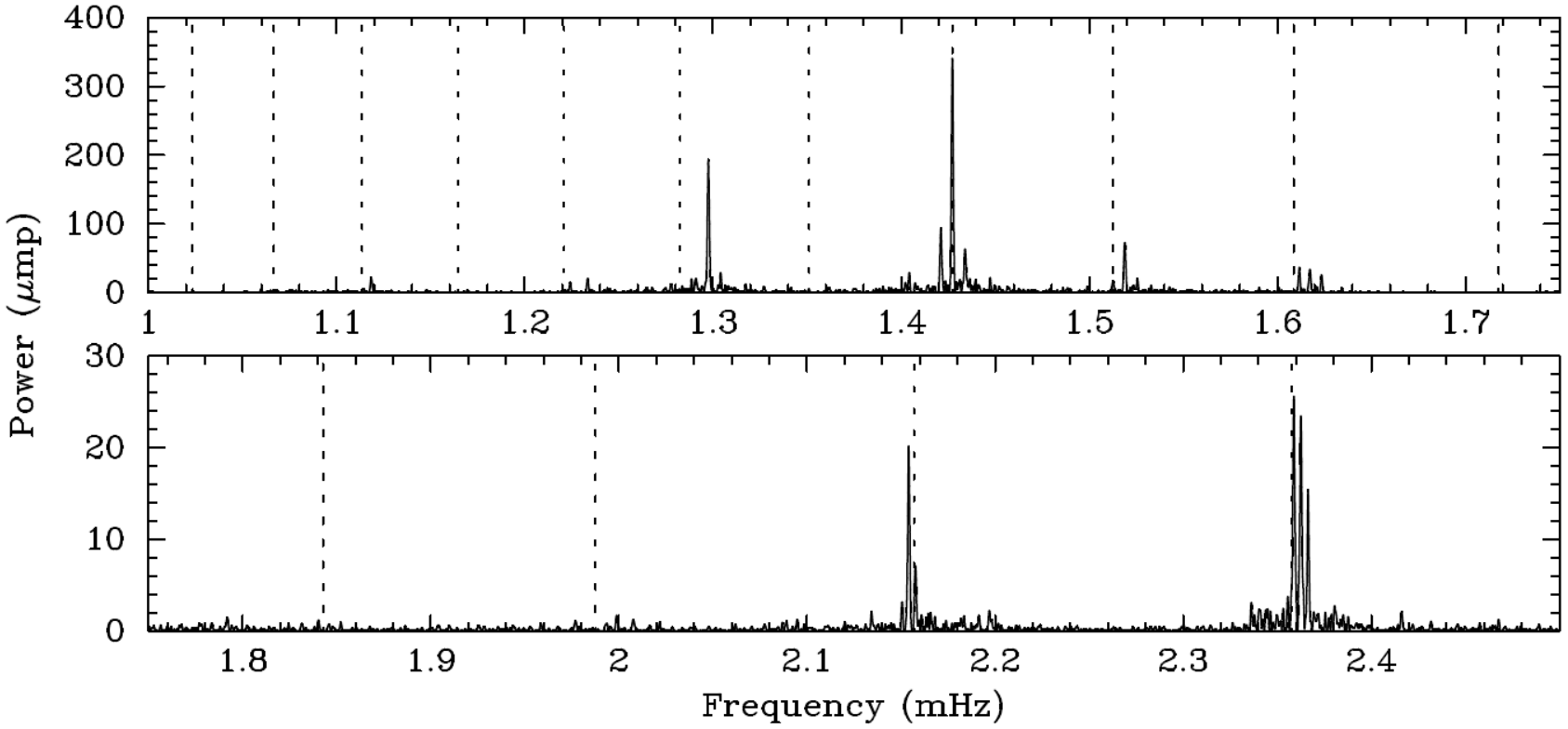

Figure 8: High-overtone g mode spectrum of the pulsating DB white dwarf star GD 358 (Winget et al. 1994). The vertical dotted lines denote periods with an equal spacing of 39.5 seconds.

Identyfikacja modów z danych wielobarwnej fotometrii

$$\Delta m(\lambda,t) = -1.086\epsilon P_l^{|m|}(\mu_0)((T_1+T_2)\cos(\omega t+\psi_T)+(T_3+T_4+T_5)cos(\omega t))$$

Przykład – zmienna 12 Lacertae

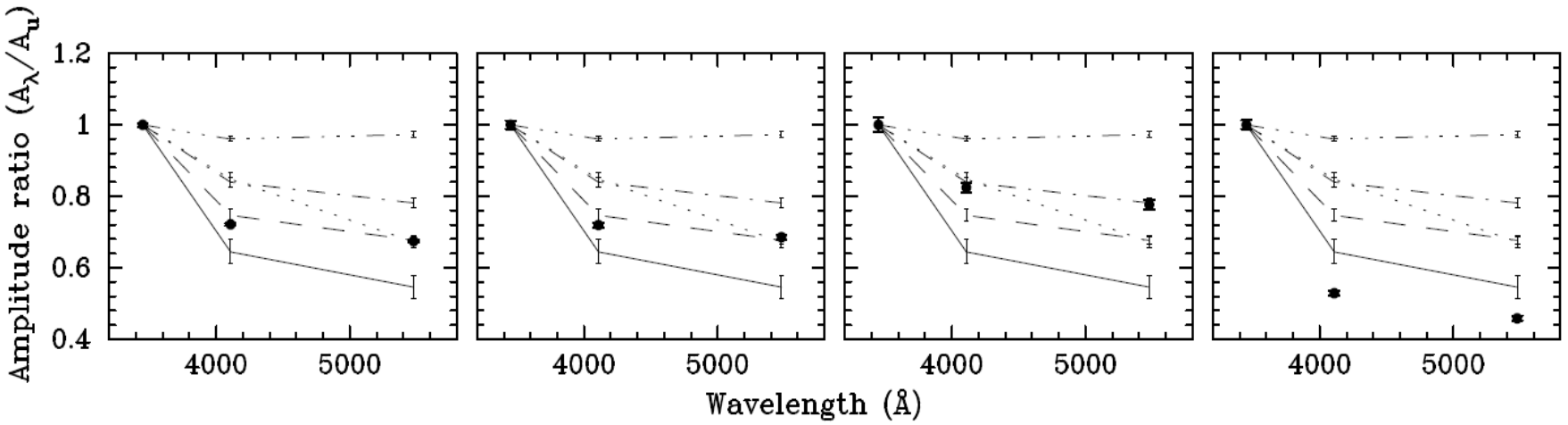

Figure 9: Identification of the four strongest pulsation modes of the β Cephei star 12 Lacertae from multicolour photometry (taken from Handler et al. 2006). The amplitudes are normalized to unity in the ultraviolet and compared with theoretical predictions. The full lines are for $l = 0$, the dashed lines for $l = 1$, the dashed-dotted lines for $l = 2$, the dotted lines for $l = 3$, and the dashed-triple dotted lines for $l = 4$. The modes investigated in the two left panels are $l = 1$, the next is $l = 2$ and the rightmost one is $l = 0$.

Zmiany profili linii widmowych podczas oscylacji nieradialnych. Identyfikacja rzędu azymutalnego.

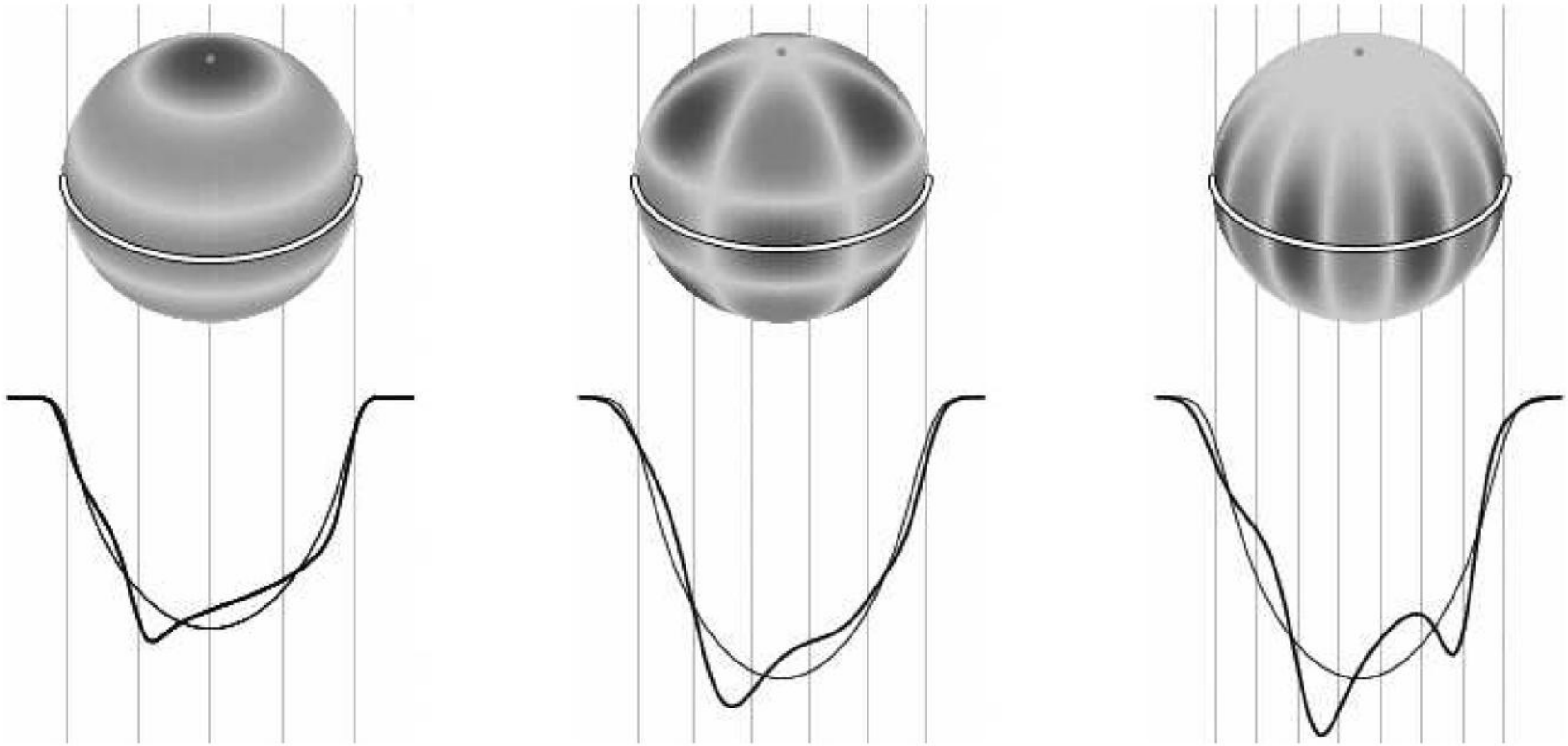

Figure 10: Line profile variations due to stellar pulsation. The upper parts of the graph show the shape of the oscillation mode on the surface, whereas the thin lines in the lower halves represent the unperturbed rotationally broadened line profile, and the thick lines are the superpositions with the pulsation. Each individual mode (from left to right: $l = 4, m = 0; l = 5, |m| = 3; l = |m| = 7$) generates a different distortion of the line profile. Adapted from Telting & Schrijvers (1997).

Pole prędkości i zmiany profilu linii widmowej

Oktupolowe pulsacje
***l*=3, m=3**

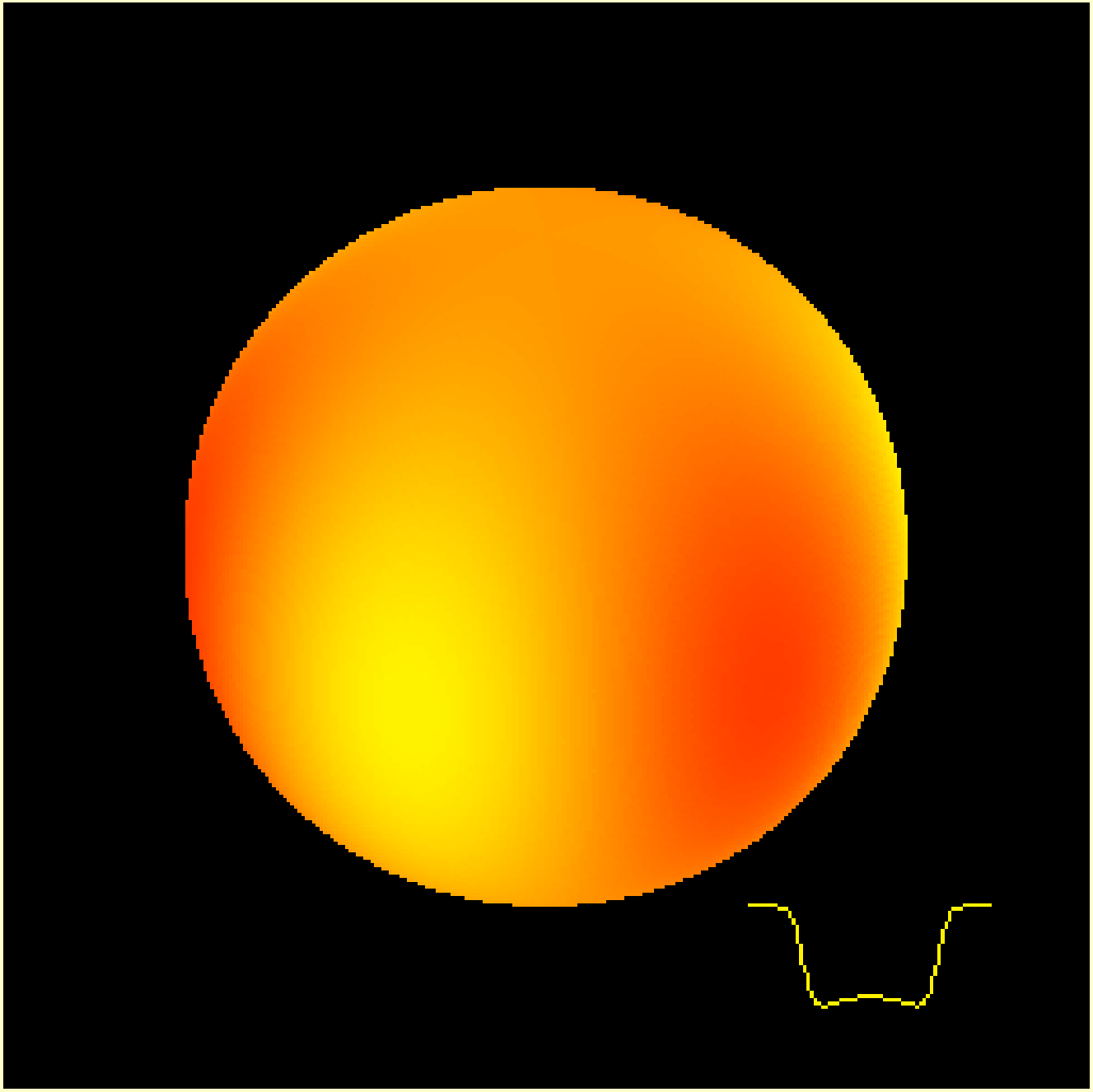

ν Eridani

14 frequencies (degree *l* is identified for 8 of them),
Sp B2 III,
mV = 3.920,
π = 5.56 +- 0.88 mas,
Vrot = 6 km/s (SIMBAD: Vsini = 7, 20, 25 km/s),
[m/H] = 0.05 +- 0.09,
Teff = 22200 +- 600 K

Oscillation spectra of ν Eri and 12 Lac

ν Eri: Jerzykiewicz et al. 2005

12 Lac: Handler et al. 2006

Dziembowski & Pamyatnykh 2008

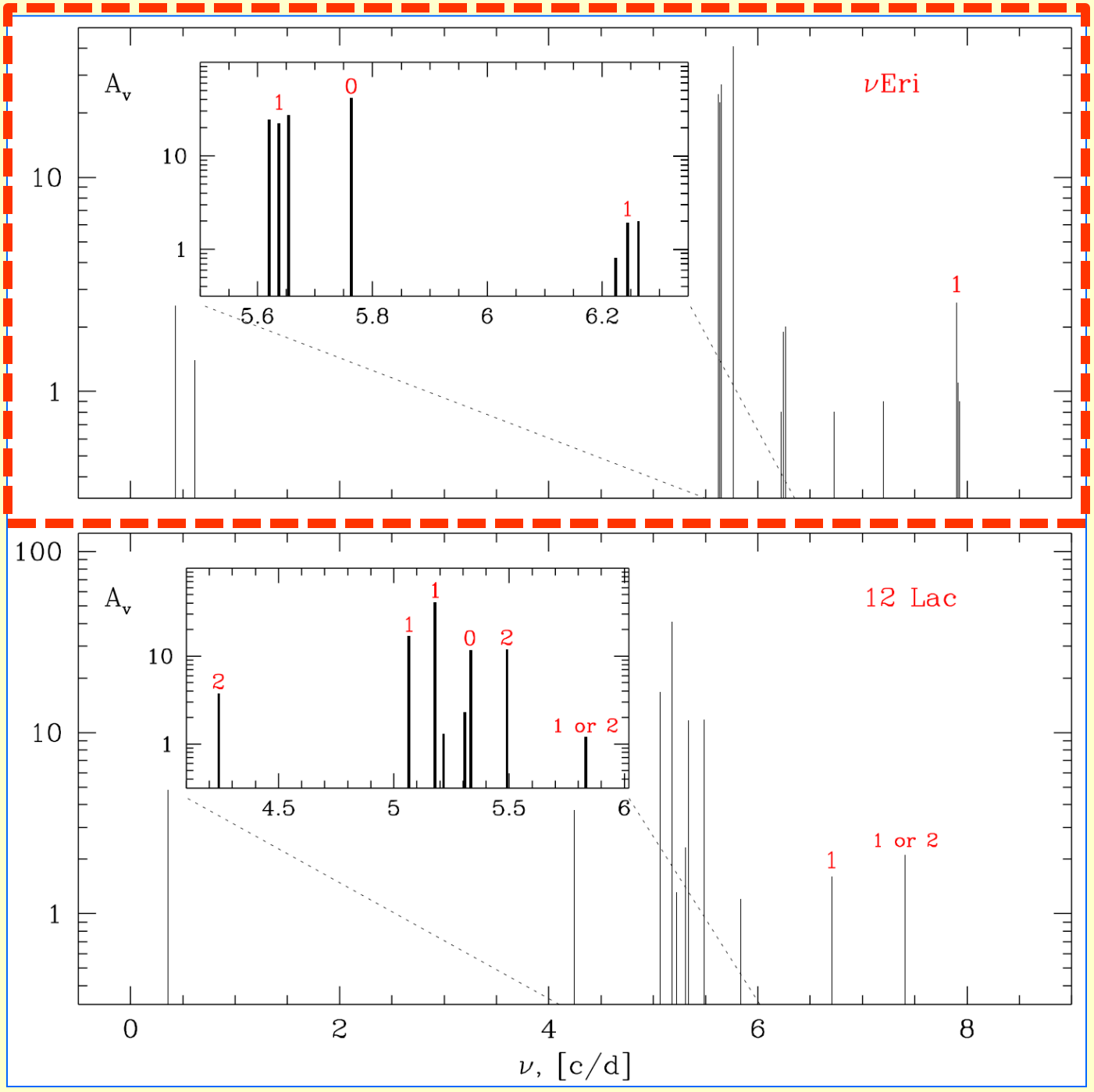

Oscylacje ν Eridani

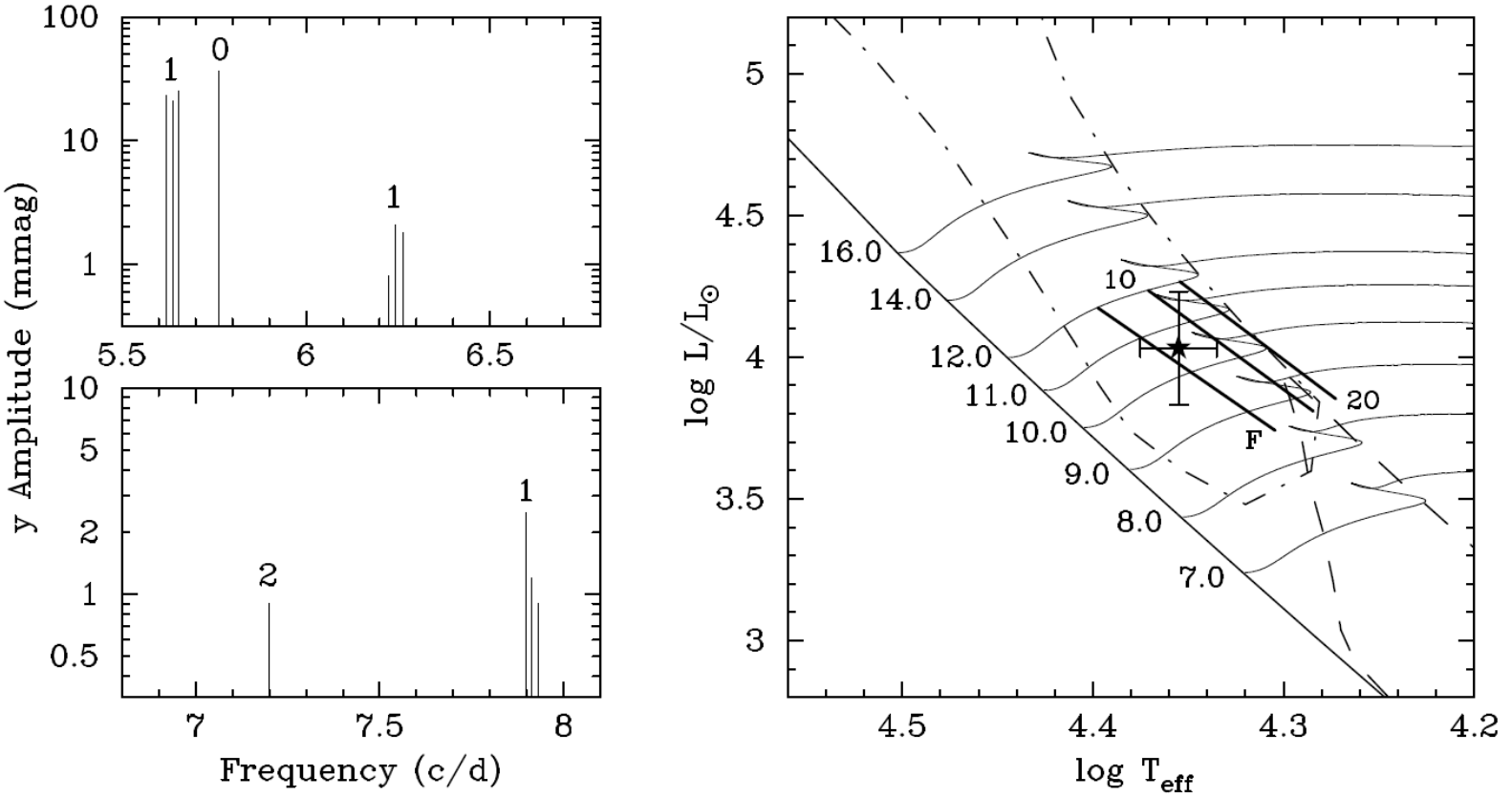

Figure 11: Left: schematic oscillation spectrum of ν Eridani. The numbers on top of each mode (group) are their l identifications, consistent in photometry and spectroscopy (De Ridder et al. 2004). Right: a plot of the star's position in the theoretical HR Diagram (star symbol) with its error bars and lines of equal mean density for the observed radial mode periods assuming they the fundamental, first and second overtones, respectively (thick lines). Some model evolutionary tracks labelled with their masses, the Zero-Age Main Sequence, and the borders of the β Cephei (dashed-dotted line) and SPB star (dashed lines) instability strips are also shown.

ν Eri

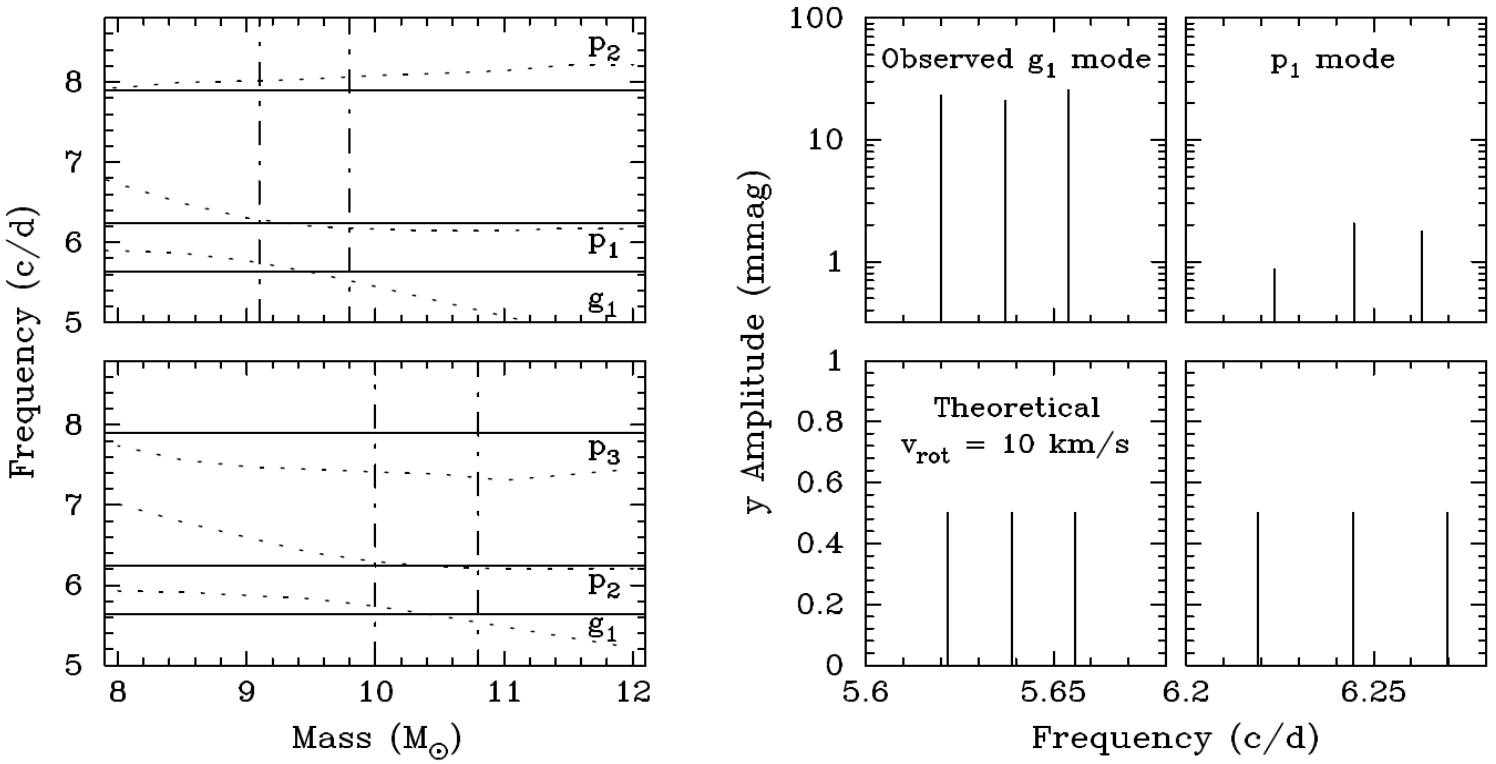

Figure 12: Left: a figure showing the match of the $l = 1, m = 0$ modes of ν Eri for models of different mass but same mean density. The full horizontal lines are the observed frequencies, the dotted lines are theoretical model frequencies. Upper panel: assuming that the radial mode is the fundamental. The vertical dashed-dotted lines show the mass range in which the first g mode and the first p mode fit the observed frequencies ($9.1 - 9.8\,M_\odot$). Lower panel: the same, but assuming the radial mode is the first overtone. Here it would be the first g mode and the second p mode that give an acceptable fit between $10.0 - 10.8\,M_\odot$. However, the observed $l = 1$ mode with highest frequency is not compatible with the more massive models. Right: a comparison of the rotational splittings of a rigidly rotating model, with a rotation rate chosen to fit the observed $l = 1, g_1$ triplet, with the observations. The observed splitting of the $l = 1, p_1$ triplet is not reproduced with this assumption, demonstrating the presence of differential interior rotation.

Fitting frequencies of the $l = 0$ and two $l = 1$ modes

κ OPAL GN93

Constraints on overshooting

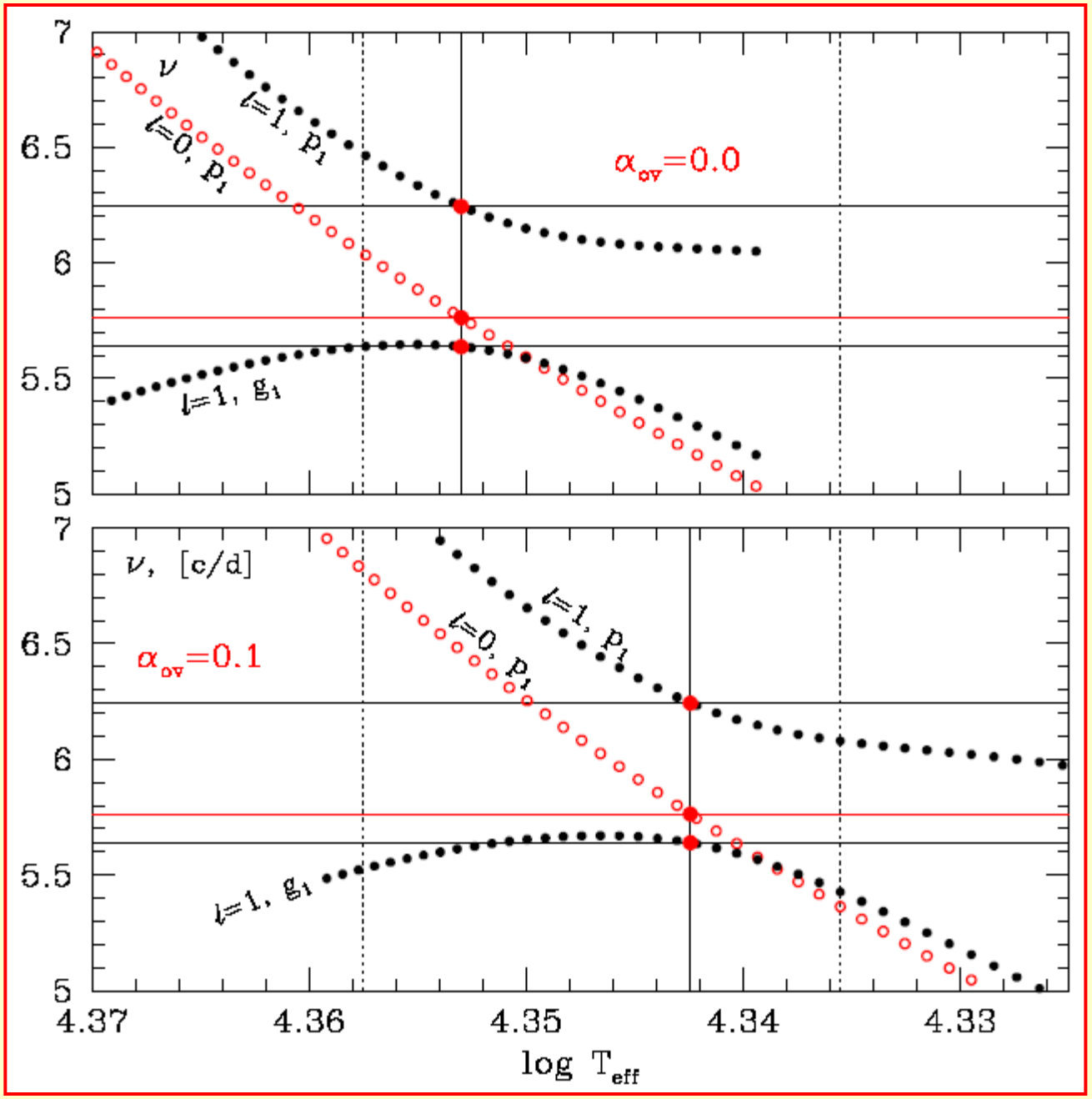

Pamyatnykh et al.2004

Testing rotation in interiors

Oscillation spectra of ν Eri and 12 Lac

Two rotationally splitted triplets of $l = 1$ modes (g1 and p1)

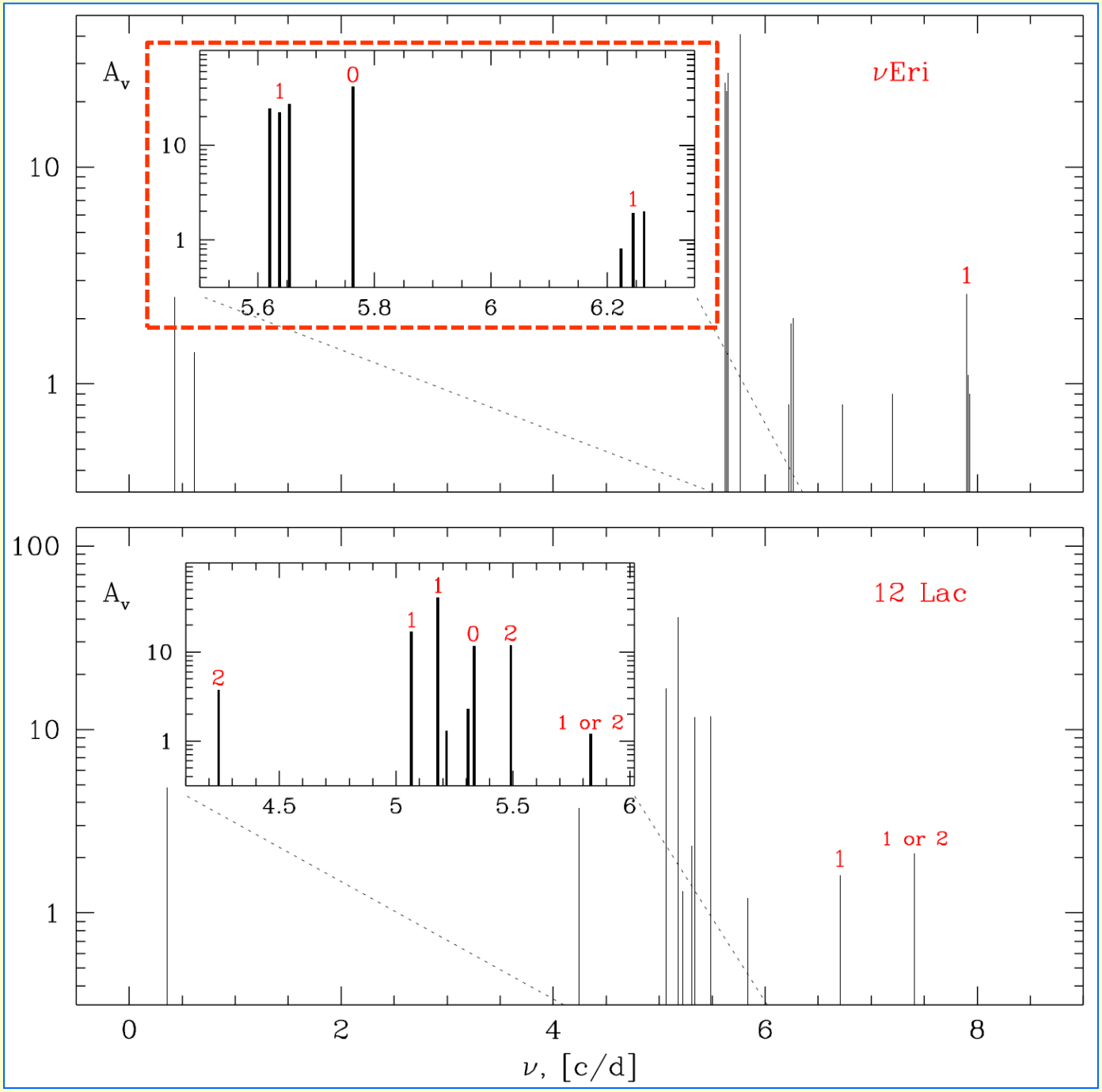

Dziembowski & Pamyatnykh 2008

Asterosejsmologiczna ocena rotacji we wnętrzu ν Eridani

$\ell = 1$ mode

Mean splitting $\quad S = \frac{1}{2}(\nu_{+1} - \nu_{-1})$

Asymmetry $\quad A = \nu_{-1} + \nu_{+1} - 2\nu_0$

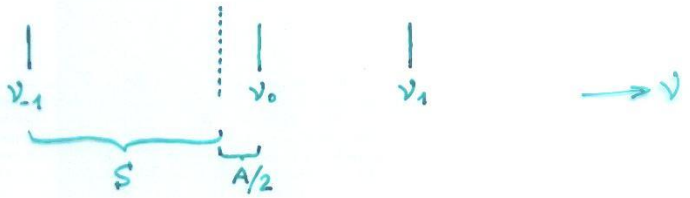

$\Omega = \Omega(r) \Rightarrow$

$$\nu_m = \nu_0 + \frac{m}{2\pi}\int_0^R \mathcal{K}\cdot\Omega\cdot\frac{dr}{R} + D_0 + m^2 D_1$$

$D_0, D_1 \sim \Omega^2$

$$\mathcal{K} = \frac{(\xi_r^2 - 2\xi_r\xi_h + [\ell(\ell+1)-1]\xi_h^2)\, r^2\rho}{\int_0^R [\xi_r^2 + \ell(\ell+1)\xi_h^2]\, r^2\rho\, dr/R}$$

$$\vec{\xi} = (\xi_r \vec{e}_r + \xi_h \vec{\nabla}_h) Y_\ell^m$$

$$\begin{cases} 2\pi S_g = K_{c,g}\bar{\Omega}_c + K_{e,g}\bar{\Omega}_e \\ 2\pi S_p = K_{c,p}\bar{\Omega}_c + K_{e,p}\bar{\Omega}_e \end{cases}$$

$$K_{c,j} = \int_0^{r_{co}} \mathcal{K}_j \frac{dr}{R} \qquad K_{e,j} = \int_{r_{co}}^R \mathcal{K}_j \frac{dr}{R}$$

$$\Rightarrow \bar{\Omega}_c \simeq 3\bar{\Omega}_e$$

Mean rotation rate in the μ-gradient zone is about 3 times faster than in the envelope.

Pamyatnykh et al.2004

ν Eri: the splitting kernels for two normal modes: l = 1, g1 (solid line), l = 1, p1 (dashed line). Triangles mark boundaries of the μ-gradient zone.

$$S \equiv 0.5(\nu_+ - \nu_-) = \int_0^1 dx \mathcal{K}(x)\Omega/2\pi$$

S_g=0.017, S_p=0.020 c/d

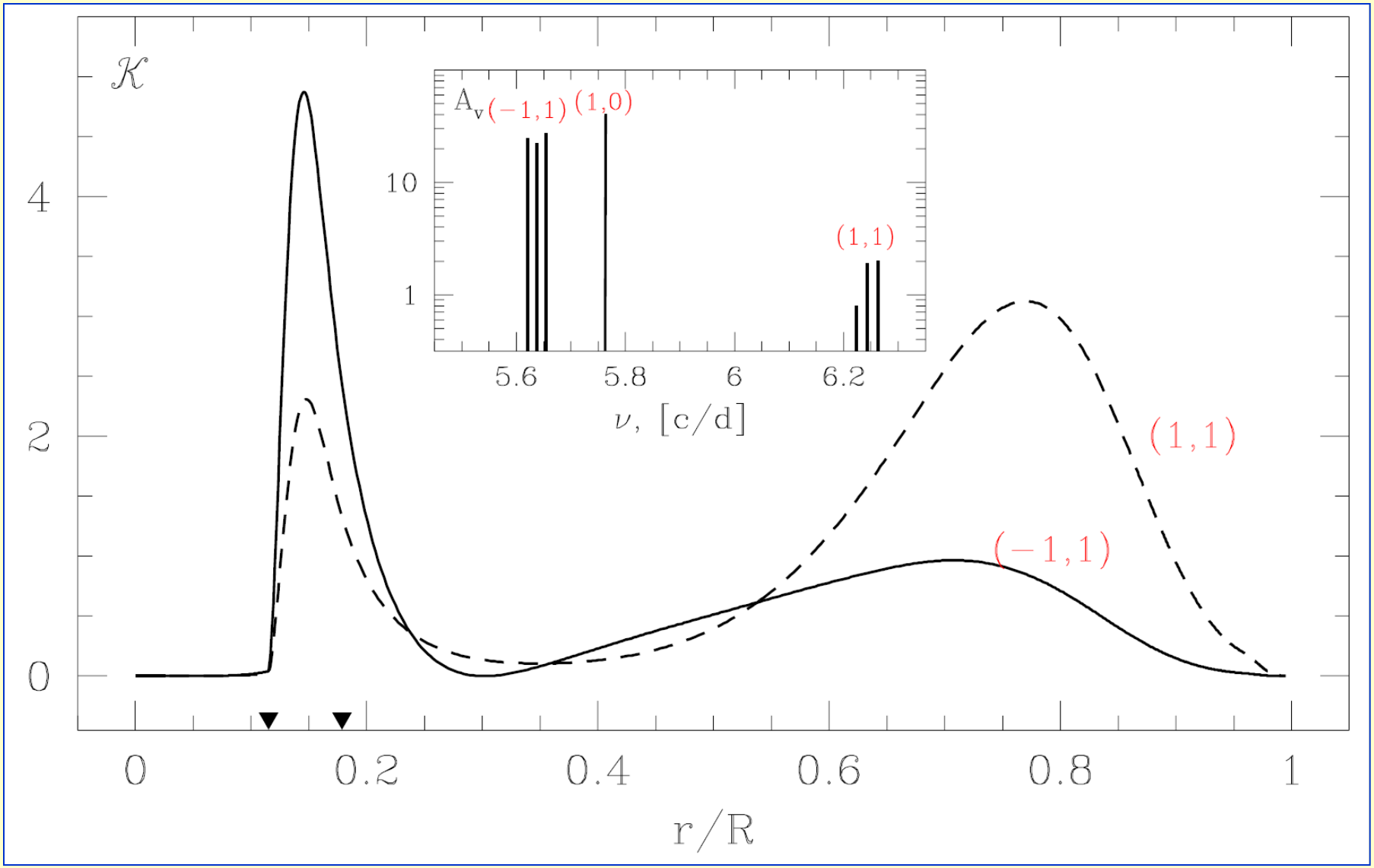

Simple rotation law

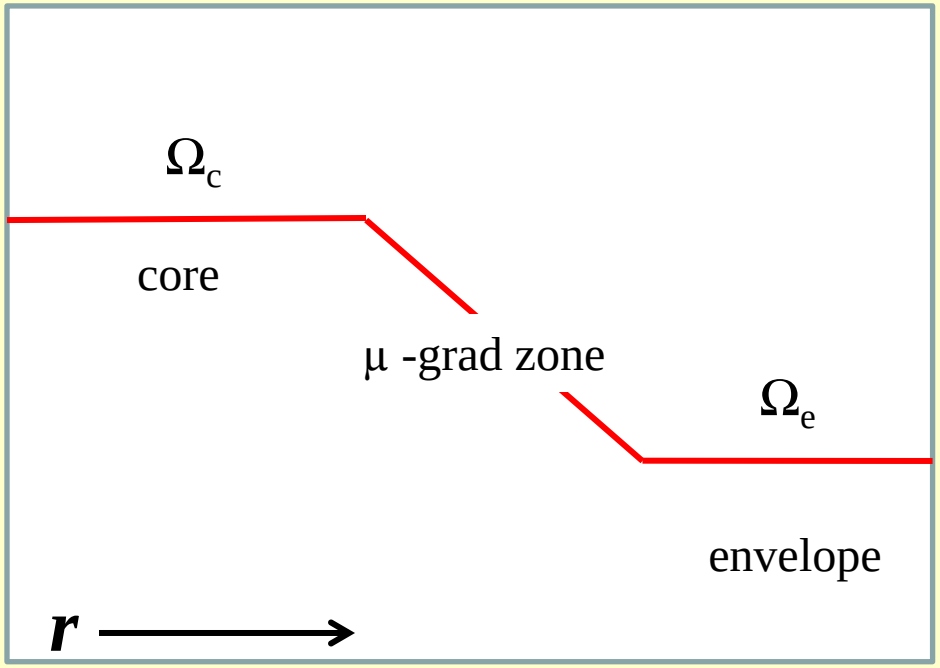

Results:

$V_{rot} = 6$ km / s

$\Omega_{core} = 5 * \Omega_{envelope}$

Table 1. The O-C (in cd^{-1}) for the $\ell = 1$, p_2 mode frequencies and the differences between observed effective temperature and that of the seismic model, $\Delta \log T_{eff} = \log T_{eff,obs} - \log T_{eff,cal}$. The observational uncertainty in effective temperature is $\Delta \log T_{eff} = 0.011$. Models with $\alpha_{ov} > 0$ were calculated with $w = 8$. V_{rot} is given in km s^{-1}.

κ	Mixture	α_{over}	OC	$\Delta \log T_{eff}$	Ω_c/Ω_e	V_{rot}
OP	A04	0.0	−0.127	−0.0103	5.55	5.93
OP	GN93	0.0	−0.151	−0.0075	5.36	5.95
OPAL	A04	0.0	−0.188	−0.0044	5.36	5.99
OP	A04	0.1	−0.085	−0.0159	5.82	5.91
OP	A04	0.2	−0.034	−0.0244	5.78	5.93

Dziembowski, Pamyatnykh 2008

Symulacja obserwacji z jednego obserwatorium

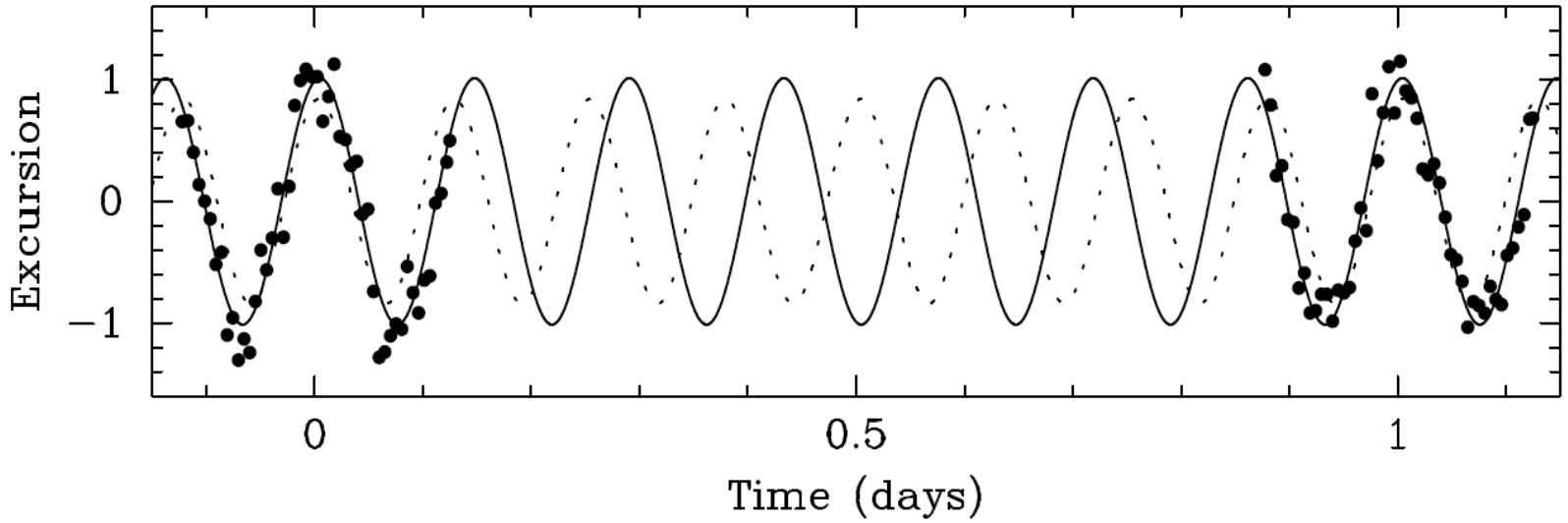

Figure 13: Simulation of observations from a single astronomical site. The filled circles represent the measurements, including noise. The full line is a fit with the correct frequency present in the data, and the dotted line is a fit with a frequency different by 1 cycle per day. The two fits represent the data almost equally well. However, they would be completely out of phase, and therefore easily separable, if measurements were available in between the present data, from a site 180 degrees different in geographical longitude. This led to the setup of multisite telescope networks.

Podkreślenie kilku ważnych cech oscylacji gwiazd

(powtór albo dodatek do poprzednich lekcji)

Kappa-mechanism and Z-bump.
β Cep and SPB instability domains.

Pamyatnykh, 1999, Acta Astronomica, 49, 119

Opacity inside a β Cephei star model (M=12 Msun, X=0.70, Z=0.02): OP (Seaton) versus OPAL (Livermore) versus LAOL (Los Alamos)

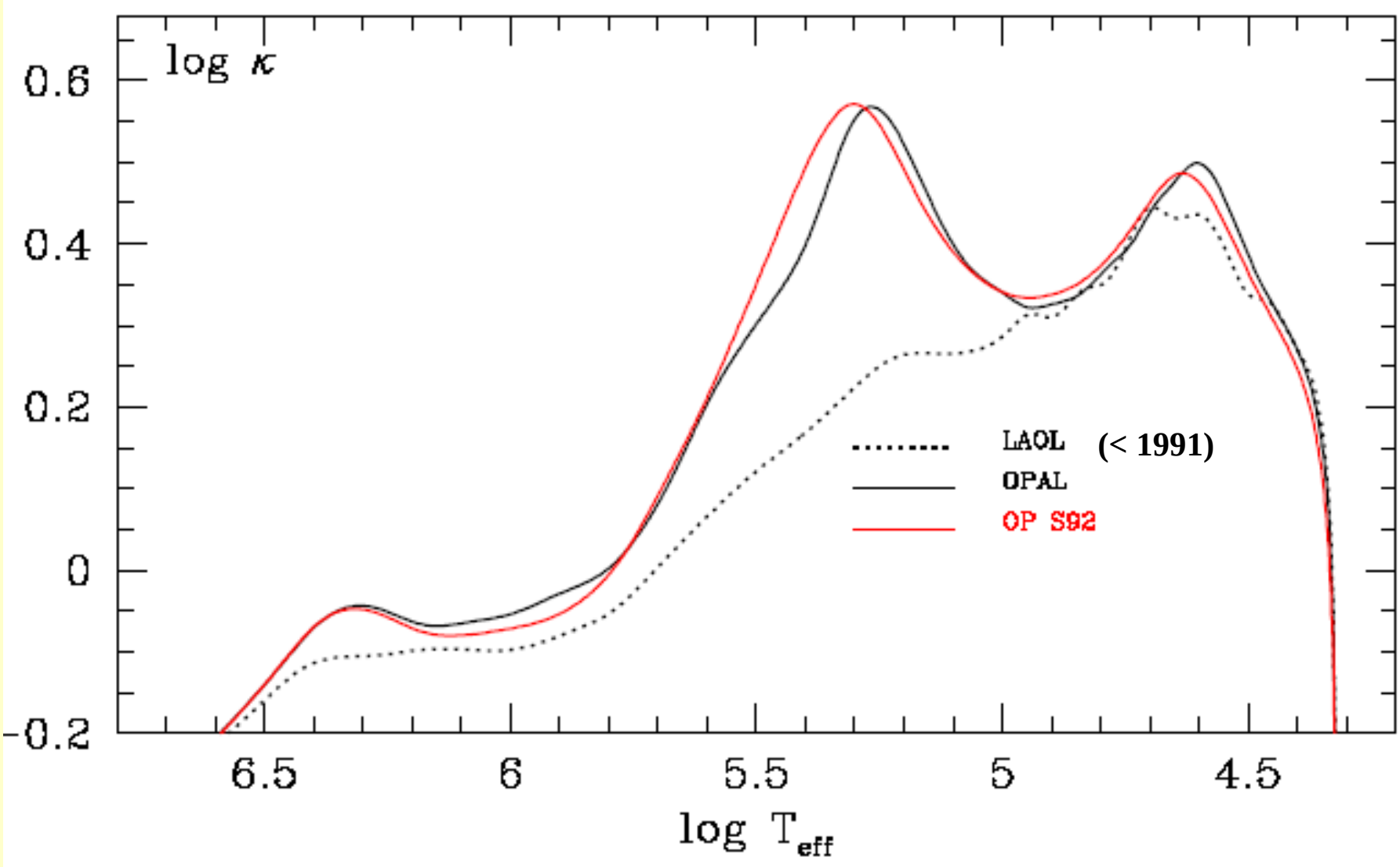

Opacity behaviour at astrophysical conditions [κ OPAL 1996]

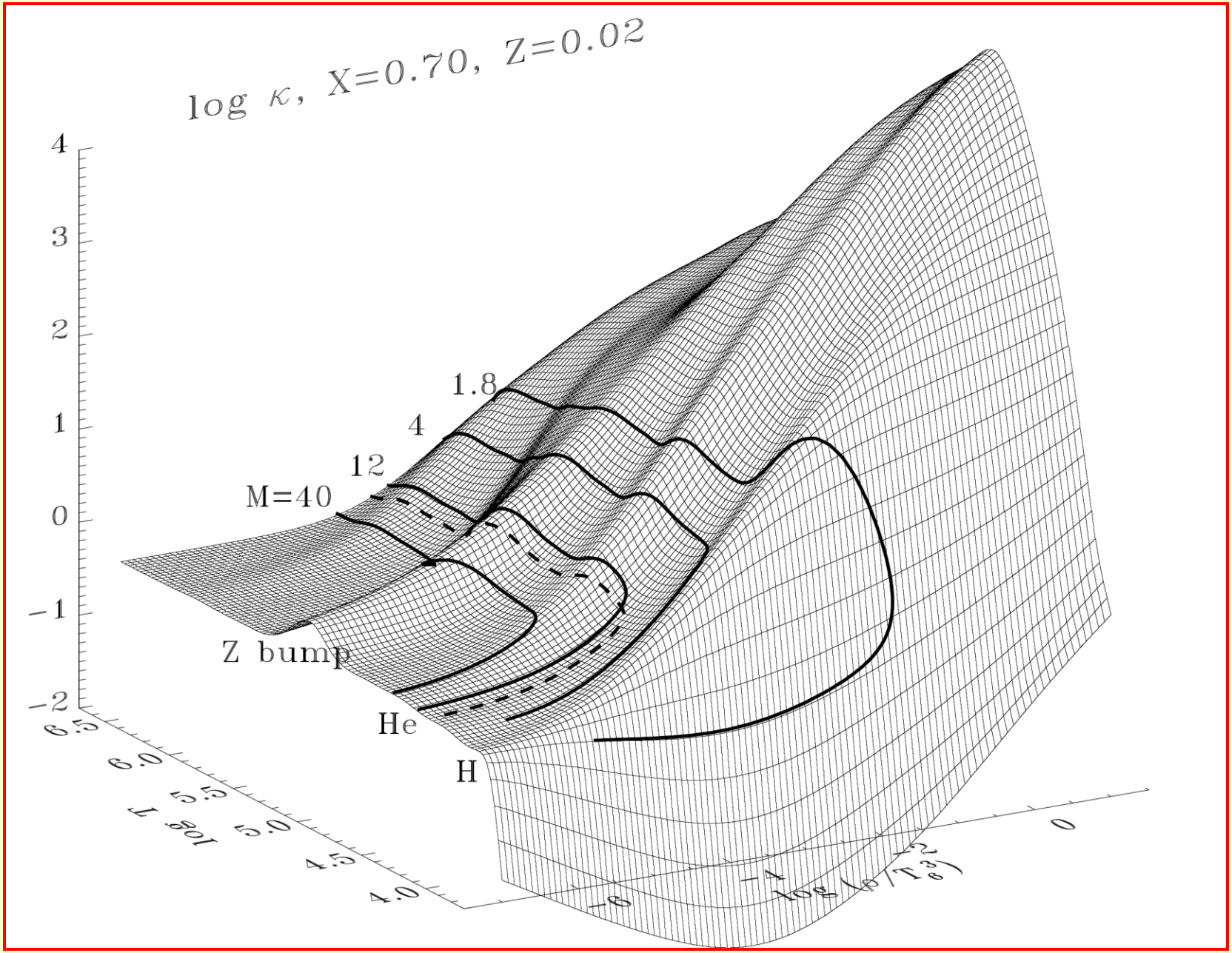

Pamyatnykh, 1999, Acta Astronomica, 49, 119

Two additional conditions must be fulfilled to excite global stellar pulsations in a mode under consideration:

- **In the driving zone, the amplitude of oscillation ($\delta P/P$) must be large and must vary only slowly with r.**

- **In the driving zone, the thermal timescale,**

$$\tau_{\rm th}(r) = \int_r^R T c_P \, {\rm d}M/L,$$

must be comparable or longer than the oscillation period. Otherwise, the potentially driving region remains in thermal equilibrium during pulsation (neutral stability).

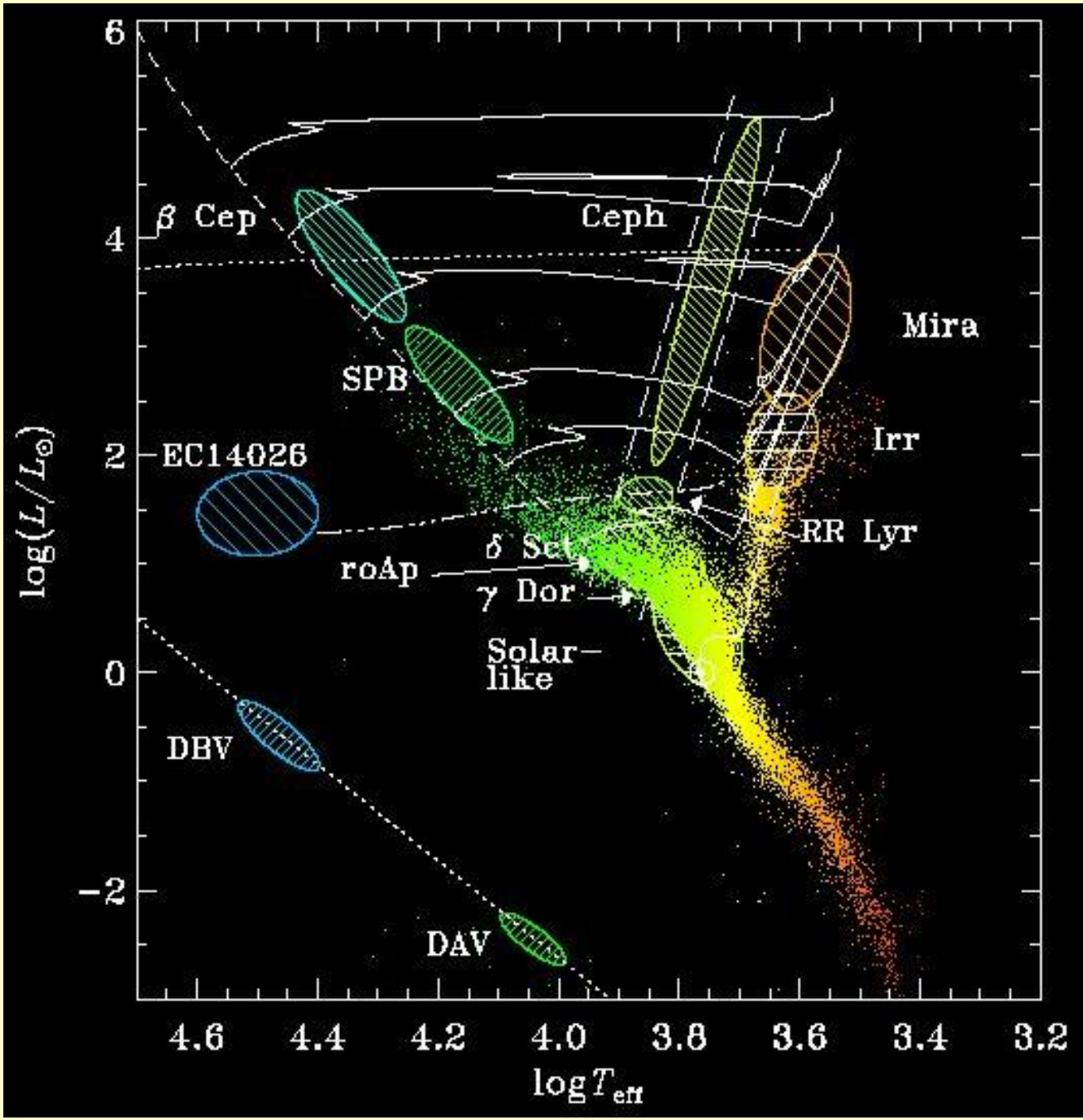

J. Christensen-Dalsgaard

κ OPAL GN93 (Livermore, 1996):

Instability domains

in the Upper MS

X=0.70, Z=0.02

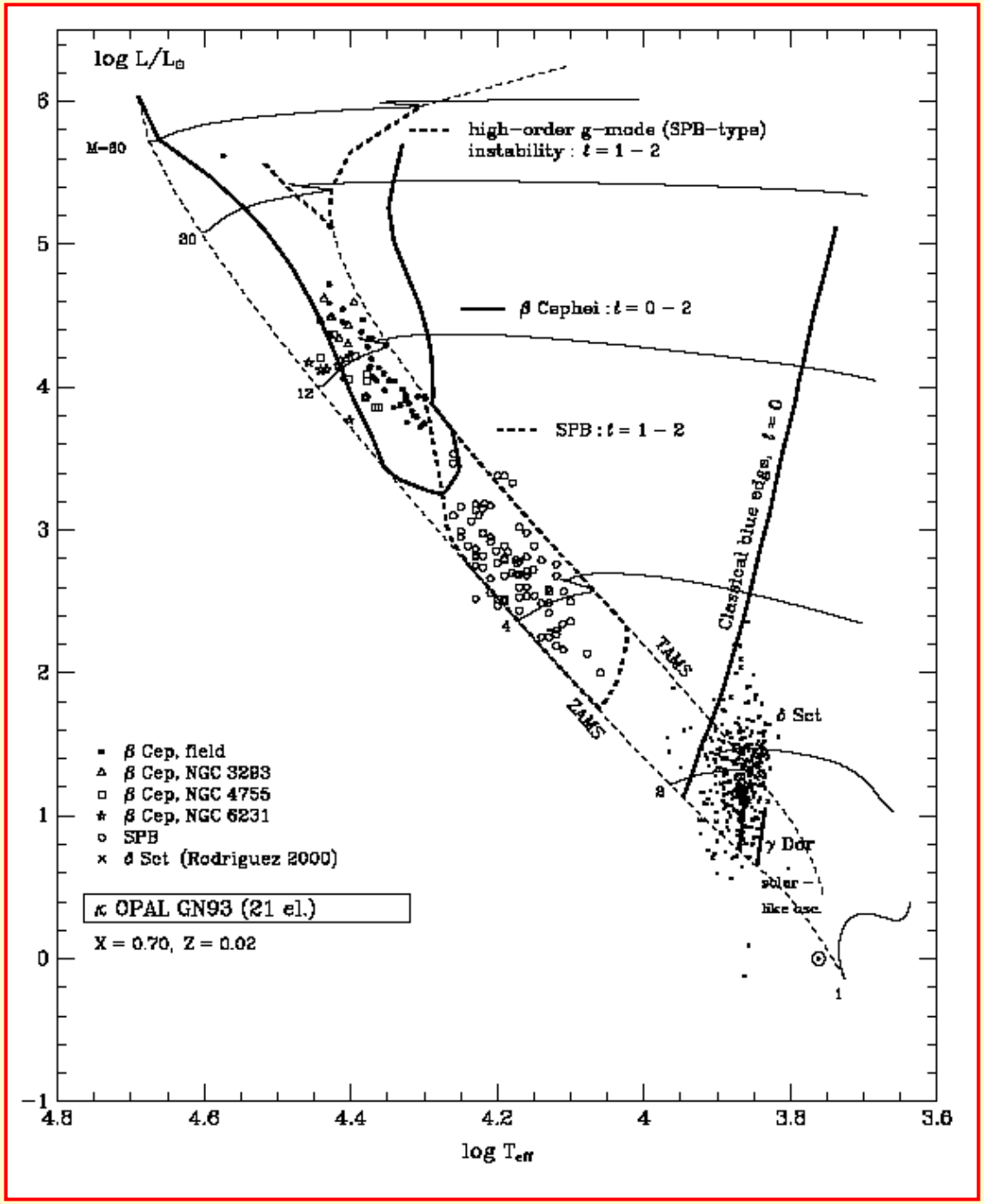

Pamyatnykh, 1999, Acta Astr., 49, 119

Effect of changes in the heavy element abundances on evolution and stability of the upper MS stars:

κ OPAL,
Z = 0.01, 0.015, 0.02

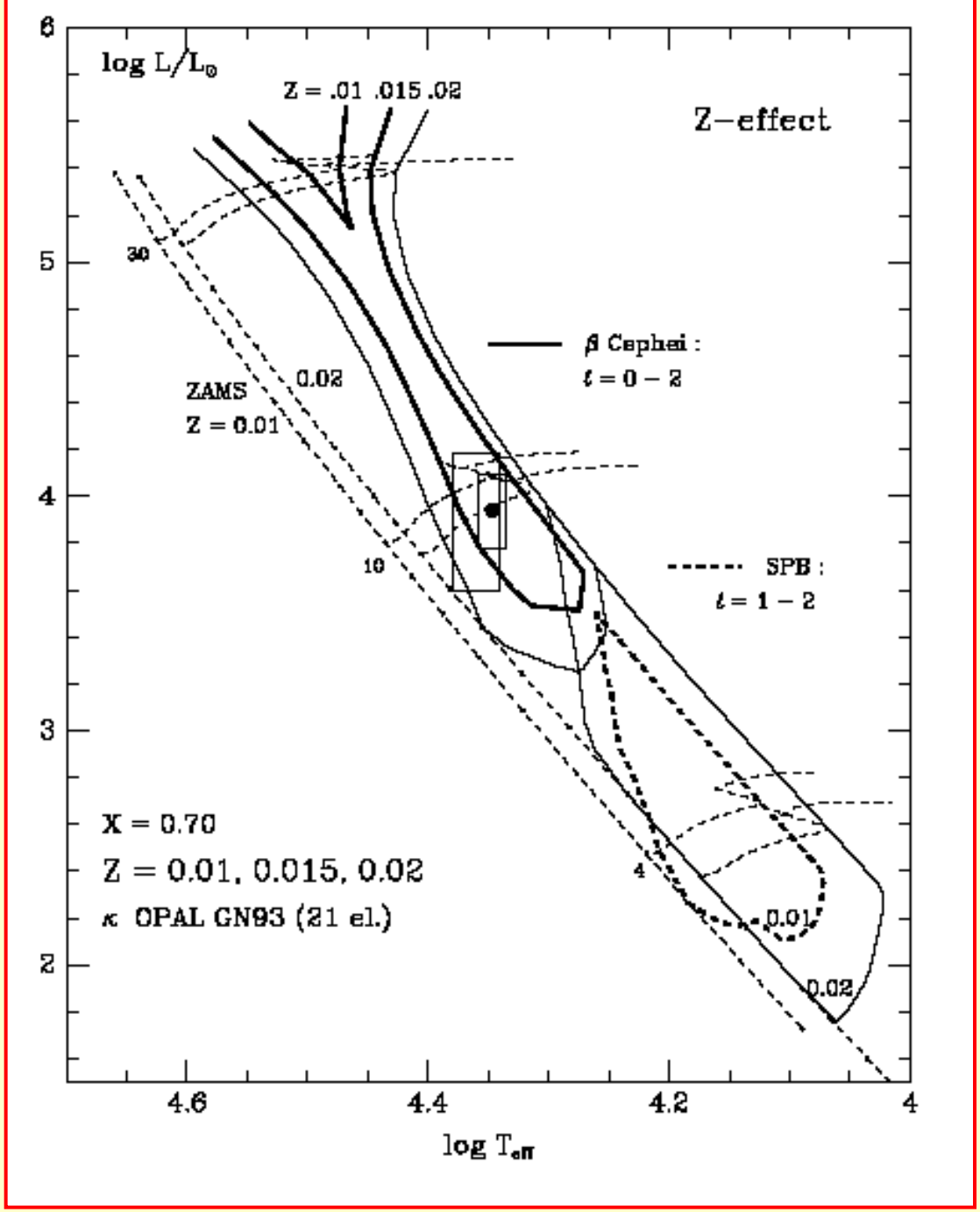

Pamyatnykh, 1999, Acta Astr., 49, 119

Opacity source	Z for β Cep instability
LAOL (< 1991)	no excitation
OPAL 1991	Z = 0.03-0.04
OPAL 1992	Z = 0.02-0.03
OPAL 1996	Z = 0.02-0.03
OP S92 >1993	Z = 0.02
OP A04 2005	Z = 0.01-0.02

With newest opacities and abundances it is possible to explain β Cep pulsations using models with significantly lower Z value than before.

Okresy radialnych, dipolowych i kwadrupolowych oscylacji ewolucyjnych modeli gwiazd z M = 10 Msun (od ZAMS do TAMS)

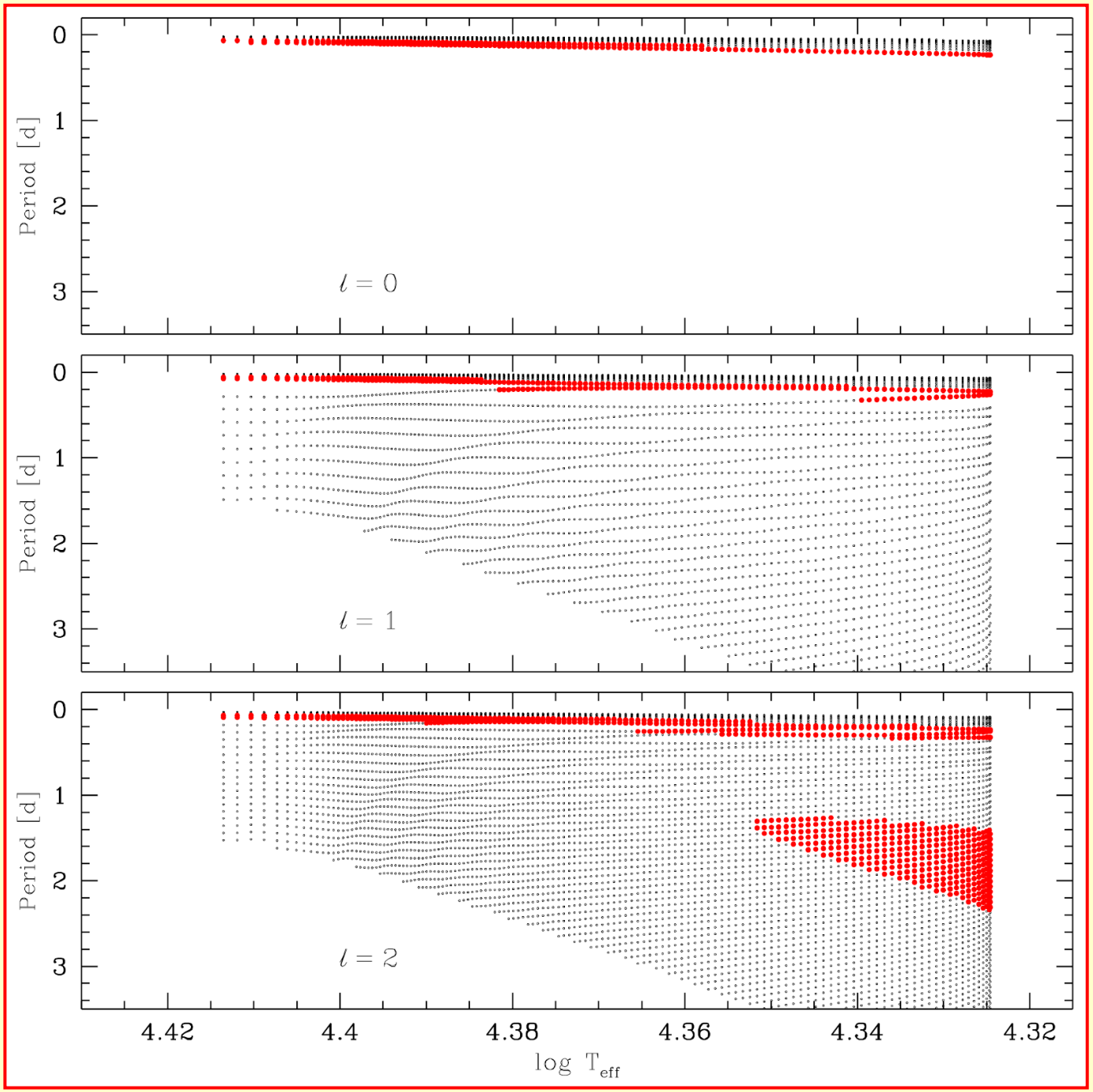

Differential work integral and density of kinetic energy for two modes in the 10 Msun model 130

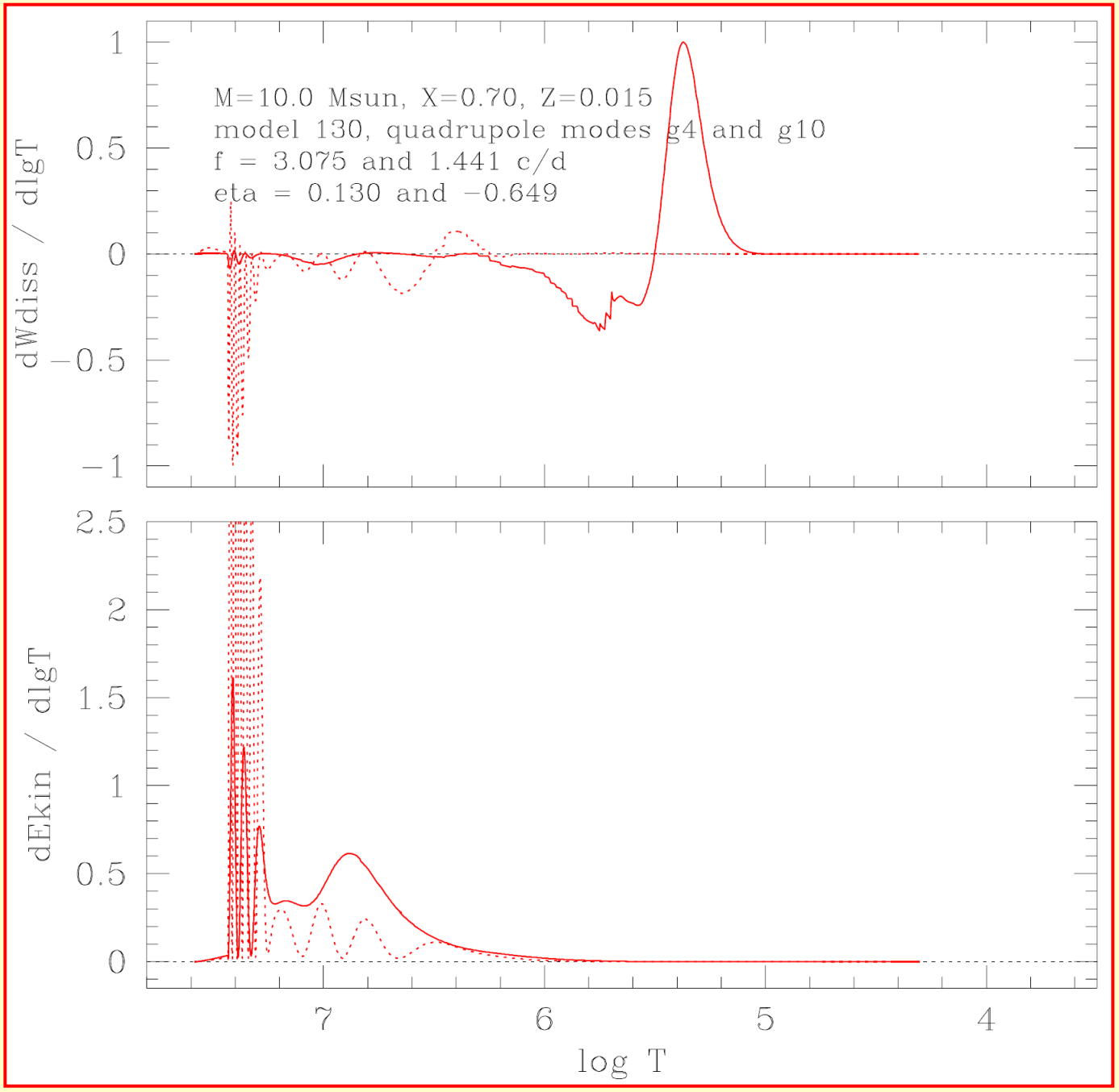

Differential work integral and pressure perturbation for two modes in the 10 Msun model 130

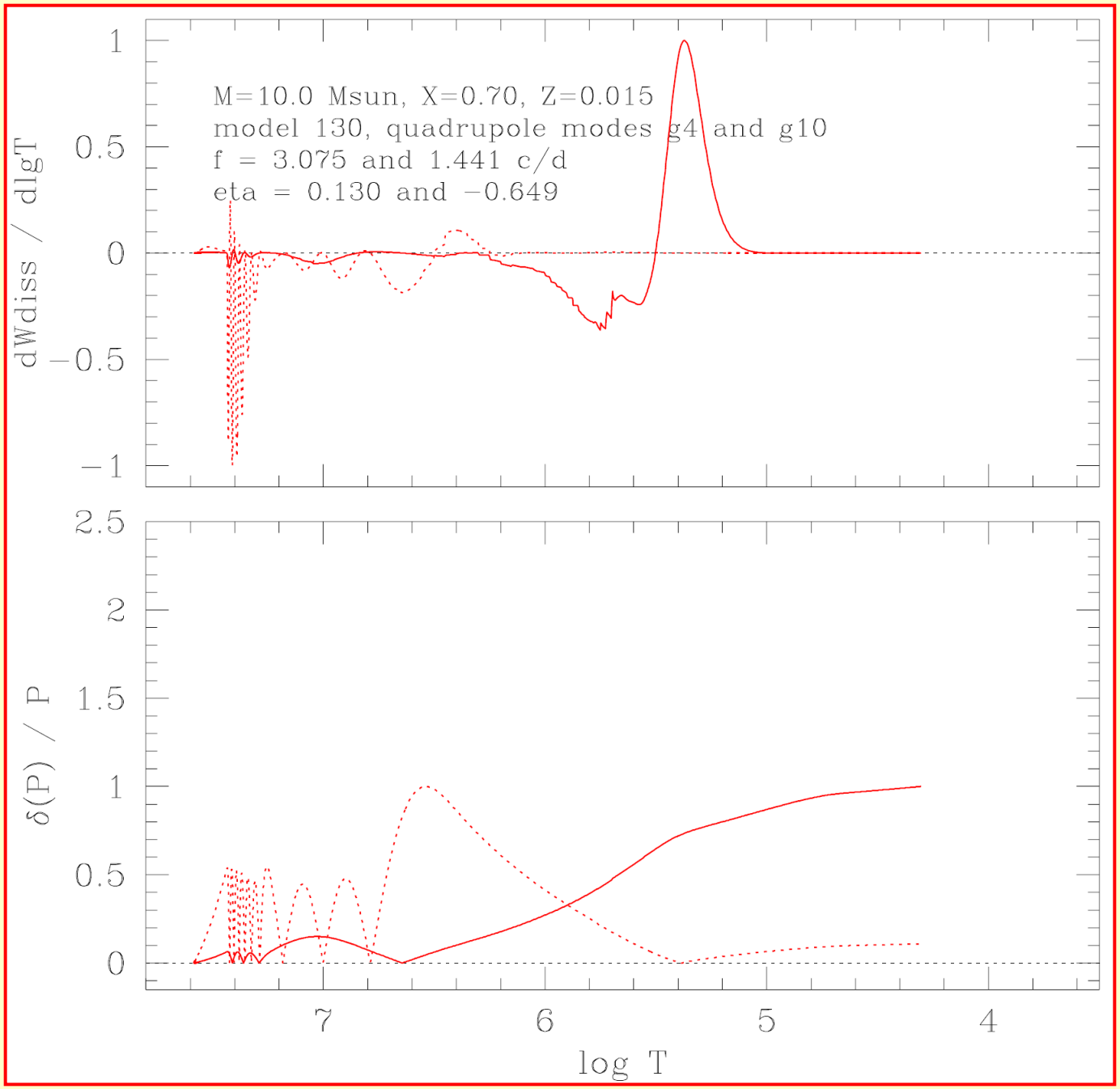

Differential work integral and density of kinetic energy for two modes in the 10 Msun model 130

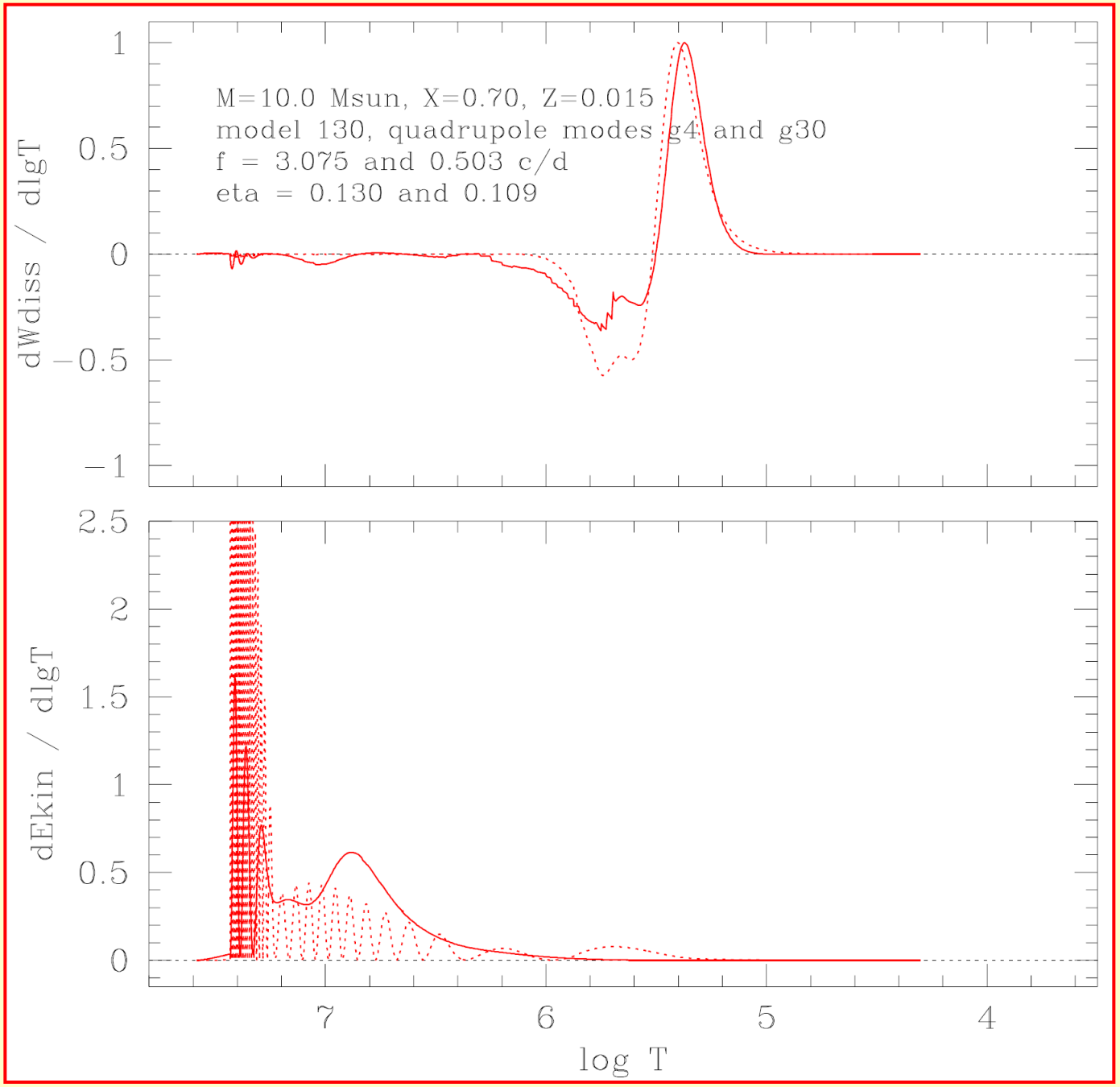

Differential work integral and pressure perturbation for two modes in the 10 Msun model 130

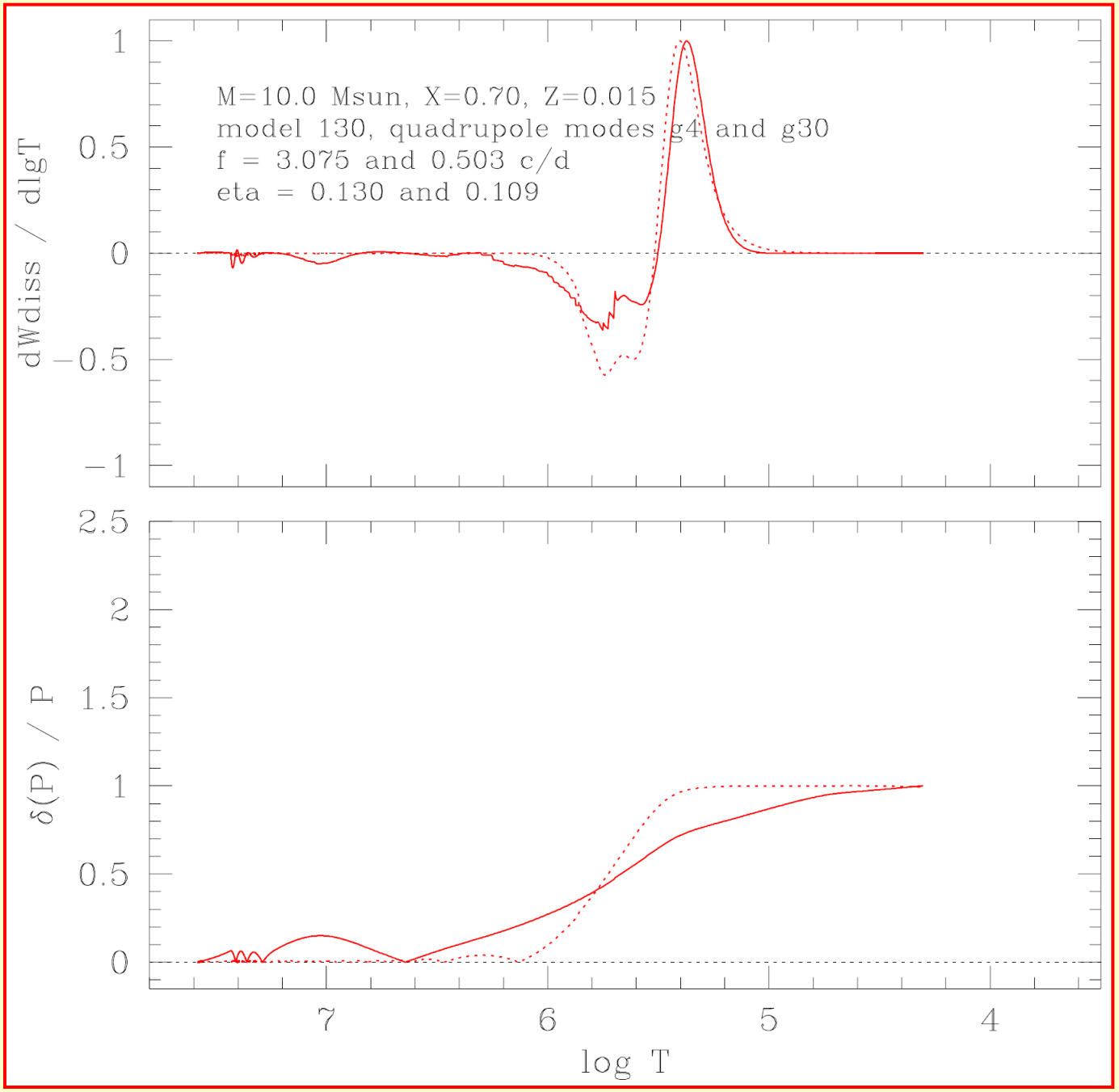

Two frequency ranges of unstable modes (*p* and *g)* in a 30 Msun model

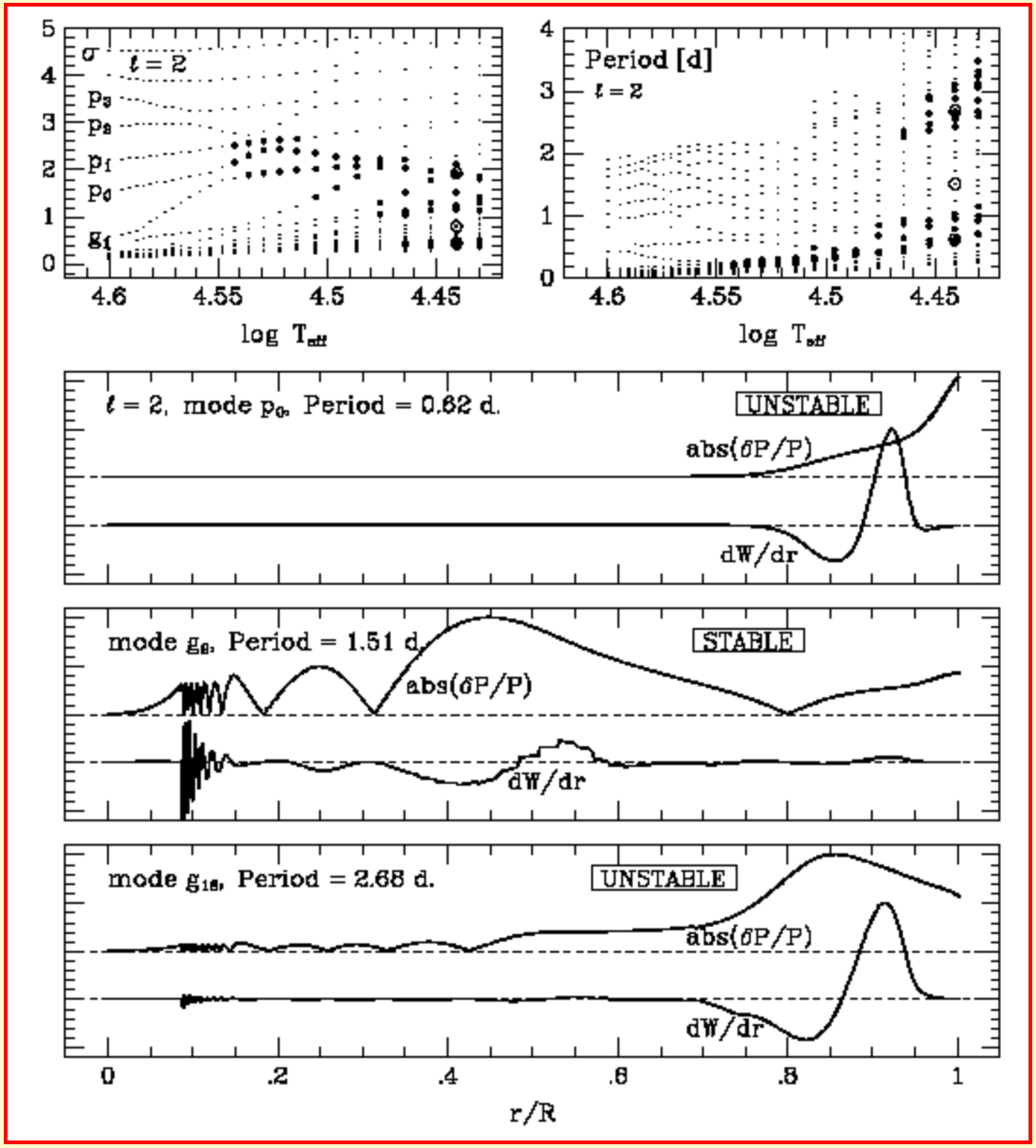

UNSTABLE

STABLE

UNSTABLE

UNSTABLE

STABLE

UNSTABLE

Pamyatnykh, 1999, Acta Astr., 49, 119

Delta Scuti instability domain

Pamyatnykh, 2000, ASP Conf. Ser., vol. 210, pp. 215-246.

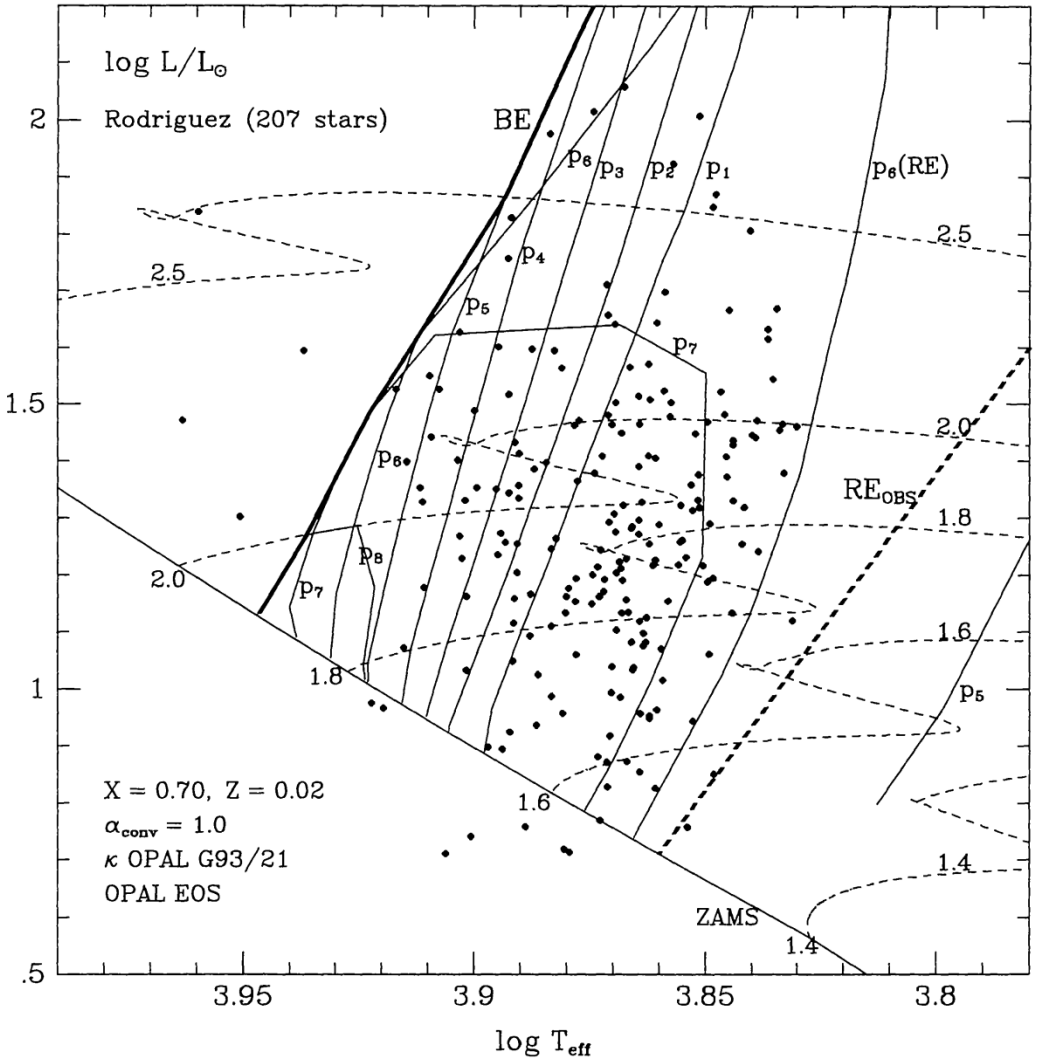

Figure 3. Theoretical Blue Edges of the δ Scuti instability domain for radial oscillations (symbols p_1 - p_8 mark corresponding modes, starting from fundamental one). The symbol BE stands for the general Blue Edge, which is the hotter envelope of unstable models. The symbol RE_{obs} marks the empirical Red Edge. The Zero-Age Main Sequence (ZAMS) and a few evolutionary tracks for the indicated values of $M/M_{\odot}$ are shown. Observational data are from the catalogue of Rodriguez et al. (1994). See text for details.

Pamyatnykh 2000

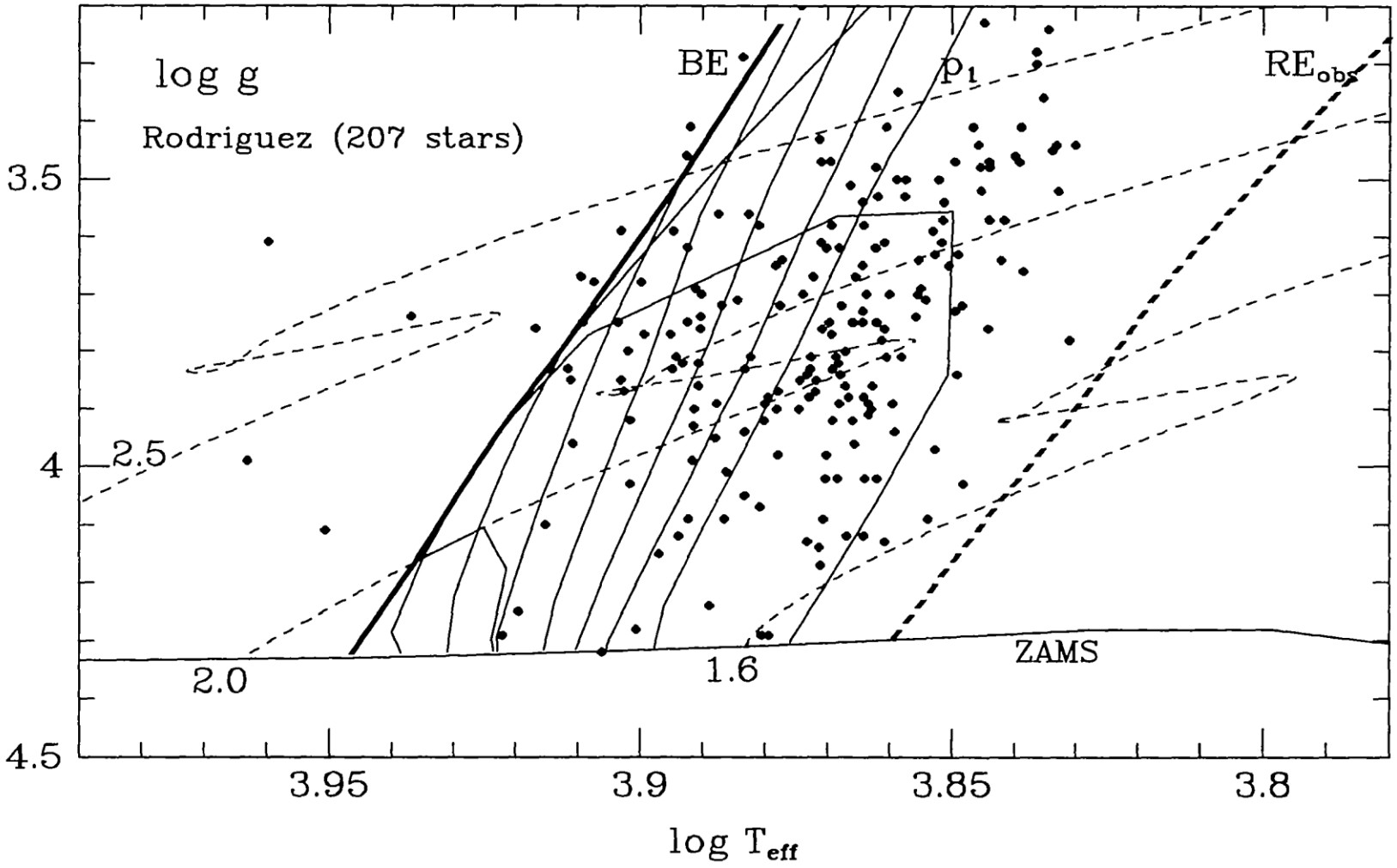

Figure 4. The δ Scuti instability domain in the $\log g - \log T_{\rm eff}$ diagram. The same models and the same calibrations for observed stars as in Fig. 3 were used. A few evolutionary tracks for the indicated values of $M/M_\odot$ are shown.

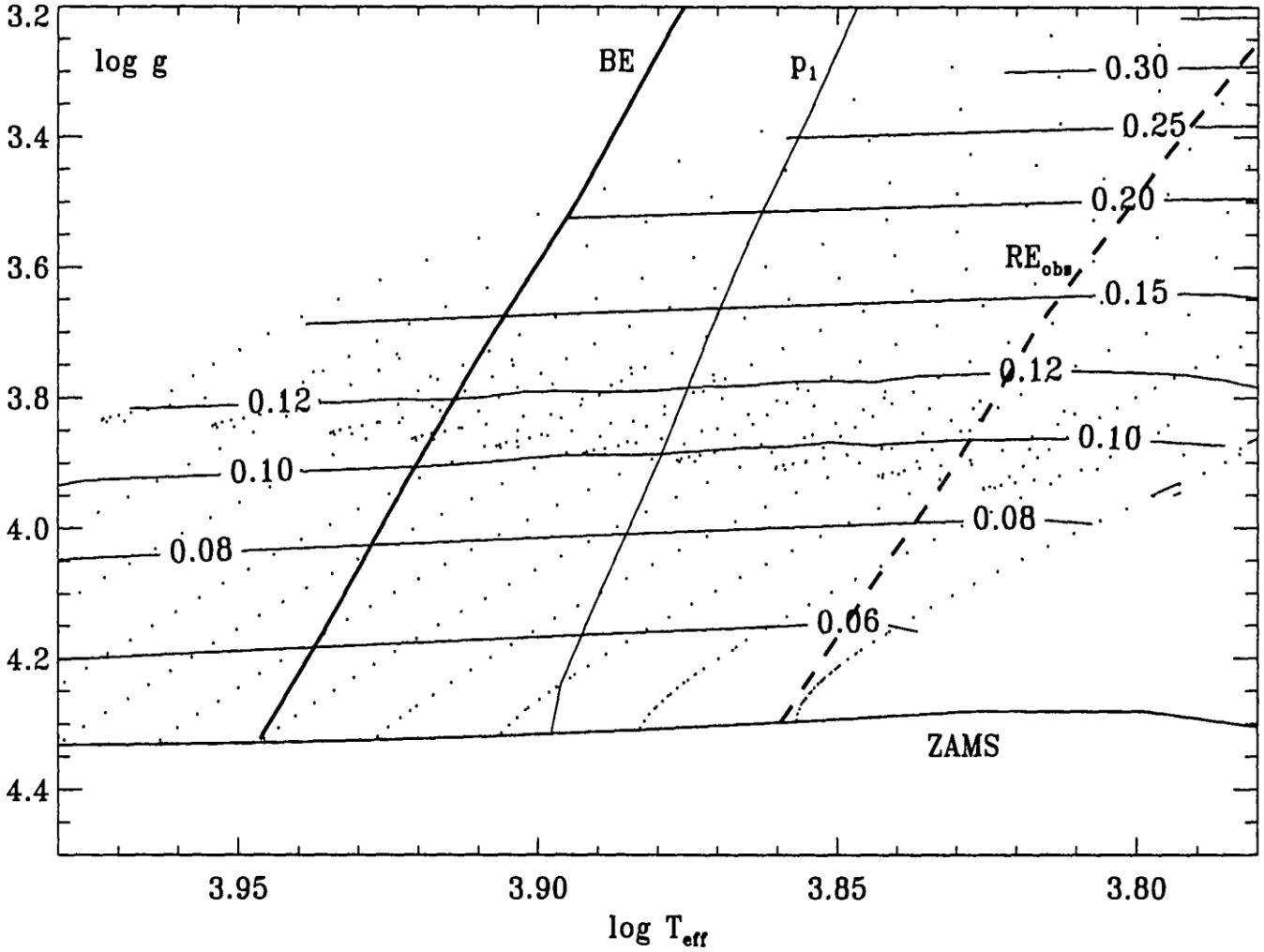

Figure 5. Lines of constant period for the radial fundamental mode in the $\log g - \log T_{\rm eff}$ diagram. The same models as in Fig. 4 were used. Period values are given in days.

Pamyatnykh 2000

The effect of overshooting on the MS evolution

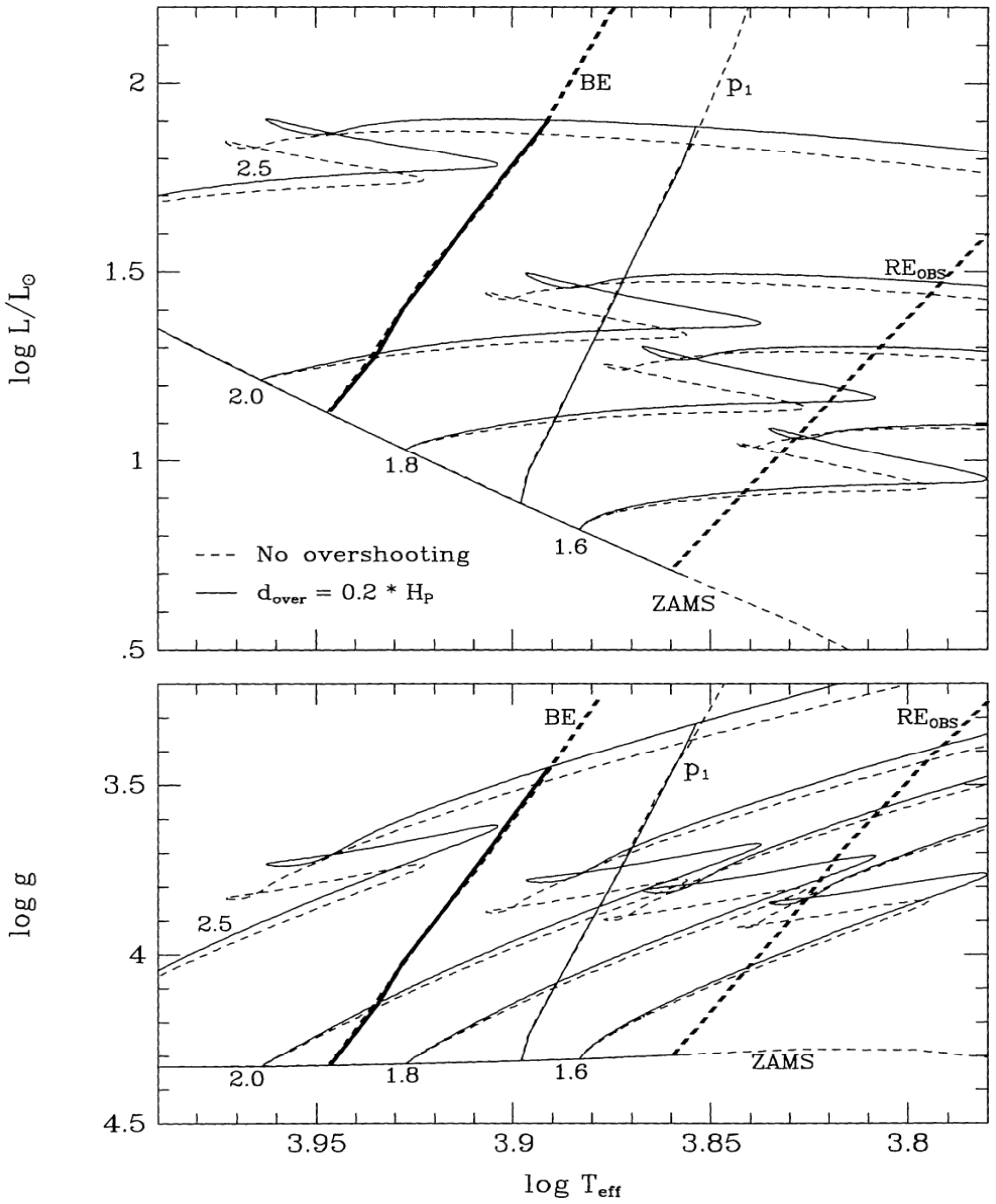

Figure 10. The effect of overshooting from the convective stellar core on the evolution and on the position of the blue edges of the δ Scuti instability domain in the HR and in the $\log g - \log T_{\rm eff}$ diagrams. The Zero-Age Main Sequence (ZAMS) and a few evolutionary tracks for the indicated values of $M/M_{\odot}$ are shown.

Pamyatnykh 2000

Rotational splitting of frequencies of low-degree modes

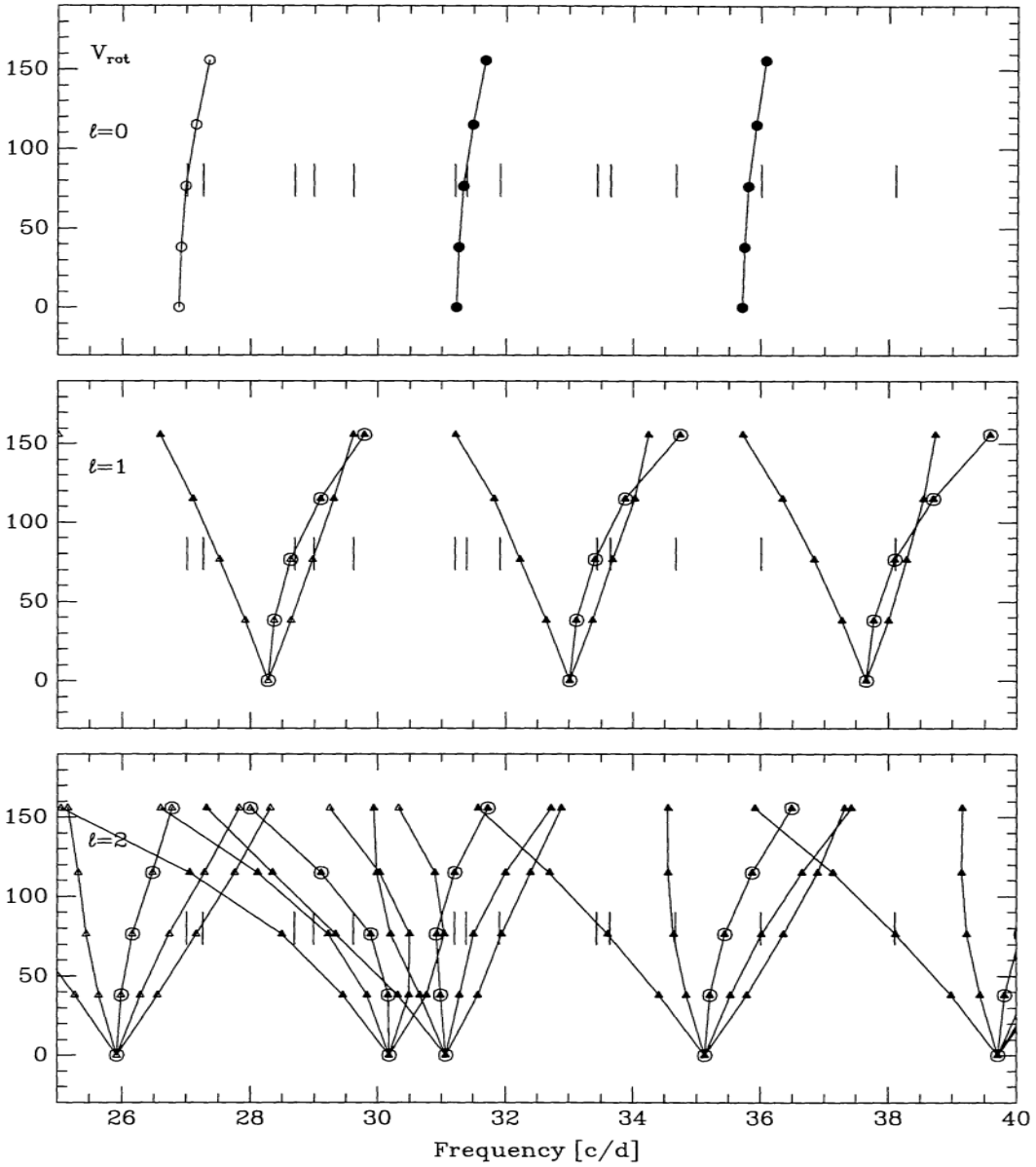

Figure 12. Rotational splitting of the frequencies of low-degree oscillation modes for models of 1.9 $M_\odot$ near the Main Sequence. All models of different $V_{\rm rot}$ have the same effective temperature $\log T_{\rm eff} = 3.91$. The luminosity of the models varies from $\log L = 1.21$ to $\log L = 1.23$ depending on $V_{\rm rot}$ (smaller for faster rotation). Vertical lines mark the observed frequency spectrum of XX Pyxidis.

Pamyatnykh 2000

Avoided crossing as a test of convective overshooting

Dziembowski & Pamyatnykh, 1991, A&A, 248, L11-L14.

Avoided crossing, testing overshooting

Frequencies of dipole and quadrupole modes for models of a 2 Msun in the MS evolutionary stage (from ZAMS to TAMS)

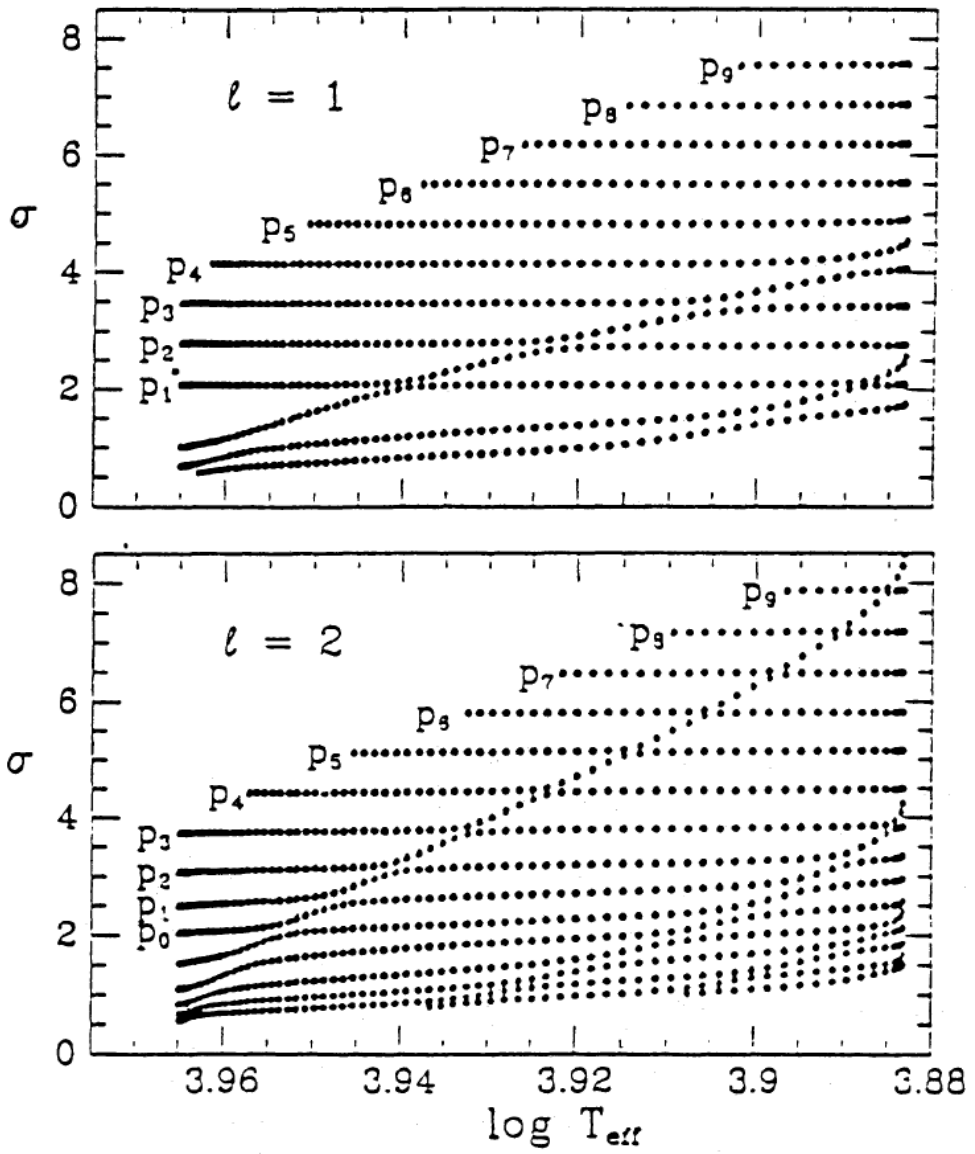

Fig.1 Dimensionless frequences of low order modes corresponding to $l = 1$ and 2 spherical harmonics for models of a $2M_{\odot}$ star in the Main-Sequence evolutionary phase. Pulsation instability begins at $\log T_{\rm eff} \approx 3.94$.

Dziembowski & Pamyatnykh 1991

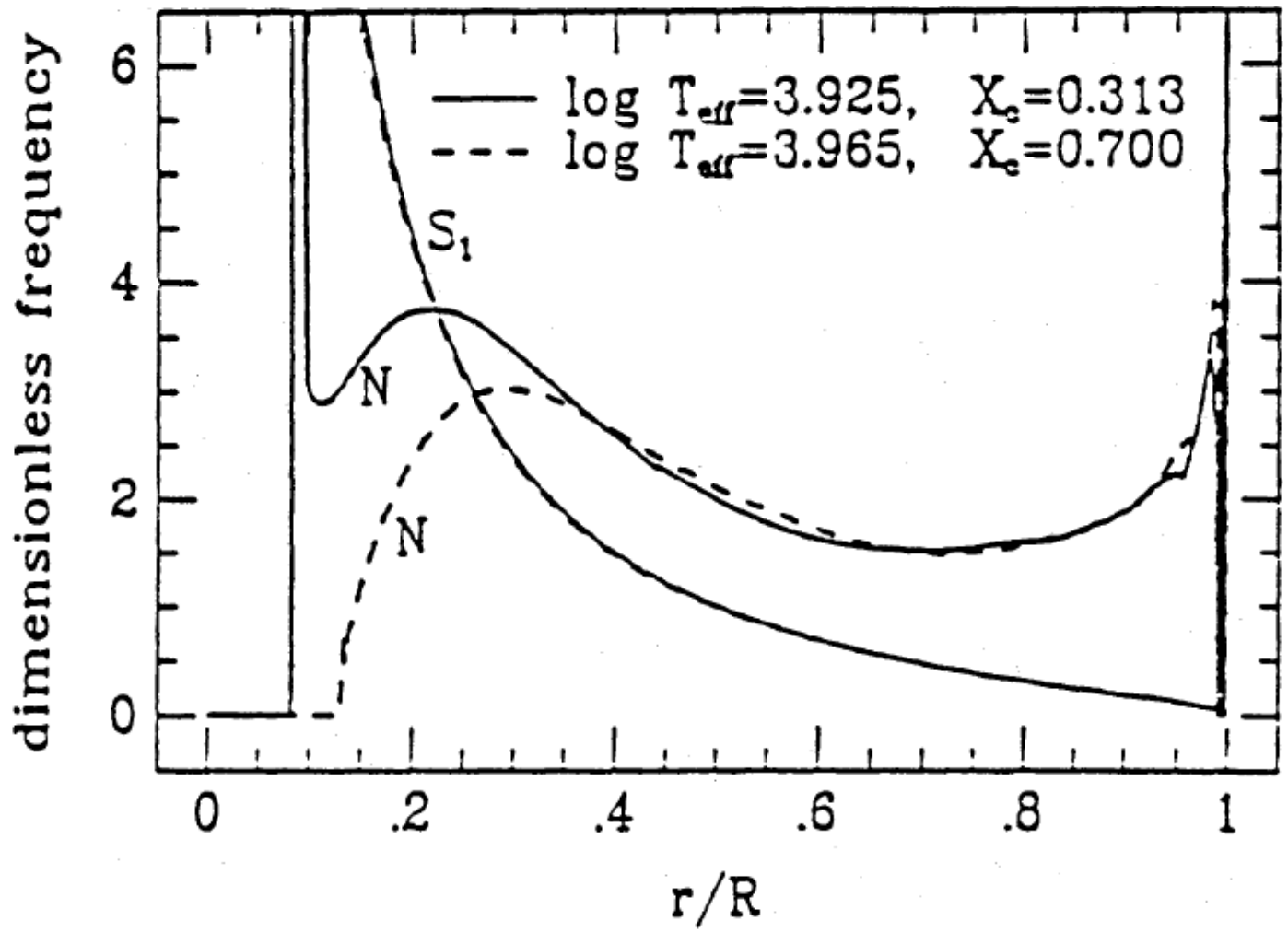

Fig.2 Brunt-Väisälä and Lamb frequencies in two models of $2M_\odot$ during the Main Sequence evolution. The frequencies are expressed in the $\sqrt{4\pi G<\rho>}$ units. Maximum value of N in the interior of the evolved model is ≈ 12.

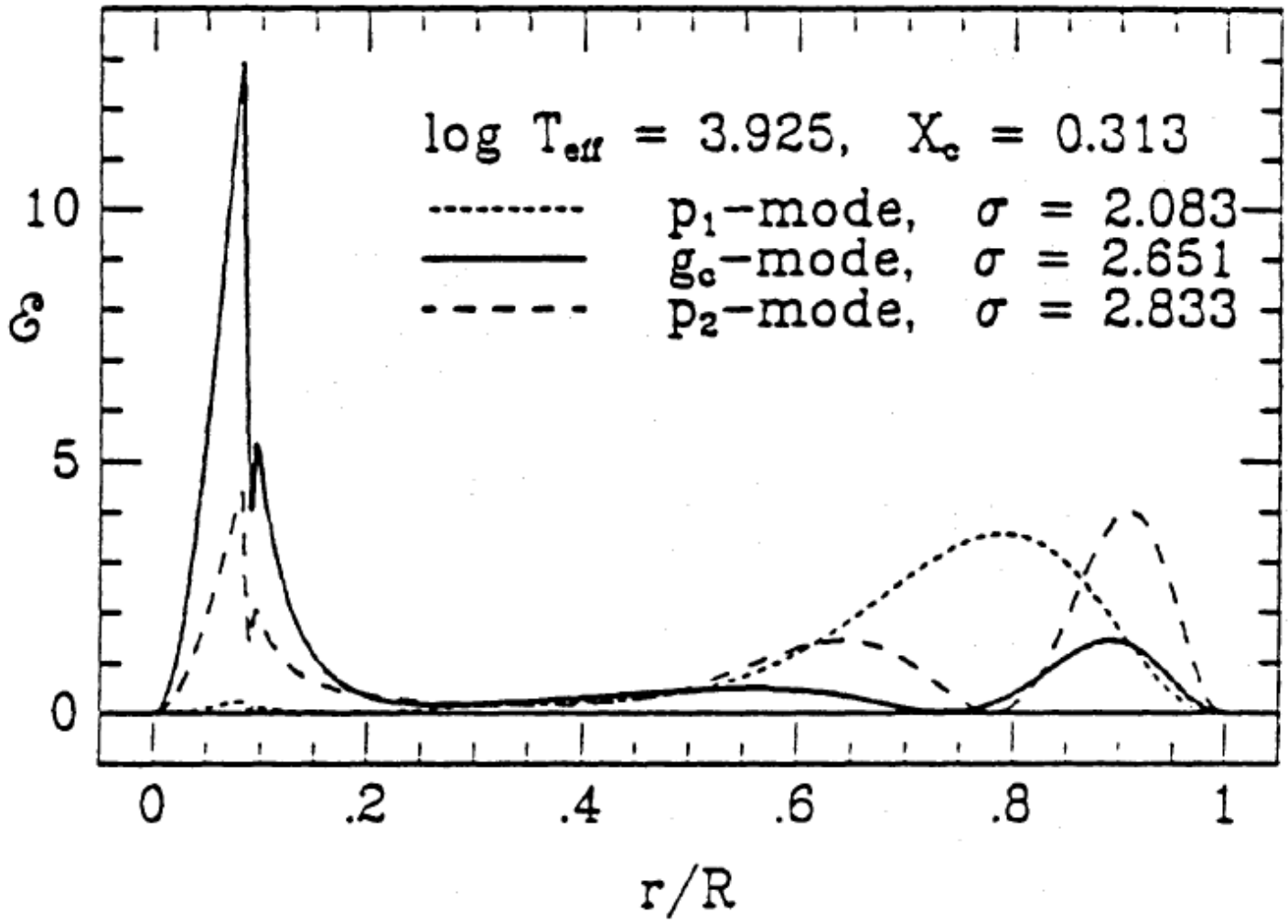

Fig.3 Kinetic energy density for for g_c- mode and two neighbouring p-modes. Normalization $\int_0^1 \mathcal{E} dx = 1$ is adopted. The inner maximum of $\mathcal{E}$ occurs at the boundary of the convective core.

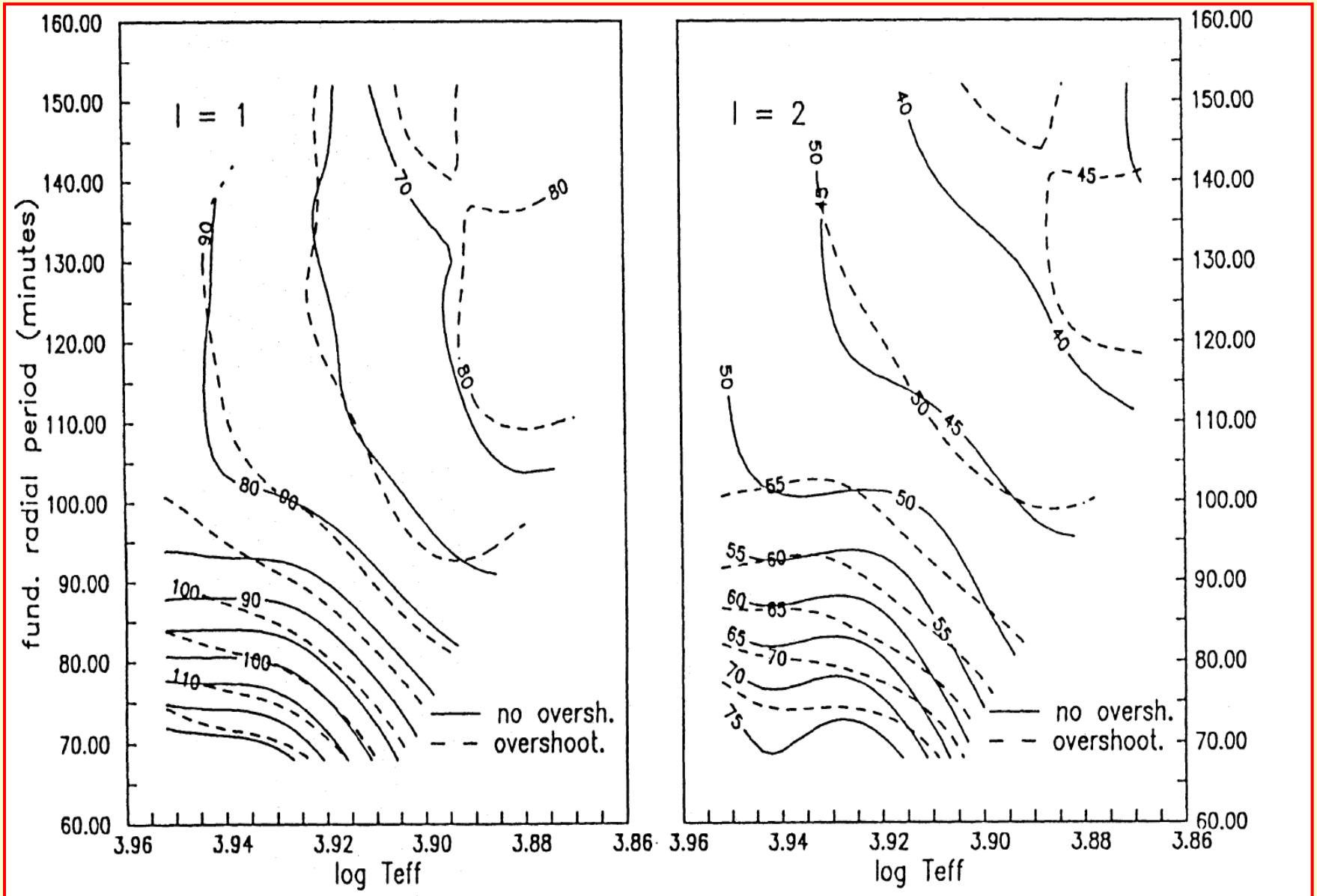

Fig.4 Lines of constant of g_c-mode period (in minutes) obtained for sequences of Main Sequence stellar models with $M = 1.8{-}2.2M_\odot$ calculated by assuming no overshooting (continues lines) and overshooting with a distance $d_{\rm over} \approx 0.25H_p$ (dashed lines).